

DESIGN AND CONTROL OF NOSE ACTUATION KIT FOR POSITION
CORRECTION OF SPIN STABILIZED MUNITIONS UNDER WIND EFFECT

A THESIS SUBMITTED TO
THE GRADUATE SCHOOL OF NATURAL AND APPLIED SCIENCES
OF
MIDDLE EAST TECHNICAL UNIVERSITY

BY

MESUT EROĞLU

IN PARTIAL FULFILLMENT OF THE REQUIREMENTS
FOR
THE DEGREE OF MASTER OF SCIENCE
IN
AEROSPACE ENGINEERING

FEBRUARY 2016

Approval of the thesis:

**DESIGN AND CONTROL OF NOSE ACTUATION KIT FOR
POSITION CORRECTION OF SPIN STABILIZED MUNITIONS UNDER
WIND EFFECT**

submitted by **MESUT EROĞLU** in partial fulfilment of the requirements for the degree of **Master of Science in Aerospace Engineering Department, Middle East Technical University** by,

Prof. Dr. Gülbin Dural Ünver _____
Director, Graduate School of **Natural and Applied Sciences**

Prof. Dr. Ozan Tekinalp _____
Head of Department, **Aerospace Engineering**

Asst. Prof. Dr. Ali Türker Kutay _____
Supervisor, **Aerospace Engineering Dept., METU**

Examining Committee Members:

Prof. Dr. Ozan Tekinalp _____
Aerospace Engineering Dept., METU

Asst. Prof. Dr. A. Türker Kutay _____
Aerospace Engineering Dept., METU

Prof. Dr. Metin U. Salamcı _____
Mechanical Engineering Dept., Gazi University

Assoc. Prof. Dr. Dilek Funda Kurtuluş _____
Aerospace Engineering Dept., METU

Asst. Prof. Dr. Kıvanç Azgın _____
Mechanical Engineering Dept., METU

Date: 05.02.2016

I hereby declare that all the information in this document has been obtained and presented in accordance with academic rules and ethical conduct. I also declare that, as required by these rules and conduct, I have fully cited and referenced all material and results that are not original to this work.

Name, Last Name:

Signature:

ABSTRACT

DESIGN AND CONTROL OF NOSE ACTUATION KIT FOR POSITION CORRECTION OF SPIN STABILIZED MUNITIONS UNDER WIND EFFECT

Erođlu, Mesut

M.S., Department of Aerospace Engineering

Supervisor : Asst. Prof. Dr. Ali Türker Kutay

February 2016, 127 pages

Unguided munitions have been replaced with guided munitions over the century. There are two main reasons for this change; to increase damage to target with fewer munitions and reduce collateral damage due to deflection of munitions. Moreover, there are two options, building new guided munitions and modification of unguided munitions to convert dummy munitions to smart ones. Modifying unguided munitions to have guided munitions instead of building a completely new one is preferable due to economic reasons [1].

This thesis aims at ensuring position correction for spin stabilized munitions under wind effect by using a one degree of freedom nose actuation mechanism. A model of the standard 155 mm spin stabilized munitions is created by PRODAS software to obtain aerodynamic coefficients. Aerodynamic coefficients are calculated between 0.6 and 3 Mach number for the model by the software. A computer code is developed that calculates the forces and moments acting on the munition by using the aerodynamic coefficients given by PRODAS. The code also calculates the trajectory by solving for the equations of motion. Results of the code developed are compared with results of PRODAS for verification. A mechanism that attaches to the nose of the munition with roll degree of freedom is designed. Two wings with a fixed incidence angle are mounted on the mechanism that creates a force normal to the axis

of the mechanism. The orientation of the mechanism with respect to the munition can be controlled by an electric motor, which gives the ability to steer the munition as desired. Solid and dynamic models of the mechanism are derived and a controller is designed for its roll position. First the baseline munition without the mechanism is simulated with varying disturbance wind direction and magnitude to obtain munition dispersion zones due to wind effect. The same analysis is repeated with the mechanism with varying wing platform areas and roll angles. The roll angle of the mechanism is kept constant at the chosen value for each flight. These analyses yielded the optimum wing size that ensured stability with maximum effectiveness.

Keywords: Spin stabilized munition, ballistic flight, nose actuation kit, design, control, position correction, wind

ÖZ

DÖNÜ KARARLI MÜHİMMATLARIN RÜZGÂR ETKİSİ ALTINDA KONUM DÜZELTMESİNİ SAĞLAYACAK BİR BURUN TAHRİK SİSTEMİNİN TASARIMI VE KONTROLÜ

Erođlu, Mesut

Yüksek Lisans, Havacılık ve Uzay Mühendisliđi Bölümü

Tez Yöneticisi : Yrd. Doç. Dr. Ali Türker Kutay

Şubat 2016, 127 sayfa

Son yüzyıldır kullanılan güdümsüz mühimmatlar günümüzde yerini akıllı yani güdümlü mühimmatlara bırakmaktadır. Bunun başlıca iki sebebi vardır. Bunlar; daha az mühimmat kullanarak düşmana maksimum zarar vermek ve mühimmat yolunun sapmasından dolayı oluşabilecek sivil kayıpları minimuma indirmektir. Ayrıca güdümlü bir mühimmat birkaç yolla elde edilebilir. Bunlar biri, yeni bir mühimmat üretmek; bir diğeri ise hâlihazırda var olan güdümsüz mühimmatların bazı modifikasyonlarla güdümlü mühimmatlara dönüştürmektir. Ancak, ekonomik nedenlerden dolayı güdümsüz mühimmatların bazı modifikasyonlarla güdümlü mühimmatlara dönüştürülmesi çok daha akılcı bir çözüm olarak kabul edilir [1].

Bu tez çalışmasında, dönü kararlı mühimmatların sabit açılı kanatçıkların tek eksenli bir burun tahrik mekanizması ile hareketinin kontrol edilerek mühimmatın rüzgâr etkisi altında konum düzeltmesinin sağlanması amaçlanmıştır. Bu amaçla öncelikle PRODAS programı kullanılarak klasik bir 155 mm dönü kararlı mühimmatın modeli çıkartılmış ve aerodinamik katsayıları bu model kullanarak hesaplanmıştır. Daha sonra mühimmatın hareket denklemleri çıkarılmış ve mühimmat üzerine etki eden kuvvet ve momentler aerodinamik katsayılar kullanılarak hesaplanmıştır. Mühimmat yörünge hesapları, geliştirilen kod yardımı ile yapılmıştır. Oluşturulan modelinin doğruluğunu ispat etmek amacıyla model

sonuları PRODAS sonuları ile karşılařtırılmıřtır. Ardından mhimmatın gerekli manevraları yapmasını saėlayacak kontrol mekanizmasının ve kontrolcsnn tasarım seenekleri zerinde durulmuř ve en uygun modeller tasarlanmıřtır. Mekanizma etkisi olmadan farklı byklkte ve ynlerde mhimmata etki edecek rzgrın mhimmatı hedeften ne kadar saptıracaėı hesaplanmıř ve bu sonular mhimmatın dřebileceėi alanlar řeklinde ifade edilmiřtir. Son olarak tasarlanan kontrol mekanizması ile rzgr etkisi olmaksızın aynı hesaplamalar tekrarlanmıř ve benzer alanlar mekanizma etkisi iin ıkarılmıřtır. Sonu olarak, kullanılabilir en byk mekanizma kanatık alanı ile mekanizmanın kontrol edebileceėi maksimum rzgr byklė hesaplanmıřtır.

Anahtar kelimeler: Dn kararlı mhimmat, balistik atıř, burun tahrik mekanizması, tasarım, kontrol, konum dzeltme, rzgr

*To
My Wife
and
Son*

ACKNOWLEDGMENTS

I would like to express my appreciation to my supervisor Dr. Ali Türker KUTAY, co-supervisor Dr. Galip Serdar TOMBUL for their helpful criticism, guidance and patience in the progress and preparation of this thesis.

I want to send my thanks to Dr. Bülent ÖZKAN and Dr. İsmail İlker DELİCE for their technical support and guidance, endless help and patience during the thesis.

I am very grateful to all members of my family for their endless support not only during my thesis preparation, but also throughout my life.

Finally I would like to thank to my great love and future Tuğba. She is the source of my all motivation and energy, I adore her. Without her endless support, I could not finish this work.

TABLE OF CONTENTS

ABSTRACT	v
ÖZ	vii
ACKNOWLEDGMENTS	x
TABLE OF CONTENTS	xi
LIST OF TABLES	xiii
LIST OF FIGURES	xiv
LIST OF SYMBOLS	xvii
CHAPTERS	
INTRODUCTION	1
1.1 Aim of the Study	1
1.2 Scope of the Thesis	3
1.3 Background and Basic Concepts.....	4
1.3.1 Spin Effect on Munition	5
1.3.2 PRODAS.....	7
1.3.3 Basic Concepts in PI and PID Controller	7
1.4 Literature Survey.....	9
1.5 Contributions of the Thesis	11
BALLISTIC ANALYSES USING PRODAS	15
2.1 Ballistic	15
2.2 Mass Properties	15
2.3 Aerodynamic Prediction.....	16
2.4 Stability Evaluation.....	17
2.5 Trajectory Analysis	20
BALLISTIC ANALYSES USING DEVELOPED CODE.....	27
3.1 Coordinate System	27
3.2 Aerodynamic Coefficients	29
3.2.1 Drag Force	31
3.2.2 Lift Force	33

3.2.3 Axial and Normal Force.....	33
3.2.4 Magnus Force.....	34
3.2.5 Pitching Moment.....	35
3.2.6 Pitch Damping Moment.....	35
3.2.7 Magnus Moment	36
3.2.8 Spin Damping Moment.....	36
3.3 Equations of Motion.....	37
3.4 Model of the Munition	40
THE NOSE ACTUATION KIT.....	47
4.1 Kit Design	47
4.1.1 Design of the Nose Actuation Kit.....	47
4.1.2 Selection of Standard Elements	52
4.2 Kit Control.....	57
4.2.1 Mechanism Moment of Inertia.....	58
4.2.2 Transmission Ratio of the Mechanism	60
4.2.3 Mechanism Mathematical Model	61
4.2.4 Controller Design.....	66
RESULTS AND DISCUSSION	75
5.1 Ballistic Flight Database	75
5.2 Results and Discussion of the Developed Code.....	79
5.3 Comparison between PRODAS and the Developed Code.....	87
5.4 Control Authority Results and Discussion	93
CONCLUSION AND FUTURE WORK.....	101
6.1 Conclusion.....	101
6.2 Future Work	104
REFERENCES.....	107
APPENDICES.....	113
Appendix A: PRODAS Results.....	113
Appendix B: The Developed Code	118
Appendix C: The Developed Code Analyses for Spin Velocities.....	125

LIST OF TABLES

TABLES

Table 1. Mass Properties	15
Table 2. Aerodynamic Coefficients	17
Table 3. Stability Factors	20
Table 4. Aerodynamic Coefficients Description [22]	37
Table 5. Initial Conditions for Ballistic Flight	43
Table 6. EC 22 Brushless Motor Properties	57
Table 7. Ballistic Flight Database for Longitudinal Dispersion	76
Table 8. Ballistic Flight Database for Lateral Dispersion	77
Table 9. Munition Trajectory Analysis by PRODAS Software	113

LIST OF FIGURES

FIGURES

Figure 1. Stability of Fin Stabilized Munitions [3]	1
Figure 2. Spin Effect on Munitions [8]	6
Figure 3. Gyroscopic Effect on Spinning Object	6
Figure 4. PI Controller Block Diagram	8
Figure 5. PID Controller Block Diagram	9
Figure 6. PGK Munition [14]	10
Figure 7. PGMM Munition [13]	11
Figure 8. Excalibur [16]	11
Figure 9. Munition Geometry	16
Figure 10. Munition movement	19
Figure 11. Range vs Time for PRODAS	21
Figure 12. Deflection vs Time for PRODAS	21
Figure 13. Height vs Time for PRODAS	22
Figure 14. Range vs Height for PRODAS	23
Figure 15. Spin Velocity vs Time for PRODAS	23
Figure 16. Gyroscopic Stability vs Time for PRODAS	24
Figure 17. Total Angle of Attack vs Time for PRODAS	25
Figure 18. Velocity vs Time for PRODAS	25
Figure 19. Earth Fixed Coordinate System	28
Figure 20. Body Fixed Coordinate System	28
Figure 21. Aerodynamic Forces on Munition [22]	30
Figure 22. Aerodynamic Moments on Munition [22]	30
Figure 23. Total Angle of Attack Plane of the Munition	31
Figure 24. Standard 155 mm Munition [16]	48
Figure 25. Designed 155 mm Munition	49
Figure 26. Designed 155 mm Munition with Case	50
Figure 27. Designed 155 mm Munition with Bearings	50

Figure 28. Designed 155 mm Munition with Bearings.....	51
Figure 29. NACA 6412 Data [27].....	52
Figure 30. Forces on Bearings [28].....	53
Figure 31. Mechanism Forces during the Flight	54
Figure 32. Motion of Dynamic Mechanism.....	59
Figure 33. Mechanism with Munition.....	60
Figure 34. Motor Basic Work Principle [32]	61
Figure 35. Brushless Motor Circuit.....	63
Figure 36. Simulink Model for Current Input and Roll Angle Output	65
Figure 37. S-Plane	66
Figure 38. Close Loop Model from Reference to Output	67
Figure 39. Simulink Model for Desired Roll Angle Input and Roll Angle Output ...	69
Figure 40. Roll Angles of Mechanism	70
Figure 41. Roll Velocity of Body.....	72
Figure 42. Necessary Current of Motor	73
Figure 43. Circular Error Probable [36].....	78
Figure 44. Alpha vs Beta for the Developed Code	79
Figure 45. Spin Velocity vs Time for the Developed Code.....	80
Figure 46. Height vs Range for the Developed Code	82
Figure 47. Positions vs Time for the Developed Code	83
Figure 48. Gyroscopic Stability vs Dynamic Stability for the Developed Code	84
Figure 49. Total Angle of Attack vs Time for the Developed Code.....	85
Figure 50. Velocity vs Time for the Developed Code	86
Figure 51. Velocities vs Time for the Developed Code.....	87
Figure 52. Range vs Time for Comparison.....	88
Figure 53. Height vs Time for Comparison	89
Figure 54. Deflection vs Time for Comparison	90
Figure 55. Spin Velocity vs Time for Comparison	91
Figure 56. Gyroscopic Stability vs Time for Comparison	92
Figure 57. Velocity vs Time for Comparison	93

Figure 58. Wind Effects on the Munition	95
Figure 59. Mechanism Effect on the Munition	97
Figure 60. Mechanism and Wind Effects on the Munition	99
Figure 61 Alpha vs Beta for Different Spin Velocities	125
Figure 62 Velocity vs Time for Different Spin Velocities	125
Figure 63 Total Aoa vs Time for Different Spin Velocities	126
Figure 64 Gyroscopic vs Dynamic Stability for Different Spin Velocities	126
Figure 65 Height vs Range for Different Spin Velocities	127

LIST OF SYMBOLS

S	: Reference area
D	: Reference diameter
P	: Air density
V	: Velocity of munition
C_D	: Drag coefficient
\vec{i}	: Unit vector in the direction of the velocity vector
C_{D_0}	: Zero-yaw drag coefficient
$C_{D\alpha^2}$: Yaw drag coefficient according to Mach number
α_M	: Total angle of attack
δ	: $\sin(\alpha_M)$
α	: Angle of attack
β	: Sideslip angle
$C_{L\alpha}$: Lift force coefficient
\vec{x}	: Unit vector along the munition's nose axis of symmetry
$C_{L\alpha_0}$: Linear lift force coefficient
$C_{L\alpha^2}$: Cubic lift force coefficient [2]
C_X	: Axial force coefficient
C_{X_0}	: Linear axial force coefficient
$C_{X\alpha^2}$: Cubic axial force coefficient [2]
$C_{N\alpha}$: Linear normal force coefficient
$C_{N\alpha\delta^3}$: Cubic normal force coefficient [2]
C_{Yp}	: Magnus force coefficient
p	: Axial spin
$C_{Yp\alpha}$: Linear Magnus force coefficient
$C_{Yp\alpha\delta^3}$: Cubic Magnus force coefficient [2]
C_M	: Pitching moment coefficient
$C_{M\alpha}$: Linear pitching moment coefficient

$C_{M\alpha 3}$: Cubic pitching moment coefficient
$C_{M\alpha 5}$: Cubic pitching moment coefficient [2]
C_{mq0}	: Linear pitch damping moment coefficient
C_{mq2}	: Cubic pitch damping moment coefficient
C_{mq4}	: Cubic pitch damping moment coefficient [2]
C_{np}	: Magnus moment coefficient
$C_{np\alpha}$: Linear Magnus moment coefficient
$C_{np\alpha 3}$: Cubic Magnus moment coefficient
$C_{np\alpha 5}$: Cubic Magnus moment coefficient [2]
C_{lp}	: Spin damping coefficient
C_{np0}	: Linear Magnus moment coefficient
$C_{np\alpha 2}$: Cubic Magnus moment coefficient [2]
\vec{F}_T	: Total force
m	: Munition mass
\vec{F}_A	: Aerodynamic force
\vec{F}_M	: Magnus force
\vec{W}	: Munition weight
\vec{F}_C	: Mechanism force
G	: Gravity
B_{avg}	: Average flux density
τ_m	: Motor torque
r_r	: Rotor radius
F_m	: Magnetic force
i	: Current
l_m	: Motor axial length
θ	: Rotor position
k_t	: Motor torque constant
Φ	: Flux

w	: Motor rotational speed
k_v	: Motor velocity constant
V	: Voltage
L	: Motor inductance
R	: Motor resistance
e	: Inverse electro motor force
τ_L	: Load
τ_m	: Motor torque
J	: Total inertia
B	: Viscous friction constant
Slant	: Line of sight distance

CHAPTER 1

INTRODUCTION

1.1 Aim of the Study

Munitions cover everything which is used in war zone. They are basically divided into two groups. One of them is fin stabilized munition, whose stability is supported by fins or wings. Center of gravity of fin stabilized munitions must be in front of center of the pressure point so that it is naturally stable. They are usually launched from aircraft due to presence of fins and wings. The other one is spin stabilized munitions, whose stability is supported by high roll velocity of the munition. Center of gravity of spin stabilized munitions must be behind the center of the pressure point for stable flight because these munitions are statically unstable but dynamically stable [2]. There is a large amount of spin stabilized munitions compared to fin stabilized munitions respectively all around the world. Moreover, both groups have also been divided into guided and unguided in the last few decades. All munitions were used as unguided munitions before guidance technology emerged.

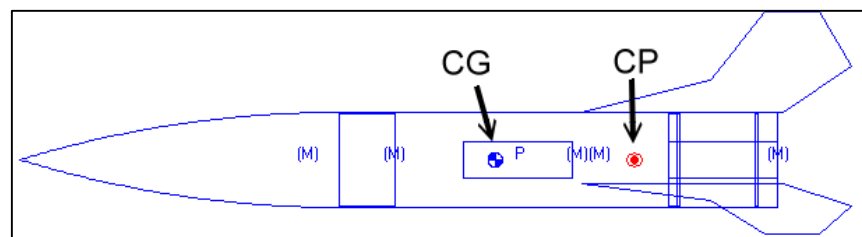


Figure 1. Stability of Fin Stabilized Munitions [3]

Guided munitions are something, which are used in war zone that can hit a target precisely by guidance orders. These munitions use aerodynamic surfaces which are fins, canards, wing or etc. to maneuver to hit a target precisely. Air effects on the aerodynamic surfaces create aerodynamic forces on a flying system. Motion of the aerodynamic surfaces creates forces to control the munition to follow the desired trajectory. Aerodynamic surfaces are mechanically developed by actuation

systems. Actuation systems deliver a range of technology options including electro mechanic and hydraulic powered actuators and advanced carbon-fiber products for commercial aerospace and defense applications. The use of electro mechanic actuation on aircraft, rather than hydraulic, comes from customer and airworthiness requirements for cleaner, more environmentally friendly aircraft. Electro mechanic actuation has the potential to help fulfill this requirement as well as providing health and usage monitoring to reduce in-service removals [4], [5].

After the World War I, countries have understood the importance of hitting the target more accurately. While the target could not be hit at the first attempt, the enemy detects your position and destroys you; therefore, all countries have given more importance and budget to guidance technology. This technology like laser guided, GPS guided or etc. has grown rapidly all over the World.

Although countries have given more budgets to guidance technology, there are always limits of this budget. At first part of guidance technology, new guided munitions are created by engineers to hit the target precisely. However, engineers have worked on upgrading dummy munitions to smart munitions instead of developing completely new munitions for decades because upgrading munitions is cheaper than developing new munitions.

Although guidance technology has been developed for many years, guided munitions cannot find sufficient fields in the world because of lack of their reliability and cost efficiency. Guided munitions must be produced more reliable, accurate and with low lost product for successful design.

In this study, 155 mm unguided spin stabilized munitions are investigated. It is known that control surfaces must be created for converting the unguided munitions to guided munitions. Therefore, the nose actuation kit, which is also called a nose actuation kit or mechanism, will be developed and assembled on to a standard 155 mm spin stabilized munition. The mechanism will be controlled by orders come as an input. The aim is position correction of the munitions with the mechanism under wind effect.

1.2 Scope of the Thesis

This thesis aims that position correction of spin stabilized munition under wind effect by the nose actuation kit which generates necessary forces and moments to the munition to maneuver it.

A standard 155 mm spin stabilized munition is modelled by PRODAS software. The program is also used to obtain aerodynamic coefficients for the munition. Trajectory analyses are done with the model and aerodynamic coefficients by using PRODAS. Equations of motion are the most critical factor to understand the motion behavior of the munition. Equations of motion could be obtained easily for general air vehicles [6]. Angular and linear accelerations are calculated by using forces and moments that act on the munition body. After equations of motion are determined for spin stabilized munition, they should be checked with the other program. These equations are coded in Matlab software with initial conditions, which are same with the PRODAS examples. After the developed code is run, the results, which include alpha vs beta, roll rate vs time, position vs time, dynamic stability vs gyroscopic stability, total angle of attack vs time and velocities vs time are achieved. The results are checked by the other program for correction of the results and it is seen that the trends are similar in each other; thus, the results are reasonable.

PRODAS is used to analyze 155 mm spin stabilized munition without control mechanism to check the results. The software is run with the same initial conditions. Results are compared with PRODAS results to check especially position and velocity graphs in 5.3. It could be seen that PRODAS results support the results in 5.2 with some error.

The nose actuation kit is called a mechanism in shortly in this thesis. Mechanism is the most important part of the thesis because position correction of the munition is supported by the mechanism under wind effect. Moreover; some factors like space limitations, high roll rate and technologic knowledge are challenges for mechanism design and control. Solid model of mechanism is designed and standard elements such as the motor and bearings should be selected before controller model of mechanism is designed because some parameters of the controller come from

standard elements. Design of solid model starts from standard elements and then the other components are designed. The motor and bearings should be selected according to space, velocity, acceleration and force limitations. Selected standard elements are placed into the solid model and then draft of solid model is prepared. The mechanism mainly consists of motor, shaft and fins. Controller model requires motor parameters and inertias of moments of mechanism components. Inertias of shaft and fins are calculated easily in 4.2.1. However, inertia of motor is taken from catalog data so selection of motor is very important for controller model design. Transmission ratio is also other important factor for controller model design. It is ratio between velocity of mechanism and velocity of motor. The transmission ratio is equal to between torque of motor and torque of mechanism. Mathematical model of mechanism is called the transfer function of the system and controller model is designed by using transfer function. Motor properties, transmission ratio and inertias of components are used to determine transfer function. Input and output of the transfer function with controller are current and angular velocity respectively. Moreover controller block diagram includes current disturbance and sensor errors, which are needed for simulation of the real situation. It is expected that position of the mechanism follow reference inputs with minimum errors.

Consequently, wind effects on the munition are obtained for different magnitudes and directions. On the other hand mechanism effects on the munition are also determined for different fin surface areas and force directions. Maximum fin surface area which does not cause instability of the munition is found and it is used to perform position control for the munition under wind effect.

1.3 Background and Basic Concepts

Spin stabilized munitions have been used about 300 years but the control concept of these munitions is a completely new subject all over the world. Because there are some challenges for this concept like very high spin velocity of munitions, stability of munitions, high accurate sensor for control, control method for mechanism of munition and guidance of system. Motion behavior of spin stabilized

munitions is too complex to solve easily so there are some concepts that should be explained in 1.3.1, 1.3.2, 1.3.3.

1.3.1 Spin Effect on Munition

Spin effect, which is shown in Figure 2, supports the stability for spin stabilized munitions. Nose vector of spin stabilized munition always tends to have same axis with velocity vector because of gyroscopic effect of munition. Gyroscopic effect could be described that a device consisting of a wheel or disc mounted so that it can spin rapidly about an axis which is free to alter in direction. The orientation of the axis is not affected by tilting of the mounting, so gyroscopes can be used to provide stability or maintain a reference direction in navigation systems, automatic pilots, and stabilizers [7]. Cylindrical objects are unstable at nature because the objects leave from its own trajectory under any disturbance. Canards, wings are used for fin stabilized munitions, which does not spin about nose axis to satisfy the stability. When velocity and nose vector of spinning objects are not coincide due to disturbance, Magnus effect occurs. Magnus effect, which is discussed in 3.2.4 and 3.2.7 in depth, spin the munition about velocity vector so with spinning about nose vector, there are two spinning axis which are about nose and velocity vector. Gyroscopic effect occurs because of these two spinning axes and this effect tends to coincide these spinning axes. If the munition spins with ω angular velocity about nose axis with I inertia of body, there is an angular momentum in direction same with nose of munition. Figure 3 shows that the munition spins at O point about nose axis with ω and about velocity vector with ω_p which is an angle $\delta\theta$ in δt .

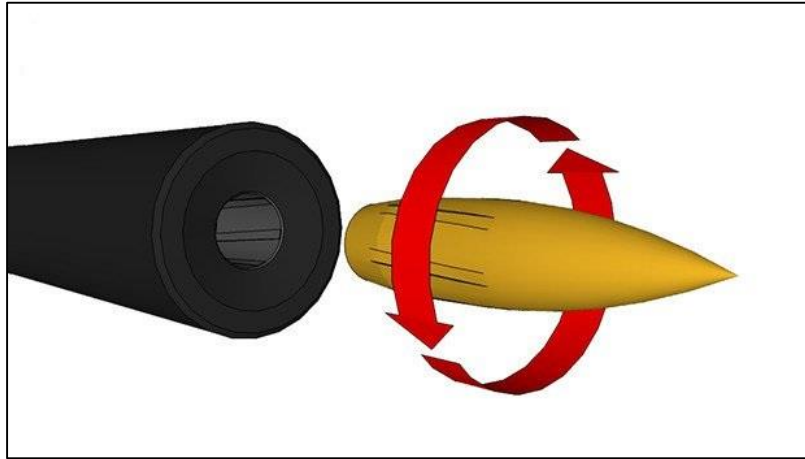


Figure 2. Spin Effect on Munitions [8]

The angular momentum in horizontal axis is given in (2.1).

$$L = I\omega \tag{2.1}$$

Equation (2.2) gives a torque.

$$T = Ls\phi\omega_p \tag{2.2}$$

Phi angle shows the angle between spin axis about ω and spin axis about ω_p . The torque direction could be found from cross product vector of spin about nose and velocity of the munition. If the angle is zero between vector of spin about nose and velocity of the munition, there is no torque.

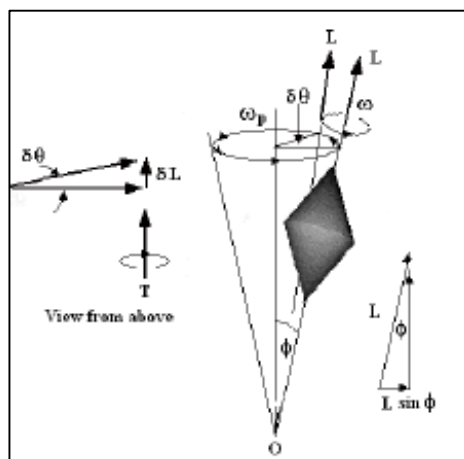


Figure 3. Gyroscopic Effect on Spinning Object

1.3.2 PRODAS

Prior to the publication of the Miller Twist Rule (Miller, 2005), the most common methods for estimating bullet stability were the relatively inaccurate Greenhill formula and the expensive computer modeling program called PRODAS. The modeling program is known to be accurate and is widely used by government laboratories and bullet companies [9]. PRODAS is designed to facilitate the rapid design of new projectiles and to analyze the effectiveness of new and existing munitions. Objectives of PRODAS are shortening design duration with evaluation cycle, documentation package, rapid correlation with test data and rapid evaluation on the performance of ammunition characteristics.

The program is developed by Arrow Tech Cooperation. Arrow Tech is an Engineering Consulting business with a focus on the defense industry. PRODAS has the capability to design projectiles and evaluate their trajectories. PRODAS is a deterministic ballistic model that determines model trajectory at a time. PRODAS conducts several different analyses which it relates together into a common database so that each subsequent analysis can utilize the results of a prior analysis [10]. Software skills are in structural analysis, dynamic analysis, weapons system simulation and all aspects of munition design and analysis.

PRODAS software program could create a projectile model, calculate mass properties, estimate aerodynamics and stability and simulate a test firing. Design problems could be detected before building prototypes. Software Tools of PRODAS have been in use every day all around the world for more than 30 years [11]. Therefore, it could be said that the software is reliable so it is useful tool to compare ballistic flight calculation and check accuracy of calculations.

1.3.3 Basic Concepts in PI and PID Controller

A PI Controller (proportional integral controller) is a special case of the PID controller in which the derivative (D) of the error is not used [12].

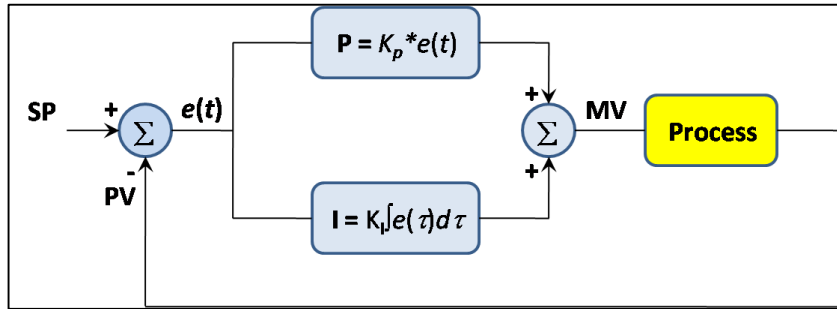


Figure 4. PI Controller Block Diagram

The controller output is given,

$$\text{Controller Output} = K_p \Delta + K_i \int \Delta dt \quad (2.3)$$

where Δ is the error.

The lack of derivative action may make the system steadier in the steady state in the case of noisy data. This is because derivative action is more sensitive to higher frequency terms in the inputs. Without derivative action, a PI controlled system is less responsive to real (no noise) and relatively fast alterations in state and so the system will be slower to reach set point and slower to respond to perturbations than a well-tuned PID system may be. Moreover, PI controller is more suitable for speed control to PID controller according to literature survey [12].

The PID controller algorithm involves three separate constant parameters, and is accordingly sometimes called three-term control: the proportional, the integral and derivative values, denoted P, I, and D. These values can be interpreted in terms of time: P depends on the present error, I on the accumulation of past errors, and D is a prediction of future errors, based on current rate of change. The weighted sum of these three actions is used to adjust the process via a control element such as the position of a control valve, a damper, or the power supplied to a heating element [12].

A PID controller relies only on the measured process variable, not on knowledge of the underlying process, making it a broadly useful controller. By tuning the three parameters in the PID controller algorithm, the controller can provide control action designed for specific process requirements. The response of

the controller can be described in terms of the responsiveness of the controller to an error, the degree to which the controller overshoots the set point, and the degree of system oscillation [12].

Most of the control engineering problems can be solved by using classical control theory. It is possible to obtain perfectly satisfactory solution in both frequency and time domains by using just proportional-integral-derivative (PID) type controllers, especially when the system is almost linear and its mathematical model is well-defined. PID controller is a control loop feedback mechanism (controller) widely used in industrial control systems. A PID controller uses an error value as the difference between a measured process variable and a desired set point. The controller attempts to minimize the error by adjusting the process through use of a manipulated variable [12].

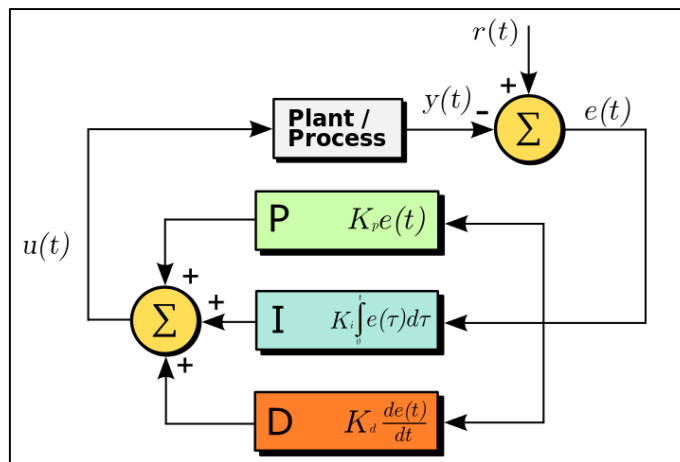


Figure 5. PID Controller Block Diagram

1.4 Literature Survey

Trend of the World is smart munitions because designing of new smart munition could be very expensive for countries instead of modifying existing munitions. For this reason, JDAM, HGK, KGK and similar kits have been designed and used for fin stabilized munitions for 50 years. The Joint Direct Attack Munition (JDAM) is a guidance kit that converts unguided bombs, or "dumb bombs" into all-weather "smart" munition. JDAM-equipped bombs are guided by an integrated inertial guidance system coupled to a Global Positioning System (GPS) receiver,

giving them a published range of up to 15 nautical miles (28 km). The JDAM is not a stand-alone weapon; rather it is a "bolt-on" guidance package that converts unguided gravity bombs into Precision-Guided Munition, or PGMs [13].

On the other hand, there are some challenging works to convert unguided bombs, or dumb bombs into smart munition for spin stabilized munition. PGK program utilizes an add-on kit that add to the fuse portion of a standard spin stabilized munition to make the "dumb" artillery round smart. However, PGK depends on GPS data to reach the target. If the GPS is jammed by enemy, the munition does not know its own position and it could not reach exact target [1].



Figure 6. PGK Munition [14]

Another munition is PGMM, utilizes the existing gun system to make a new smart weapon which can be used in tactical applications, when a smart round is needed. The PGMM round employs a thruster ring about the center of mass to maneuver. However, PGMM uses semi active laser seeker to reach the target so it requires direct contact with the enemy. Thus it could be dangerous for military units [1], [15].

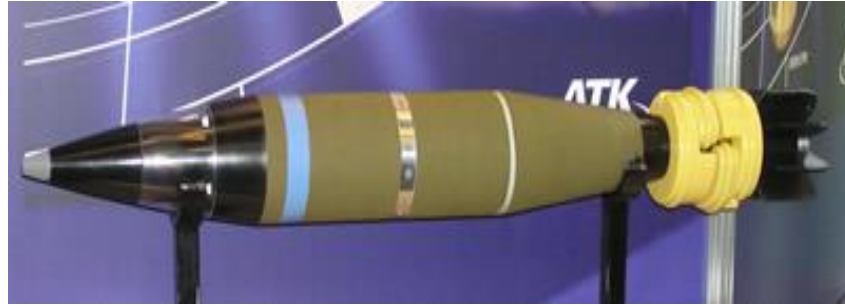


Figure 7. PGMM Munition [13]

Another example is Excalibur. Excalibur is equipped with a high cost IMU and four canards on the front of the projectile for guidance and basic control. This system has proved itself in war area and is still in the test and evaluation stages. However, high cost IMU and four actuation systems make the munition impractical [1].



Figure 8. Excalibur [16]

1.5 Contributions of the Thesis

In this thesis, position correction of standard 155 mm spin stabilized munition is aimed by changing trajectory under wind effect. The nose actuation kit is designed and it generates forces and moments, act on the munition for position correction of

the munition. Moreover the mechanism has drag force and this force causes munition maximum range to decrease. The mechanism also decreases the munitions' spin velocity, which is very critical for stability of the munition.

Mechanism forces and moments are created by fitting mechanism fins with an angle to maintain the munition range and deflection correction. Munition body spins about nose axis with an angular velocity on the contrary mechanism spins about opposite direction according to body spin direction with the same angular velocity.

Development of microchips and sensor technology allow that complex actuation system design. Spin stabilized munition control had not been possible because of high roll velocity of these munitions until now. However, there is some advance in this area with recent developments in technology. This thesis includes mechanism design which produces force and moment to change munition trajectory, control block design which help to follow the reference inputs with minimum error, ballistic flight analysis without thrust, mechanism and wind effect.

Aerodynamic coefficients are obtained by PRODAS software and trajectory is also analyzed with the software. Aerodynamic coefficients for the standard 155 mm spin stabilized munition are used in developed code. All calculations are done by the code developed and the results are compared with PRODAS solutions. Different solution methods, which are simple Euler and modified Euler, are tried. At first, simple Euler Method, which is also called forward Euler method is used. Run time of developed code is about an hour. The calculation time is too long for ballistic flight to repeat the analyses many times for different theta angle, spin velocity and muzzle velocity. Therefore, solution method is changed to reduce run time of developed code so modified Euler is replaced with forward Euler method to solve the munition trajectory. The results are better according to forward Euler method but the main benefit is for run time of code. Run time of the code reduce to about few minutes with modified Euler solution method.

Moreover, the nose actuation kit is designed uniquely and control block diagram is created by using PI control to follow the orders with an error. However, it is seen that PI controller performance is not enough for the system which has high

roll velocity. PID controller has derivative term and it follows the reference input less error according to PI controller. Coefficients of PID controller are determined by two ways that are tune command of Matlab and Butterworth method talked about in 4.2.4. Coefficients are determined by Butterworth method, show better performance in PID controller compare to coefficients, which are determined by Tune method.

Wind effects on the munition are obtained for different wind magnitudes and directions. Mechanism force changes with velocity of the munition so mechanism force could not be taken constant through the flight. Mechanism effects on the munition are obtained for different fin surface areas and force direction. Therefore, position correction could be done with the mechanism under wind effect.

CHAPTER 2

BALLISTIC ANALYSES USING PRODAS

2.1 Ballistic

Ballistic is the science of mechanics that deals with the launching, flight, behavior, and effects of projectiles, especially bullets, gravity bombs, rockets, or the like; the science or art of designing and accelerating projectiles so as to achieve a desired performance. External ballistics is the part of the science of ballistics that deals with the behavior of a non-powered projectile in flight. External ballistics is frequently associated with firearms, and deals with the unpowered free-flight phase of the bullet after it exits the gun barrel and before it hits the target, so it lies between transitional ballistics and terminal ballistics. However, external ballistics is also concerned with the free-flight of rockets and other projectiles, such as balls, arrows [17].

2.2 Mass Properties

Mass properties of the munition must be determined to calculate the aerodynamic coefficients. The munition physical properties could be taken easily from literature survey and it could be designed according to these physical properties [18].

Table 1. Mass Properties

Parameters	Unit	Value
Mass	kg	43.54
Transverse Inertia	kg.m ²	1.88
Axial Inertia	kg.m ²	0.148
Cg from Nose	mm	546.11
Diameter	mm	154.74

The munition geometry, which is shown in Figure 9, could be created in PRODAS according to Table 1. Geometric model of 155 mm spin stabilized munition is a general model, which is used in literature. Therefore, the model, in Figure 9, is designed by using PRODAS database.

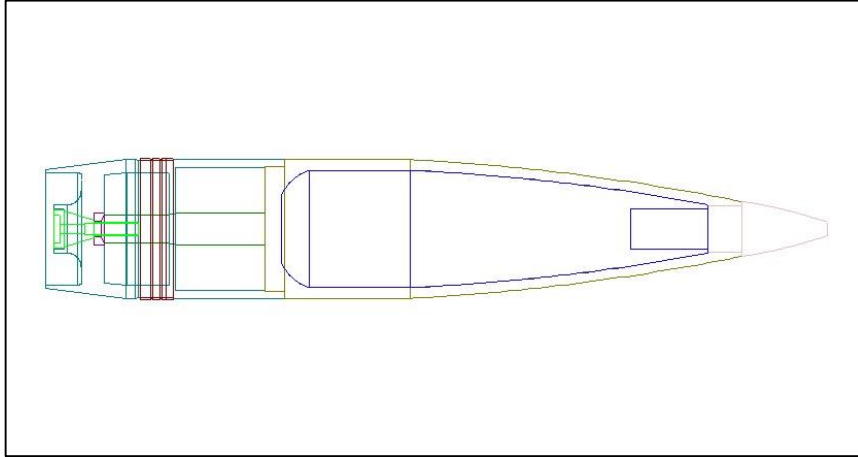


Figure 9. Munition Geometry

2.3 Aerodynamic Prediction

In this section, all aerodynamic force and moment coefficients are computed. The munition encounters these forces and moments when it flies. Aerodynamic analyses are done for standard 155 mm spin stabilized munition. After the geometry is fixed according to literature survey, aerodynamic coefficients are calculated for Mach numbers, between 0.6 and 3, and they are given in Table 2 [11].

Table 2. Aerodynamic Coefficients

Mach	C_{x0}	C_{x2}	C_{x4}	C_{Na}	C_{Na3}	C_{Ypa}	C_{Ma}	C_{Ma3}	C_{Ma5}	C_{Mq}	C_{Mq2}	C_{lp}	C_{ld}	C_{xf}	C_{PN}
0.6	0.12	5	0	1.5	10	-1	4.21	-1.3	0	-11	0	-0.027	0	0.08	0.57
0.7	0.12	5	0	1.5	10	-1	4.23	-1.3	0	-11	0	-0.027	0	0.08	0.5
0.75	0.12	5	0	1.5	10	-1	4.3	-1.3	0	-14	0	-0.027	0	0.08	0.46
0.8	0.12	5.5	0	1.5	10	-1	4.4	-1.3	0	-15	0	-0.027	0	0.08	0.43
0.85	0.13	5.7	0	1.55	10	-1	4.51	-2	0	-15	0	-0.027	0	0.09	0.13
0.88	0.13	5.85	0	1.6	10	-1	4.62	-2.5	0	-15	0	-0.027	0	0.09	0
0.9	0.14	6	0	1.65	10	-1.1	4.77	-3	0	-15	0	-0.027	0	0.09	-0.2
0.93	0.16	6.2	0	1.7	10	-1.2	4.99	-3	0	-16	0	-0.027	0	0.11	0.12
0.95	0.19	6.7	0	1.75	10	-1.4	5.2	-3	0	-16	0	-0.027	0	0.13	0.36
0.98	0.24	7	0	1.8	10	-1.3	4.8	-3	0	-18	0	-0.027	0	0.17	0.69
1	0.29	7.2	0	1.85	10	-1.2	4.25	-3	0	-22	0	-0.027	0	0.21	0.99
1.03	0.31	6.9	0	1.9	10	-1.2	4.23	-2	0	-23	0	-0.0265	0	0.22	1.12
1.05	0.33	6	0	1.95	10	-1.1	4.2	-2	0	-24	0	-0.026	0	0.23	1.23
1.1	0.33	5.5	0	2	10	-1.1	4.19	-1	0	-25	0	-0.026	0	0.23	1.3
1.2	0.32	5.3	0	2.1	10	-1	4.19	-1	0	-26	0	-0.026	0	0.23	1.4
1.35	0.31	5.1	0	2.23	10	-1	4.18	0	0	-27	0	-0.026	0	0.22	1.46
1.5	0.3	5	0	2.35	10	-1	4.17	0	0	-27	0	-0.025	0	0.21	1.51
1.75	0.28	4.8	0	2.48	10	-1	4.15	0	0	-28	0	-0.025	0	0.2	1.73
2	0.26	4.6	0	2.6	10	-1	4.13	0	0	-28	0	-0.024	0	0.18	1.92
2.25	0.24	4.4	0	2.68	10	-1	4.11	0	0	-28	0	-0.023	0	0.17	2.04
2.5	0.22	4.2	0	2.75	10	-1	4.09	0	0	-28	0	-0.023	0	0.16	2.15
3	0.2	4	0	2.75	10	-1	4.09	0	0	-28	0	-0.023	0	0.14	2.27

C_X is axial force coefficient similar to drag coefficient. The coefficient is positive in nose direction but axial force is negative according to nose of munition direction. C_N is normal force coefficient. C_{YPA} is Magnus force coefficient and it is always negative naturally. C_{MA} is pitching moment coefficient, which tends to separate the nose and velocity vector, so this coefficient should be small quantity. C_{MQ} is pitch damping moment coefficient and it is the most critic coefficient because it affects stability of the munition. It tries to coincide the nose and velocity vector so it must be negative. C_{LP} is spin damping moment and it is also should be negative. The last one is C_{PN} which is Magnus moment coefficient. Aerodynamic coefficients are nondimensional and they are nonlinearly related to velocity of munition. All coefficients are also discussed and described in 3.2.

2.4 Stability Evaluation

After creating geometry and calculation of aerodynamic parameters, munition stability should be evaluated because the munition follows its trajectory along the

flight only if the munition is stable. Some parameters, which are muzzle velocity, spin velocity and altitude, are needed to evaluate stability of the munition. Stability of the munition is determined according to its gyroscopic stability factor and dynamic stability factor.

Gyroscopic stability governs how a bullet flies and whether it remains pointing forward in early flight. Gyroscopic stability is a response to aerodynamic forces, which are change the trajectory, to align the projectile with its trajectory. This stability is only valid for spin stabilized objects. Gyroscopic stability relates to total angle of attack, which is angle between bullet's axis and movement axis. Total angle of attack is shown in Figure 10. As the spin velocity p decreases more slowly than the velocity V , the gyroscopic stability factor Sg continuously increases. Gyroscopic stability takes a minimum value at the muzzle exist because of the highest velocity. Thus, if a bullet is gyroscopically stable at the muzzle, it will be gyroscopically stable for the rest of its flight. The quantity Sg also depends on the air density and this is the reason, why special attention has to be paid to guarantee gyroscopic stability at extreme cold weather conditions.

Bullet and gun designers usually prefer $Sg > 1$, but it is also possible to introduce excessive stabilization. This is called over-stabilization.

The gyroscopic (also called static) stability factor depends on only one aerodynamic coefficient (the overturning moment coefficient derivative C_{MA}) and thus is much easier to determine than the dynamic stability factor. This may be the reason, why some ballistic publications only consider static stability if it comes to stability considerations.

Gyroscopic stability factor could be written in (2.1) [2].

$$Sg = \frac{2I_x^2 p^2}{\pi \rho I_y d^3 V^2 C_{ma}} \quad (2.1)$$

The gyroscopic stability condition is a necessary condition to guarantee a stable flight. However, both stability conditions, which are gyroscopic and dynamic stability condition, must be fulfilled to guarantee a stable flight [9].

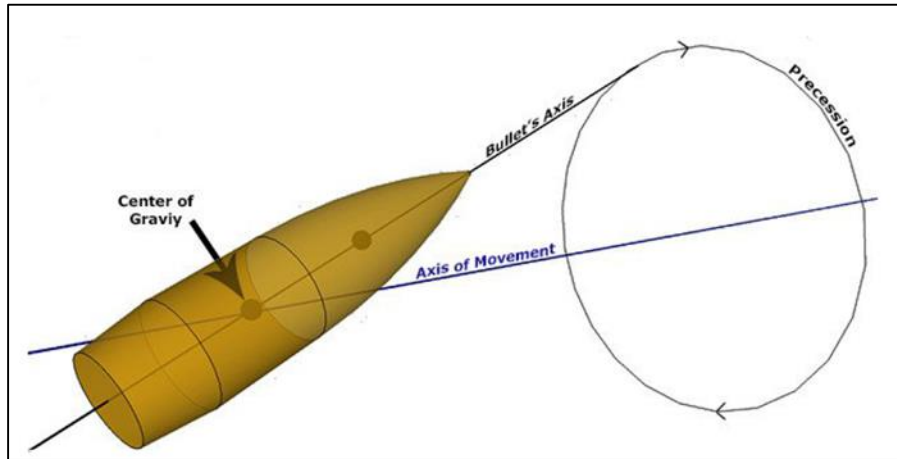


Figure 10. Munition movement

Dynamic stability factor shows whether the munition is stable or not during the flight. This is long term tendency after the munition is disturbed. If the wobbling is not dumped out, the bullet is not dynamically stabilized and beyond being less accurate, the bullet can tumble. Bullet and munition designers should prefer Sd between 0 and 2, otherwise the munition becomes unstable [19].

Dynamic stability factor could be written in (2.2) [2].

$$Sd = \frac{2(C_n - C_{x0}C_{yp})\left(\frac{md^2}{2I_x}\right)}{(C_n - C_{x0} - \left(\frac{md^2}{2I_y}\right)C_{mq} + \left(\frac{md^2}{2I_x}\right)C_{lp}} \quad (2.2)$$

Stability factors could be given in Table 3 during the flight. Dynamic stability changes with munition's angle of attack because some aerodynamic coefficients have a nonlinear behavior so they change with munition's angle of attack.

Table 3. Stability Factors

Mach	Gyroscopic Stability	Dynamic Stability Factor at Angle of attack				
		1	2	5	7.5	10
0.6	1.59	1.41	1.47	1.6	2	2.21
0.7	1.58	1.41	1.48	1.68	2.08	2.28
0.75	1.55	1.18	1.25	1.44	1.78	1.95
0.8	1.52	1.11	1.18	1.38	1.7	1.86
0.85	1.48	1.2	1.26	1.42	1.78	1.96
0.875	1.44	1.25	1.31	1.44	1.82	2.01
0.9	1.4	1.3	1.35	1.46	1.85	2.05
0.925	1.34	1.29	1.35	1.52	1.85	2.02
0.95	1.28	1.27	1.35	1.58	1.85	2
0.975	1.39	1.36	1.39	1.48	1.64	1.73
1	1.57	1.3	1.3	1.28	1.34	1.37
1.025	1.58	1.43	1.38	1.25	1.27	1.29
1.05	1.59	1.54	1.46	1.22	1.21	1.22
1.1	1.59	1.51	1.43	1.19	1.19	1.19
1.2	1.59	1.4	1.34	1.14	1.14	1.14
1.35	1.6	1.33	1.28	1.13	1.13	1.13
1.5	1.6	1.27	1.24	1.12	1.12	1.12
1.75	1.61	1.21	1.19	1.12	1.12	1.12
2	1.62	1.22	1.2	1.13	1.13	1.13
2.25	1.62	1.22	1.2	1.14	1.14	1.14
2.5	1.63	1.23	1.21	1.14	1.14	1.14

2.5 Trajectory Analysis

Trajectory analysis is done with initial conditions by using the program. Before the analysis; geometry is created, aerodynamic coefficients are calculated, stability analysis determined. After the steps are applied respectively, results of trajectory analysis are given in APPENDICES. Solutions could be taken step size whatever you want. Thus, solutions are placed in the APPENDICES for 0.5 sec step size. The results are at APPENDICES are also shown in Figure 11-Figure 18 and they are discussed one by one.

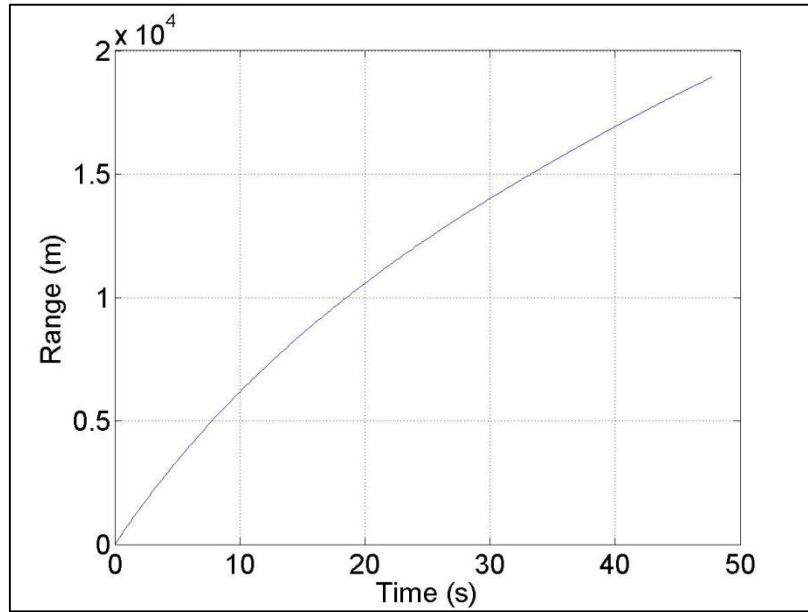


Figure 11. Range vs Time for PRODAS

Figure 11 shows the range of the munition in meter vs time in second along the flight. Range of the munition increases along the flight. The vertical axis of the figure is the range and the horizontal axis is the flight time.

The munition muzzle velocity is 826 m/s and is thrown with 23 degree elevation angle. The flight starts from origin 0 meter and it takes about 18921 m for about 47.7 sec at the end of the flight.

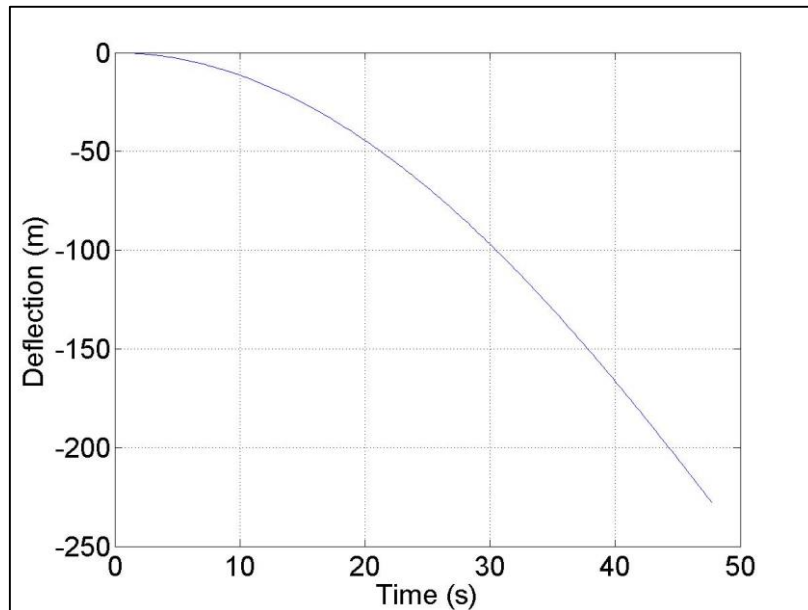


Figure 12. Deflection vs Time for PRODAS

Figure 12 shows the lateral deflection of the munition in meter vs time in second along the flight. The vertical axis of the figure is the lateral deflection, and the horizontal axis is the flight time. Figure 12 is top view of the munition during the flight without any control mechanism.

Lateral deflection of the munition reaches about 227 m to left side while looking munition behind because the munition tends to deflect to left side for spin stabilized munitions with positive spin velocity at the end of the flight. The munition deflects more with time because the munition spin velocity decreases along the flight as seen from Figure 12.

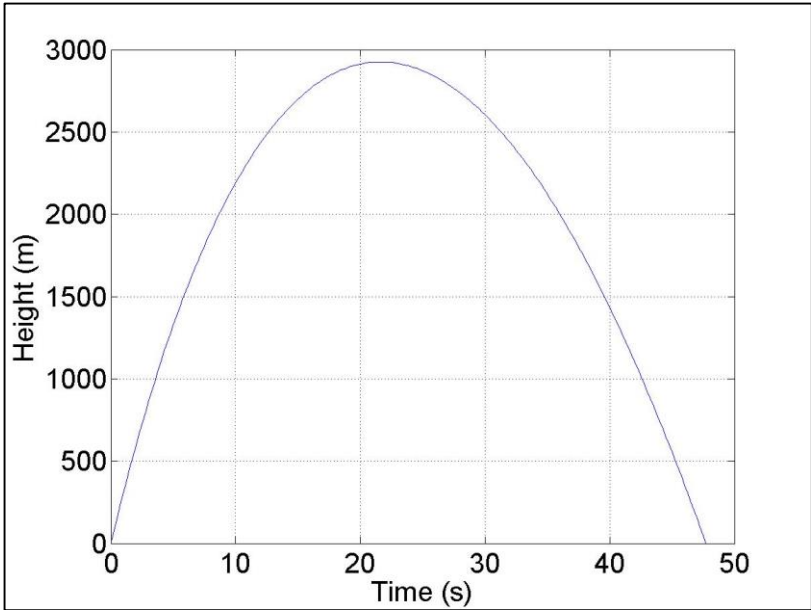


Figure 13. Height vs Time for PRODAS

Figure 13 shows the height of the munition in meter vs time in second though the flight. The vertical axis of the figure is the height of the munition, and the horizontal axis is the flight time. Figure 13 is side view of the munition during the flight without any control mechanism

Figure 13 shows variation height of munition with time. The munition start from ground and it is thrown at 23 elevation angle. Therefore, the munition rises until about 2920 m and then it falls to ground at 47.7 s.

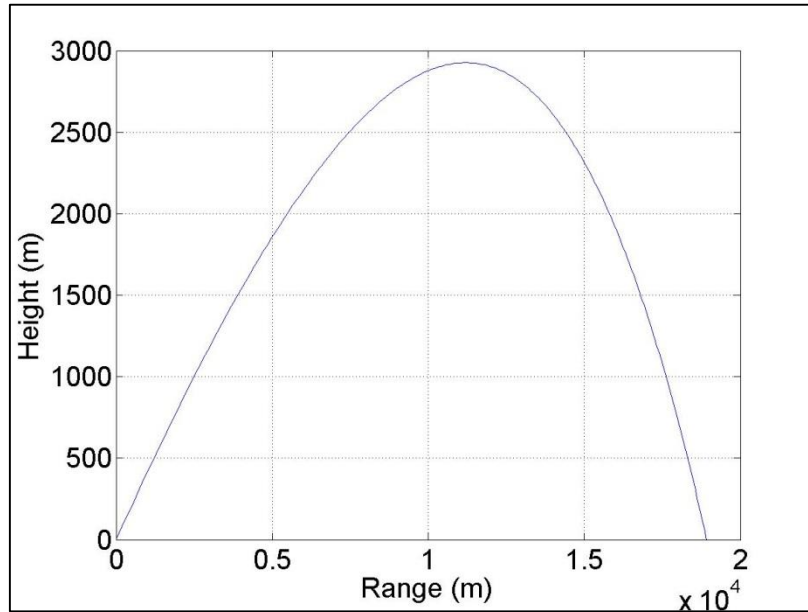


Figure 14. Range vs Height for PRODAS

Figure 14 shows the range of the munition vs the height of the munition in meter though the flight. The vertical axis of the figure is the height and the horizontal axis is the range of the munition. The graph shows side view of the munition during the flight without any control mechanism.

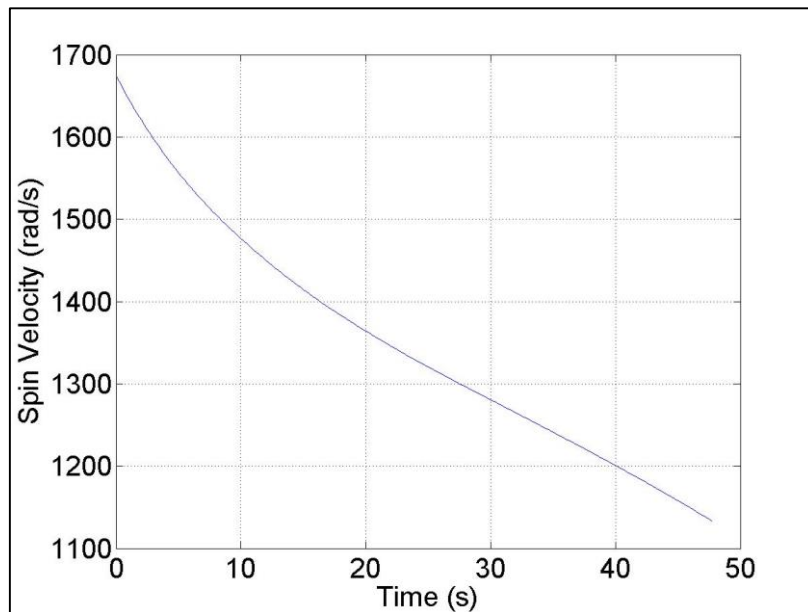


Figure 15. Spin Velocity vs Time for PRODAS

Figure 15 shows spin velocity in radian per second of the munition along the flight. The vertical axis of the figure is spin velocity and the horizontal axis is time in

second. Spin velocity of the munition is the other important parameter. It affects aerodynamic forces and moments on the munition and stability of the munition directly.

It is expected that munition spin velocity decreases with time as seen in Figure 15 because of roll damping moment on the munition. Spin velocity and its manner of munition are very essential for their stability during the flight. If the spin velocity of the munition decreases so much, the munition become unstable so it is not able to reach the target. Thus, spin velocity of the munition must be conserved possibly.

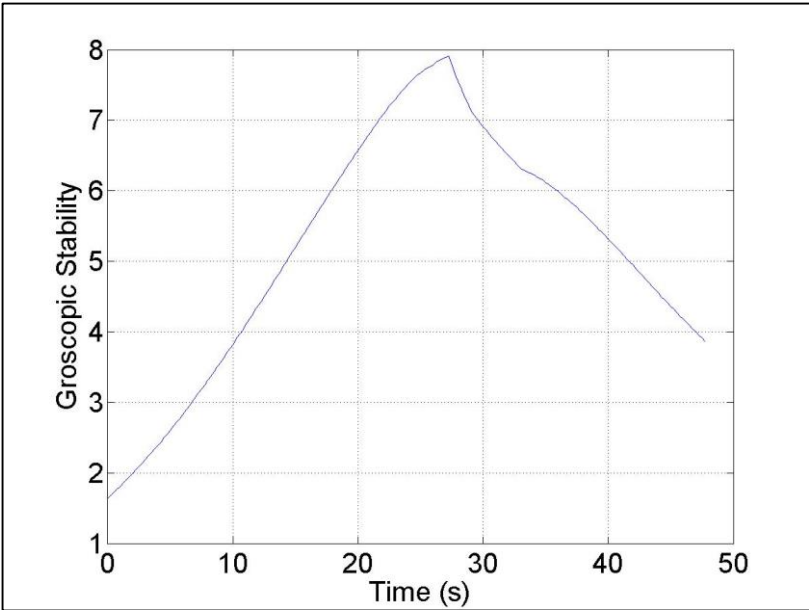


Figure 16. Gyroscopic Stability vs Time for PRODAS

Gyroscopic stability is mentioned in 2.4 must be more than 1 during the flight. Gyroscopic stability, which is in Figure 16, starts from about 1.64 and increases up to middle of flight because velocity of munition decreases until middle of flight and then then increase due to same reason. Thus, the stability condition is satisfied during the flight.

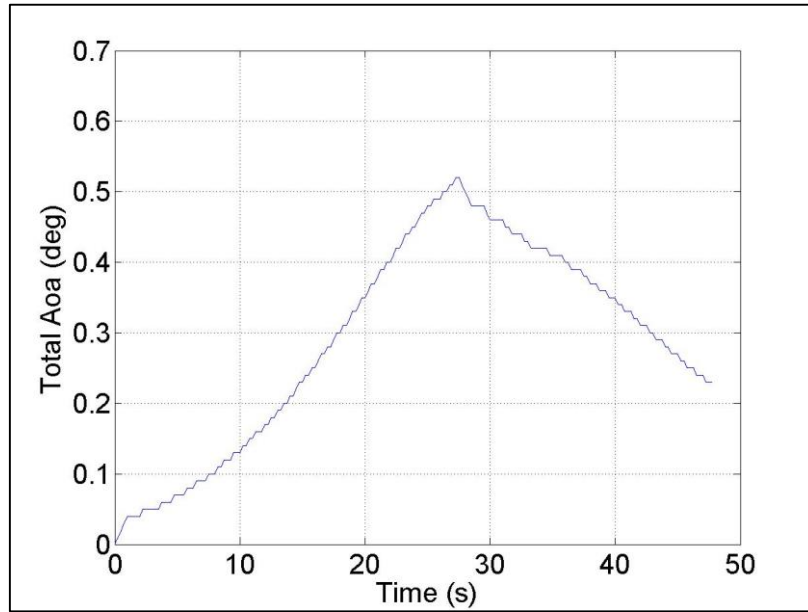


Figure 17. Total Angle of Attack vs Time for PRODAS

Figure 17 indicates the angle between nose axis of munition and velocity vector. It affects to all forces and moments because forces and moments on munition increase with total angle of attack. Thus, total angle of attack should be small not to deflect from the target.

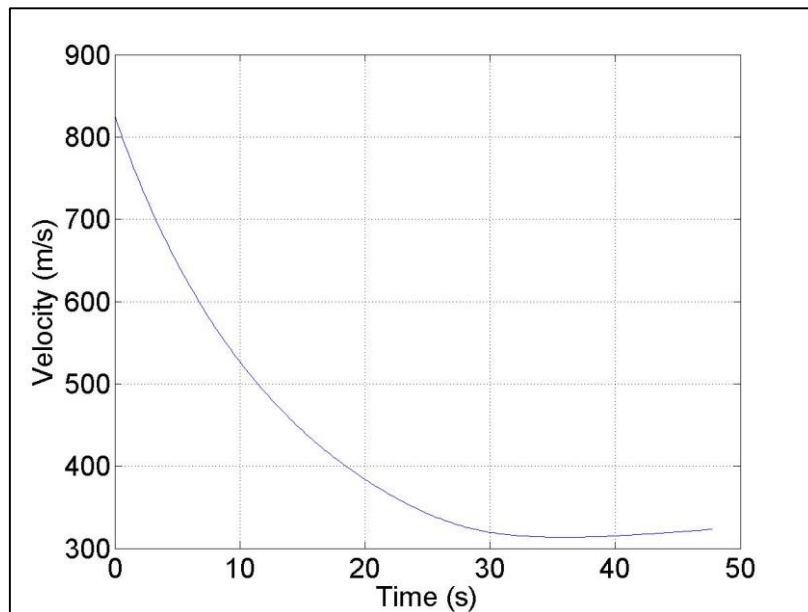


Figure 18. Velocity vs Time for PRODAS

Figure 18 shows the velocity of the munition in meter per second and time in second. The vertical axis of the figure is velocity of the munition, which is from muzzle exist to end of the flight. The horizontal axis is the time.

Velocity decreases exponentially until half of flight due to gravity force. It decreases until about 300 m/s as seen in Figure 18.

CHAPTER 3

BALLISTIC ANALYSES USING DEVELOPED CODE

It is important that dynamic model of spin stabilized munition is created exactly. If the model of munition is designed correctly, flight behavior of the munition is similar both for simulations and real flight. Angle of attack, sideslip angle, Mach number and accurate environmental model are needed to know for successful model. This chapter describes coordinate systems of the munition, aerodynamic forces and moments which are used in model, equations of motion, mathematical model, simulation ballistic database for variable step size, discussion for results and comparison of PRODAS and simulation result.

3.1 Coordinate System

In this section, two main coordinate systems, which are body fixed and earth fixed coordinate systems, will be introduced. These coordinate systems are used for describing munition equations of motion during the flight. The earth fixed coordinate system has its origin at the center of mass of munition and z axis direction is from missile center of gravity to center of the earth. The x and y axes should be chosen as pointing to the North and East directions respectively. The axes of this coordinate system are shown as X_I , Y_I and Z_I . This coordinate system is shown in Figure 19 [20].

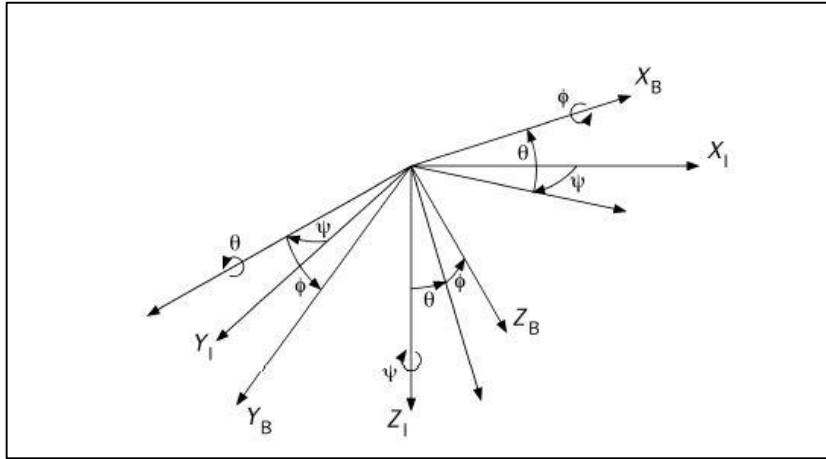


Figure 19. Earth Fixed Coordinate System

The origin of body-fixed coordinate system is at the munition center of mass and coordinate system moves with the body of munition. Its axes are X_B , Y_B , and Z_B . The X_B is direction of nose of munition and the other axes are chosen according to right hand rule. This system is also illustrated in Figure 20 [20].

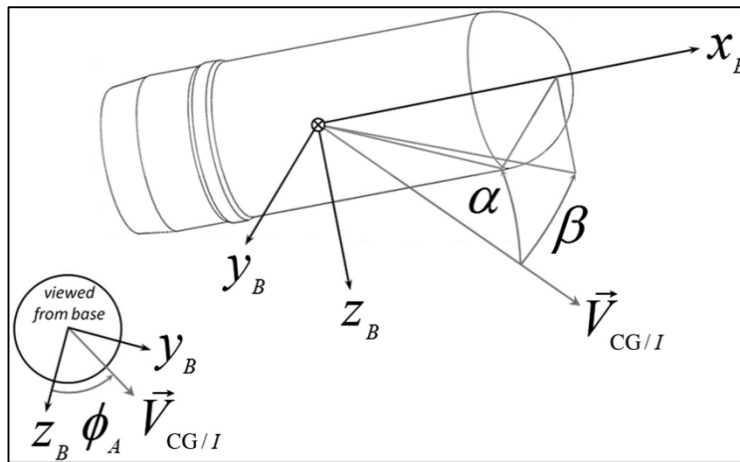


Figure 20. Body Fixed Coordinate System

Direction cosine matrix (DCM) is relation between earth fixed and body fixed coordinate systems. In analytic geometry, the DCM (or directional cosines) of a vector are the cosines of the angles between these vectors and their coordinate axes. Similarly, they are the contributions of each component of the basis to a unit vector in that direction. Parameters could be transferred from one coordinate system to another with direction cosine matrix. The yaw, pitch, roll sequence is commonly used to obtain direction cosine matrix. This sequence has Euler angles which are yaw

(ψ), pitch (Θ) and roll (Φ). All trigonometric functions are denoted with c (cos) and s (sin) notations to simplify the equations [20].

Direction cosine matrix could be obtained like (3.1).

$$T_{\psi\theta\phi} = T_{\phi}T_{\theta}T_{\psi} \quad (3.1)$$

$$T_{\psi} = \begin{bmatrix} c\psi & s\psi & 0 \\ -s\psi & c\psi & 0 \\ 0 & 0 & 1 \end{bmatrix} \quad (3.2)$$

$$T_{\theta} = \begin{bmatrix} c\theta & 0 & -s\theta \\ 0 & 1 & 0 \\ s\theta & 0 & c\theta \end{bmatrix} \quad (3.3)$$

$$T_{\phi} = \begin{bmatrix} 1 & 0 & 0 \\ 0 & c\phi & s\phi \\ 0 & -s\phi & c\phi \end{bmatrix} \quad (3.4)$$

DCM could be obtained by the yaw, pitch, roll (321) sequence as follows in (3.5).

$$T_{\psi\theta\phi} = T_{\phi}T_{\theta}T_{\psi} = \begin{bmatrix} c\theta c\psi & c\theta s\psi & -s\theta \\ s\phi s\theta c\psi - s\psi c\phi & s\phi s\theta s\psi + c\psi c\phi & c\theta s\phi \\ c\phi s\theta c\psi + s\psi s\phi & c\phi s\theta s\psi - c\psi s\phi & c\phi c\theta \end{bmatrix} \quad (3.5)$$

3.2 Aerodynamic Coefficients

Aerodynamic forces are exerted on a surface of body by the air or some other gas where the body is immersed, and is due to the relative motion between the body and the gas. Aerodynamic force arises due to two causes which are the pressure differences between surfaces of body where the air affect and the viscosity of the gas, also known as skin friction [21].

The aerodynamic forces and moments, with the gravity force, are the leading functions to the dynamic equations of motion. Moreover, mechanism forces are discussed in this chapter as well.

In aircraft aerodynamic, sideslip angle and angle of attack are defined separately according to directions of velocity vector and nose vector. However, total angle of attack is used to define combination of sideslip angle and angle of attack in modern exterior ballistic. This section explains that aerodynamic force and moment definitions and their physical meanings.

Figure 21 and Figure 22 show how aerodynamic forces and moments act on the spinning body [22].

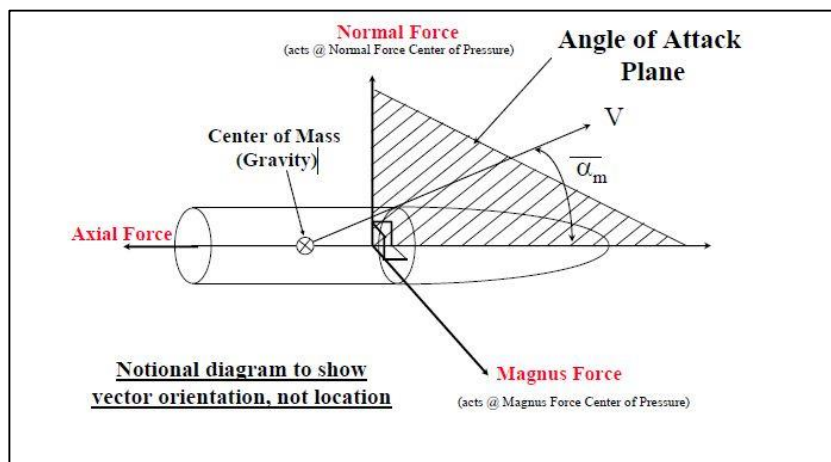


Figure 21. Aerodynamic Forces on Munition [22]

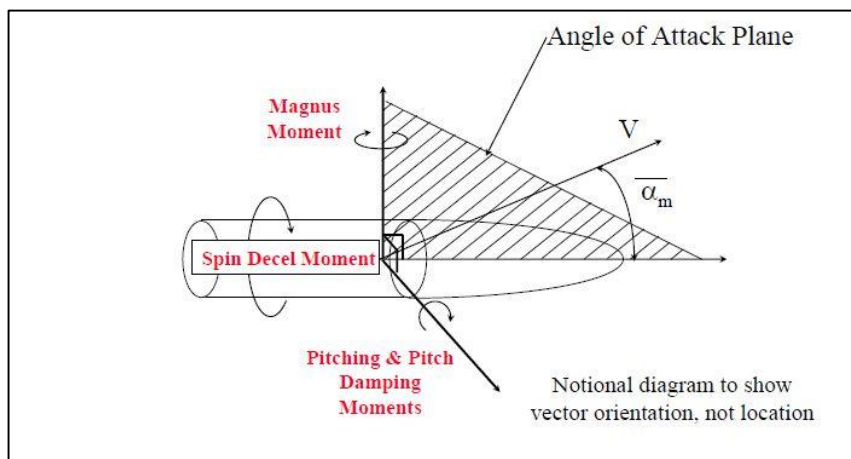


Figure 22. Aerodynamic Moments on Munition [22]

Axial, Magnus and normal forces act on center of pressure of munition. Thus, there are also moments of these forces on center of gravity point. Because it is thought that all forces and moments act on center of gravity in mathematical model of munition. When the forces, which act on center of pressure, are transferred to center of gravity, the forces are taken with their moments according to differences between center of gravity and pressure. Spin deceleration moment, pitching moment and Magnus moments act on center of gravity location. Total angle of attack is defined as $\overline{\alpha}_m$ which is combination of angle of attack and sideslip angle. This angle is defined according to velocity and nose vectors of the munition, which are shown with \vec{i} and \vec{x} respectively.

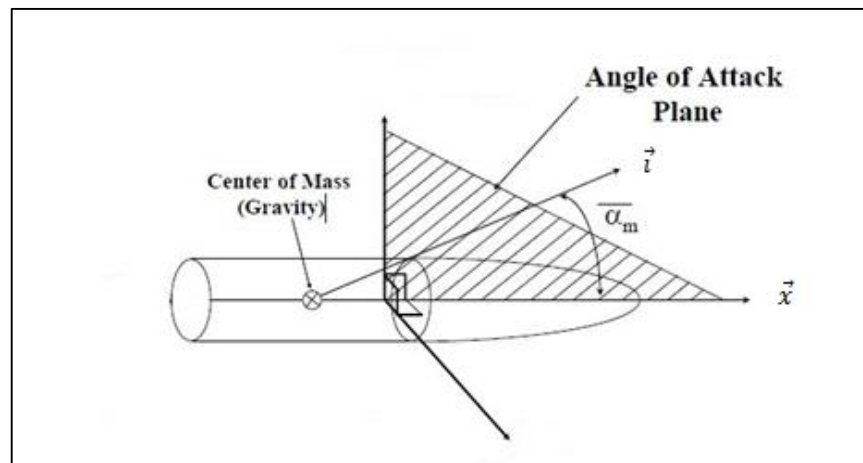


Figure 23. Total Angle of Attack Plane of the Munition

Moreover Magnus force, pitch damping force and Magnus cross force can be neglected because their quantities are too small to affect the munition [2].

3.2.1 Drag Force

The drag force is known as air resistance force. Its direction is opposite of velocity vector. In other words, drag force is force in inverse direction according to motion direction. It is related to air density, velocity, surface of body and drag coefficient varies with shape of body. Therefore, drag force is given by

$$\vec{F}_D = -\frac{1}{2}\rho V^2 S C_D \vec{i} \quad (3.6)$$

$$S = \frac{\pi d^2}{4} \quad (3.7)$$

$$q_\infty = \frac{1}{2} \rho V_w^2 \quad (3.8)$$

q_∞ is dynamic pressure, which could be used in sources. Dynamic pressure is the kinetic energy per unit volume of air. Dynamic pressure is in fact one of the terms of Bernoulli's equation. Bernoulli's equation could be derived from the conservation of energy for a fluid in motion. Similarly, the dynamic pressure is equal to the difference between the stagnation pressure and the static pressure [23].

The reference diameter is usually taken at the end of ogive nose section for spin stabilized munitions. The ogive is the tapered section of the munition. The reference diameter is almost the widest section of munitions.

Drag coefficient has a nonlinear behavior and the effect of the total angle of attack on drag coefficient is varying with total angle of attack [2]. For this reason, the expression for the Magnus moment arm is given experimentally as a Taylor series expansion with order according to the Maple–Synge hypothesis for symmetry of munition [24]. Thus,

$$C_D = C_{D_0} + C_{D\alpha^2} \delta^2 \quad (3.9)$$

$$\delta = \sin \alpha_M = \sqrt{\left(\frac{\sin \alpha}{\cos \beta}\right)^2 + (\sin \beta)^2} \quad (3.10)$$

δ is $\sin(\alpha_M)$.

3.2.2 Lift Force

The positive lift force tries to pull the munition to upward direction perpendicular to trajectory when the nose of munition is above velocity vector. Objects can fly by using the lift force. The lift force is given in (3.11).

$$\vec{F}_L = \frac{1}{2} \rho V^2 S C_{L\alpha} [\vec{i} \times (\vec{x} \times \vec{i})] \quad (3.11)$$

If the total angle of attack is zero, nose and velocity vector coincide so cross product of nose and velocity vectors is zero. Therefore, there is no lift force. This situation is because munition is symmetric in the trajectory and munition axis.

Lift force coefficient has a nonlinear behavior [2], [24]. Thus,

$$C_{L\alpha} = C_{L\alpha_0} + C_{L\alpha_2} \delta^2 \quad (3.12)$$

It is simpler that using body axis forces which are normal and axial forces than instead of using velocity axis forces which are lift and drag forces according to exterior ballistic [2].

3.2.3 Axial and Normal Force

An axial force is occurred due to wind effect on munition similar to drag force. The difference of axial force from drag force is direction of force. The positive axial has an opposite direction with nose of munition as shown in Figure 21.

$$\vec{F}_A = -\frac{1}{2} \rho V^2 S C_X \vec{x} \quad (3.13)$$

Axial force coefficient has a nonlinear behavior [2].

$$C_X = C_{X_0} + C_{X\alpha_2} \delta^2 \quad (3.14)$$

The positive normal force has same plane with total angle of attack plane as shown in Figure 21. This force tends to lift munition when the munition flies with

positive angle of attack similar to lift force. However, normal force is separate from lift force according to direction. Normal force is given in (3.15).

$$\vec{F}_N = \frac{1}{2} \rho V^2 S C_N [\vec{x} \times (\vec{i} \times \vec{x})] \quad (3.15)$$

C_N is normal force coefficient. Normal force coefficient has a nonlinear behavior [22].

$$C_N = C_{N\alpha} \delta + C_{N\alpha^3} \delta^3 \quad (3.16)$$

3.2.4 Magnus Force

The Magnus force is generation of a sidewise force on spinning munitions when there is relative motion between the spinning body and the fluid. Magnus force is because of pressure difference of sides of spinning bodies.

If the side of spinning body has the same direction with velocity vector, air velocity flows faster at this side according to other side. The side where air velocity flows faster has a low pressure and Magnus force occurs at this side. It is always perpendicular to total angle of attack plane as shown in Figure 21. However it is small quantity [22].

$$\vec{F}_{Yp} = \frac{1}{2} \rho V^2 S \frac{pd}{V} C_{Yp} (\vec{i} \times \vec{x}) \quad (3.17)$$

The Magnus force is proportional to the product of spin velocity and total angle of attack. If one of spin velocity and total angle of attack is zero, Magnus force vanishes. It could be said that Magnus force occurs only if the object spins. Magnus force coefficient has a nonlinear behavior [22].

$$C_{Yp} = C_{Yp\alpha} \delta + C_{Yp\alpha^3} \delta^3 \quad (3.18)$$

3.2.5 Pitching Moment

Pitching moment occurs at center of gravity because of normal force. However, normal force occurs at center of pressure. When normal force is transferred to center of gravity, normal force is taken with its moment. The pitching moment could be found by production of normal force and difference between center of gravity and center of pressure. It is perpendicular to total angle of attack plane as shown in Figure 22. It tends to increase total angle of attack of the munition [22].

$$\vec{F}_M = \frac{1}{2} \rho V^2 S d C_M (\vec{i} \times \vec{x}) \quad (3.19)$$

Pitching moment coefficient has a nonlinear behavior.

$$C_M = C_{M\alpha} \delta + C_{M\alpha^3} \delta^3 + C_{M\alpha^5} \delta^5 \quad (3.20)$$

3.2.6 Pitch Damping Moment

The most important moment is pitch damping moment because it tries that the nose vector collides with velocity vector to satisfy the stability of munition so it could be called as stability moment. The pitch damping moment acts in total transverse angular velocity plane and the moment must be negative along the flight for stability [22]. Pitch damping moment is perpendicular to total angle of attack plane as shown in Figure 22.

$$\vec{F}_{Mq} = \frac{1}{2} \rho V^2 S d \frac{qd}{V} C_{mq} \quad (3.21)$$

Pitch damping moment coefficient has a nonlinear behavior. So,

$$C_{mq} = C_{mq0} + C_{mq2} \delta^2 + C_{mq4} \delta^4 \quad (3.22)$$

3.2.7 Magnus Moment

The Magnus moment could be large quantity so this moment affects the trajectory dramatically. This moment could be negative or positive. It is cross product of difference between center of gravity and center of pressure and Magnus force [22]. Magnus force is given in (3.23).

$$\vec{F}_{np} = \frac{1}{2} \rho V^2 S d \frac{pd}{V} C_{np} [\vec{x} \times (\vec{i} \times \vec{x})] \quad (3.23)$$

Magnus moment coefficient has a nonlinear behavior.

$$C_{np} = C_{np\alpha} \delta + C_{np\alpha^3} \delta^3 + C_{np\alpha^5} \delta^5 \quad (3.24)$$

Magnus and pitching moment coefficients are taken from PRODAS software in Table 2.

3.2.8 Spin Damping Moment

The spin damping moment is the same direction with spin direction of the munition as shown in Figure 22. It always reduces magnitude of spin of munition so it is a negative quantity [22]. Effects of spin damping moment could be seen at Figure 45 and Figure 55.

$$\vec{F}_{lp} = \frac{1}{2} \rho V^2 S d \frac{pd}{V} C_{lp} \vec{x} \quad (3.25)$$

Spin damping moment coefficient has a nonlinear behavior.

$$C_{lp} = C_{lp0} + C_{lp\alpha^2} \delta^2 \quad (3.26)$$

NACA aeroballistics use $\frac{pd}{2V}$ instead of $\frac{pd}{V}$. However, $\frac{pd}{V}$ is used in developed code at this thesis [2].

3.3 Equations of Motion

In mathematical physics, equations of motion are equations that describe the behavior of a physical system in terms of its motion as a function of time. More specifically, the equations of motion describe the behavior of a physical system as a set of mathematical functions in terms of dynamic variables: normally spatial coordinates and time are used, but others are also possible, such as momentum components and time [25]. The equations of motion of general air vehicle are given [18].

All aerodynamic coefficients are identified at Table 4.

Table 4. Aerodynamic Coefficients Description [22]

Coefficient	Description	Coefficient
C_X	Body Axial Force Coefficient	$C_X = C_{X_0} + C_{X\alpha 2}\delta^2$
C_N	Normal Force Coefficient	$C_N = C_{N_0} + C_{N\alpha 3}\delta^2$
$C_{Yp\alpha}$	Magnus Force Coefficient	$C_{Yp\alpha}$
$C_{N\alpha}$	Normal Force Coefficient for Mechanism Wings	$C_{N\alpha}$
C_M	Pitching Moment Coefficient	$C_M = C_{M_0} + C_{M\alpha 3}\delta^2$
C_{mq}	Pitch Damping Moment Coefficient	C_{mq}
C_{lp}	Roll Damping Coefficient	C_{lp}
$C_{np\alpha}$	Magnus Moment Coefficient	$C_{np\alpha}$

$$\vec{F}_T = m(\dot{\vec{V}}_B + \vec{\omega}_B \times \vec{V}_B) \quad (3.27)$$

$$\text{where } \vec{F}_T = \begin{bmatrix} F_X \\ F_Y \\ F_Z \end{bmatrix}, \dot{\vec{V}}_B = \begin{bmatrix} \dot{u} \\ \dot{v} \\ \dot{w} \end{bmatrix}, \vec{\omega}_B = \begin{bmatrix} p \\ q \\ r \end{bmatrix}, \vec{V}_B = \begin{bmatrix} u \\ v \\ w \end{bmatrix},$$

$$\vec{M}_T = I_B \dot{\vec{\omega}}_B + \vec{\omega}_B \times (I_B \vec{\omega}_B) \quad (3.28)$$

$$\text{where } \vec{M}_T = \begin{bmatrix} L \\ M \\ N \end{bmatrix}, I_B = \begin{bmatrix} I_x & 0 & 0 \\ 0 & I_y & 0 \\ 0 & 0 & I_z \end{bmatrix} \text{ by assuming } I_{xy} = I_{xz} = I_{yz} = 0.$$

Equations of motion for spin stabilized munition are similar to general air vehicle. Moreover, high spin velocity of the munition affects the munition dramatically. Thus, equations of motion are written as,

$$F_1 = m(\dot{u} - rv + qw) \quad (3.29)$$

$$F_2 = m(\dot{v} - pw + ru) \quad (3.30)$$

$$F_3 = m(\dot{w} - qu + pv) \quad (3.31)$$

$\vec{F}_T = \begin{bmatrix} F_1 \\ F_2 \\ F_3 \end{bmatrix}$, which is total force, is defined.

Total force on the munition could also be written like as;

$$\vec{F}_T = \vec{F}_A + \vec{F}_M + \vec{W} + \vec{F}_C \quad (3.32)$$

Relationships between angular velocities and moments on the munition are derived in (3.33), (3.34) and (3.35).

$$\vec{M}_1 = I_x \dot{p} - (I_y - I_z)qr \quad (3.33)$$

$$\vec{M}_2 = I_y \dot{q} - (I_z - I_x)pr \quad (3.34)$$

$$\vec{M}_3 = I_z \dot{r} - (I_x - I_y)pq \quad (3.35)$$

where $\vec{M}_T = \begin{bmatrix} M_1 \\ M_2 \\ M_3 \end{bmatrix}$.

Total moment could be written as in (3.36).

$$\overline{M}_T = \overline{M}_{SA} + \overline{M}_{UA} + \overline{M}_M + \overline{M}_C + \overline{M}_{cgoffset} \quad (3.36)$$

All forces and moments, which are used in the munition equations of motion, are introduced. Aerodynamic forces and moments are already calculated at 3.2.

$$\overline{F}_A = q_\infty S [C_X \vec{x} + C_N [\vec{x} \times (\vec{i} \times \vec{x})]] \quad (3.37)$$

$$\overline{F}_M = q_\infty S \left[\frac{pd}{V} C_{Yp} (\vec{i} \times \vec{x}) \right] \quad (3.38)$$

$$\overline{F}_C = q_\infty S \begin{bmatrix} 0 \\ C_{N\alpha} \cos \phi_{mechanism} \\ C_{N\alpha} \sin \phi_{mechanism} \end{bmatrix} \quad (3.39)$$

The use of the transformation matrix is required to transfer weight to body fixed frame since the weight is known in the earth fixed frame.

$$\overline{W} = T_{\psi\theta\phi} \begin{bmatrix} 0 \\ 0 \\ mg \end{bmatrix} \quad (3.40)$$

$$\overline{M}_A = q_\infty S d \left[C_M (\vec{i} \times \vec{x}) + \frac{qd}{V} C_{mq} + \frac{pd}{V} C_{ip} \vec{x} \right] \quad (3.41)$$

$$\overline{M}_M = q_\infty S d \left[\frac{pd}{V} C_{np} [\vec{x} \times (\vec{i} \times \vec{x})] \right] \quad (3.42)$$

$$\overline{M}_C = q_\infty S d \begin{bmatrix} 0 \\ -\overline{F}_C(3,1)(cg - cp_{can}) \\ \overline{F}_C(2,1)(cg - cp_{can}) \end{bmatrix} \quad (3.43)$$

$$\overrightarrow{M}_{cgoffset} = q_{\infty} S \begin{bmatrix} C_{N\alpha} s \alpha c g_{offset} \\ C_X c \phi c g_{offset} \\ -C_X s \phi c g_{offset} \end{bmatrix} \quad (3.44)$$

However for all applications, the moment due to cg offset is assumed zero [1]. Some sources introduce the forces and moments distinctly. The difference often occurs due to different notation of scholars. The forces and moments in other sources are given in APPENDICES.

Thus, total force and moment on the munition can be found [15].

$$\begin{aligned} \overrightarrow{F}_T &= \begin{bmatrix} F_1 \\ F_2 \\ F_3 \end{bmatrix} \\ &= q_{\infty} S \left[C_X \vec{x} + C_N [\vec{x} \times (\vec{i} \times \vec{x})] + \frac{pd}{V} C_{Yp} (\vec{i} \times \vec{x}) \right] \\ &+ q_{\infty} S \begin{bmatrix} 0 \\ C_{N\alpha} \cos \phi_{mechanism} \\ C_{N\alpha} \sin \phi_{mechanism} \end{bmatrix} + T_{\psi\theta\phi} \begin{bmatrix} 0 \\ 0 \\ mg \end{bmatrix} \end{aligned} \quad (3.45)$$

$$\begin{aligned} \overrightarrow{M}_T &= \begin{bmatrix} M_1 \\ M_2 \\ M_3 \end{bmatrix} \\ &= q_{\infty} S d \left[C_M (\vec{i} \times \vec{x}) + \frac{qd}{V} C_{mq} + \frac{pd}{V} C_{lp} \vec{x} + \frac{pd}{V} C_{np} [\vec{x} \times (\vec{i} \times \vec{x})] \right] \\ &+ q_{\infty} S d \begin{bmatrix} 0 \\ -\overrightarrow{F}_c(3,1)(cg - cp_{can}) \\ \overrightarrow{F}_c(2,1)(cg - cp_{can}) \end{bmatrix} \end{aligned} \quad (3.46)$$

3.4 Model of the Munition

This section will explain that how the forces and moments affect behavior of the munition. Three translational and angular motions are described in (3.47) [18].

$$\begin{bmatrix} \dot{V}_{i1} \\ \dot{V}_{i2} \\ \dot{V}_{i3} \\ \dot{h}_1 \\ \dot{h}_2 \\ \dot{h}_3 \end{bmatrix} = \begin{bmatrix} \frac{F_1}{m} + h_3 V_2 - h_2 V_3 \\ \frac{F_2}{m} + h_1 V_3 - h_3 V_1 \\ \frac{F_3}{m} + h_2 V_1 - h_1 V_2 \\ \frac{M_1}{I_x} + \frac{(I_y - I_z)h_2 h_3}{I_x} \\ \frac{M_2}{I_y} + \frac{(I_z - I_x)h_1 h_3}{I_y} \\ \frac{M_3}{I_z} + \frac{(I_x - I_y)h_1 h_2}{I_z} \end{bmatrix} \quad (3.47)$$

The Earth's rotation is ignored due to small effect. Aerodynamic forces, which are F_1 , F_2 , F_3 , and aerodynamic moments, which are M_1 , M_2 , M_3 , were introduced in 3.3. There is relation between rate of Euler angles and body fixed angular velocity [2] [18] [1].

$$\begin{bmatrix} p \\ q \\ r \end{bmatrix} = \begin{bmatrix} \dot{\phi} \\ \dot{\theta} \\ \dot{\psi} \end{bmatrix} \quad (3.48)$$

Angular velocities of munition and rate of Euler angles are not on the same axis except rate of roll angle and roll velocity [6]. It is essential to know that this is not a transformation matrix because transformation matrix transforms one coordinate system to another. It is only relation between two systems.

$$\begin{bmatrix} p \\ q \\ r \end{bmatrix} = \begin{bmatrix} \dot{\phi} \\ \dot{\theta} \\ \dot{\psi} \end{bmatrix} \quad (3.49)$$

$$\begin{bmatrix} p \\ q \\ r \end{bmatrix} = \begin{bmatrix} \dot{\phi} \\ 0 \\ 0 \end{bmatrix} + T_\phi \begin{bmatrix} 0 \\ \dot{\theta} \\ 0 \end{bmatrix} + T_\phi T_\theta \begin{bmatrix} 0 \\ 0 \\ \dot{\psi} \end{bmatrix} \quad (3.50)$$

Thus,

$$\begin{bmatrix} p \\ q \\ r \end{bmatrix} = \begin{bmatrix} 1 & 0 & s\theta \\ 0 & c\phi & c\theta s\phi \\ 0 & -s\phi & c\theta c\psi \end{bmatrix} \begin{bmatrix} \dot{\phi} \\ \dot{\theta} \\ \dot{\psi} \end{bmatrix} \quad (3.51)$$

Rate of Euler angles could be found by inverse of the matrix in equation (3.51).

$$\begin{bmatrix} \dot{\phi} \\ \dot{\theta} \\ \dot{\psi} \end{bmatrix} = \begin{bmatrix} 1 & -s\phi t\theta & -c\phi t\theta \\ 0 & c\phi & -s\phi \\ 0 & \frac{s\phi}{c\theta} & \frac{\phi}{c\theta} \end{bmatrix} \begin{bmatrix} p \\ q \\ r \end{bmatrix} \quad (3.52)$$

The rate of position states of munition is transferred from velocities of munition in body fixed frame by using transformation matrix, which is given in 3.1 [6].

$$\begin{bmatrix} \dot{x} \\ \dot{y} \\ \dot{z} \end{bmatrix} = [T_\phi T_\theta T_\psi]^{-1} \begin{bmatrix} u \\ v \\ w \end{bmatrix} \quad (3.53)$$

$$\begin{bmatrix} \dot{x} \\ \dot{y} \\ \dot{z} \end{bmatrix} = \begin{bmatrix} c\theta c\psi & s\phi s\theta c\psi - s\psi c\phi & c\phi s\theta c\psi + s\psi s\phi \\ c\theta s\psi & s\phi s\theta s\psi + c\psi c\phi & c\phi s\theta s\psi - c\psi s\phi \\ -s\theta & c\theta s\phi & c\phi c\theta \end{bmatrix} \begin{bmatrix} u \\ v \\ w \end{bmatrix} \quad (3.54)$$

Therefore, all state variables are defined in equations (3.47), (3.52) and (3.54). After all forces, moments and equations are defined, ballistic flight could be simulated by using model of munition. However, aerodynamic forces and moments are calculated by using total angle of attack which is angle between munition nose vector and velocity unit vector. Initial conditions and physical properties of the munition are given in Table 5.

Table 5. Initial Conditions for Ballistic Flight

Name	Symbols	Quantity
Diameter of the Munition	d	0.1547 m
Mass	m	41 kg
Axial Moment of Inertia	I _{xx}	0.142 kg.m ²
Transverse Moment of Inertia	I _{yy} , I _{zz}	1.82 kg.m ²
Roll Rate	p	1669 rad/s
Pitch Rate	q	0 rad/s
Yaw Rate	r	0 rad/s
Roll	phi	0 degree
Pitch	theta	23 degree
Yaw	psi	0 degree
Nose Velocity	u	826 m/s
Transverse Velocity	v	0 m/s
Transverse Velocity	w	0 m/s

$$\begin{bmatrix} x_1 \\ x_2 \\ x_3 \end{bmatrix} = \begin{bmatrix} \cos(\theta) \cos(\psi) \\ \sin(\theta) \cos(\psi) \\ \sin(\psi) \end{bmatrix} \quad (3.55)$$

That it is known elevation and yaw angle of muzzle at initial help to determine nose vector of munition [2]. Angular and linear velocities of the munition are calculated by using roll velocity and muzzle velocity of munition at initial condition [2]. Angular velocity of munition is given in (3.56).

$$\begin{bmatrix} h_1 \\ h_2 \\ h_3 \end{bmatrix} = \begin{bmatrix} \frac{I_x}{I_y} p x_1 \\ \frac{I_x}{I_y} p x_2 \\ \frac{I_x}{I_y} p x_3 \end{bmatrix} \quad (3.56)$$

Moreover, linear velocity is given in (3.57).

$$\begin{bmatrix} V_1 \\ V_2 \\ V_3 \end{bmatrix} = u \begin{bmatrix} \cos(\Theta) \cos(\psi) \\ \sin(\Theta) \cos(\psi) \\ \sin(\psi) \end{bmatrix} \quad (3.57)$$

On the other hand, unit velocity vector could be found as (3.58).

$$\vec{i} = \frac{\vec{V}}{|\vec{V}|} \quad (3.58)$$

The other and most critical parameter is delta for spin stabilized munition. It is sinus of total angle of attack and it could be found by taking cross product of nose vector and velocity vector of munition [2]. Total angle of attack could be found as (3.60).

$$delta = \vec{i} \times \vec{x} \quad (3.59)$$

$$Total\ aoa = \sin^{-1} delta \quad (3.60)$$

The positions states of the munition are obtained from velocities of munition by using linear velocities are given in (3.47) [6].

$$\begin{bmatrix} x_1 \\ x_2 \\ x_3 \end{bmatrix} = \begin{bmatrix} x_{10} \\ x_{20} \\ x_{30} \end{bmatrix} + step\ time \begin{bmatrix} V_1 \\ V_2 \\ V_3 \end{bmatrix} \quad (3.61)$$

X, y and z directions imply range of the munition, height of the munition and lateral deflection respectively. Aerodynamic forces and moments are determined by using aerodynamic coefficients, where these coefficients are calculated by PRODAS software and given with Table 2, and all state variables are completed. Therefore, a developed code can be obtained and ballistic flight simulations can be performed

using the developed code and the given initial conditions. The developed code results are given and discussed in Chapter 5.

CHAPTER 4

THE NOSE ACTUATION KIT

4.1 Kit Design

The first purpose of engineering design is to apply scientific knowledge and physical solutions to technical problems of mankind. While engineers and scientists provide a technical solution, it is very essential to understand that their design implies a solution. In other words, designers are too involved to ensure that the end product is economical, effective and appeals to users [26].

Munitions, which could be given as an example for mankind objects, are designed by engineers for defense industry. Countries need to threat the other countries with something, which is a weapon, in history. Munitions are created for this aim. They could be in different sizes and material, but their aim remains unchanged basically. While the vision may differ, there is an engineering design component in a munition that makes it effective [26].

4.1.1 Design of the Nose Actuation Kit

Before engineers start to design, some parameters should be certain. These parameters could be packaging or geometrical limits, technologic limits, production limits, velocity and torque orders. The parameters of kit are not certain so kit design is draft format. However, the mechanism is created according to feasible standard elements. This feasible design help to exhibit the mechanism after the parameters are certain.

155 mm spin stabilized munition is chosen to assemble the nose actuation kit because of some reasons. One of the reasons is that large amount of 155 mm munition are commonly used all over the world. The other reason is that the munition has the largest size compared to other spin stabilized munitions. Especially in Turkey, there are a lot of vehicles like tanks and gunners to use 155 mm munition.

155 mm artillery round designed for a long range, indirect fire top attack role against armored vehicles. The shell contains two sub munitions, which decrease over the battlefield on ballets and attack hardened, large targets with explosively formed penetrator warheads. Built with multiple redundant self-destruct mechanisms, these sub munitions were specifically designed to fall outside the category of sub munition weapons prohibited in 2008 [16].

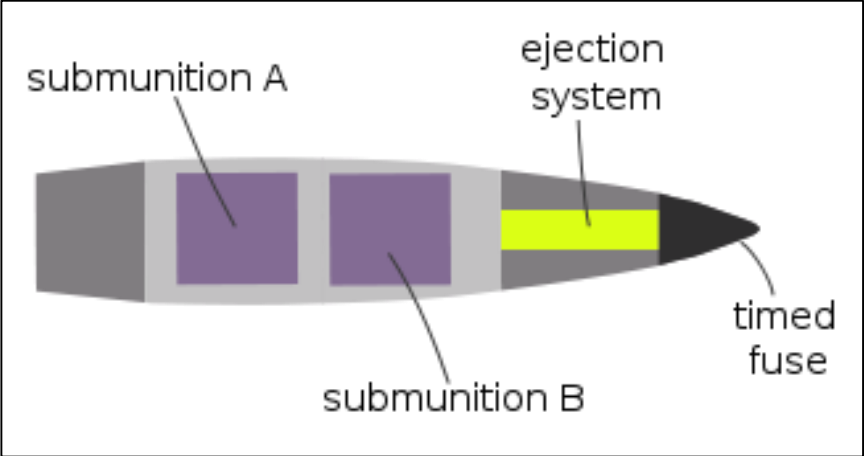


Figure 24. Standard 155 mm Munition [16]

Figure 24 shows standard 155 mm spin stabilized munition, which is used to assemble the mechanism. The nose actuation kit uses time fused section so the mechanism should include the fuse of munition but this thesis does not include fuse design and location selection. The fuse of munition could be placed back of the Kit close to center of gravity.

There is a limited space for the time fuse section in the munition. The mechanism should be also small and does not need a large space because of space limitation.

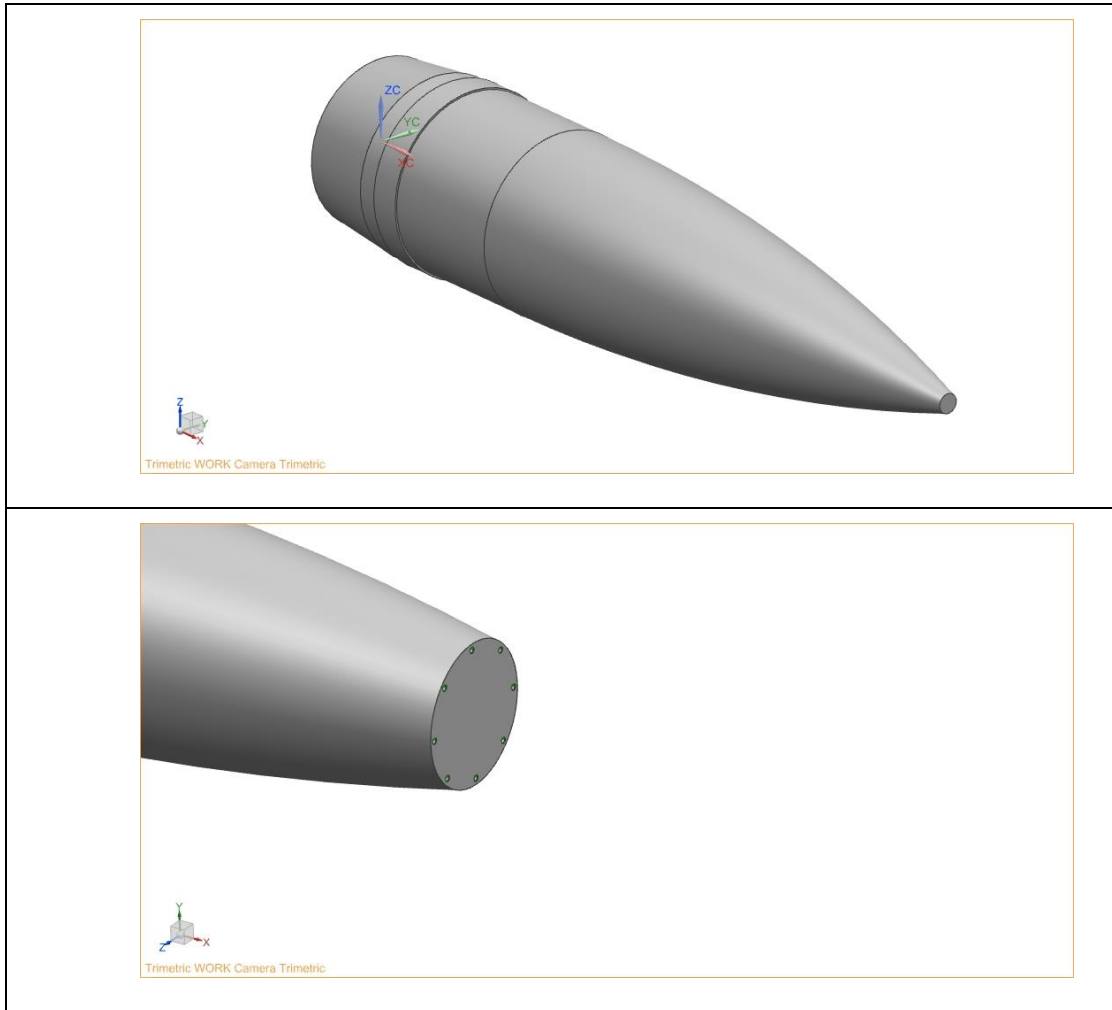


Figure 25. Designed 155 mm Munition

Munition should be cut to place the mechanism in front of the munition. Figure 25 shows 155 mm spin stabilized munition after cutting nose part of the munition. Mechanism wings are designed according to force, which is needed to control the munition, and stability criteria, which is discussed in 2.4. Motor and bearings are selected to torque and the munition's spin velocity requirements. The last component is power supply and it is selected according to current needed of motor. The summation of components volume gives necessary volume to cut from nose of the munition. Moreover, threaded holes are opened to assemble the mechanism to the munition body.

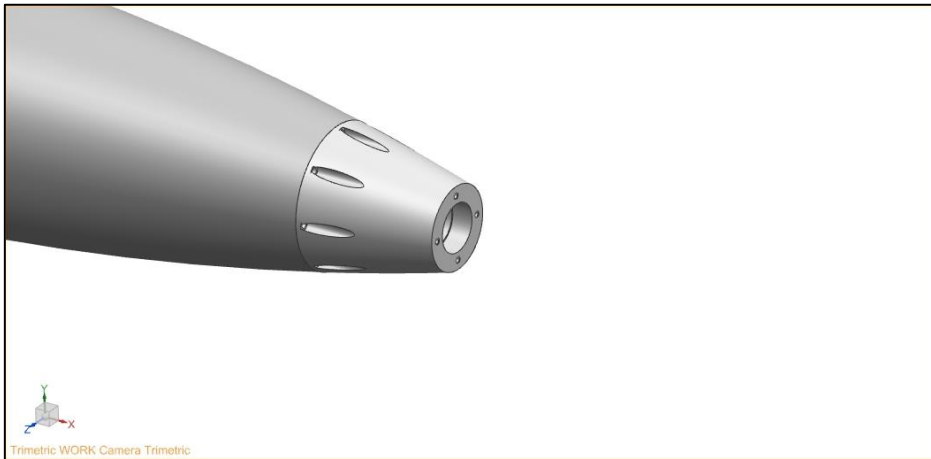


Figure 26. Designed 155 mm Munition with Case

Case of munition is rigid to the munition body and it includes the power supply of motor, motor, bearings. Shield of motor and power supply fasten to the munition body so these components spin with the munition body.

Mechanism motor should be chosen according to torque and velocity requirements of system. After the calculation of minimum torque requirement of mechanism, motor could be chosen. It should be better to take standard motor instead of custom design motor because if the selected motor is custom design, the price of motor increases dramatically. Bearings must be chosen with same procedure. The forces are thought on bearings when they are chosen as well.

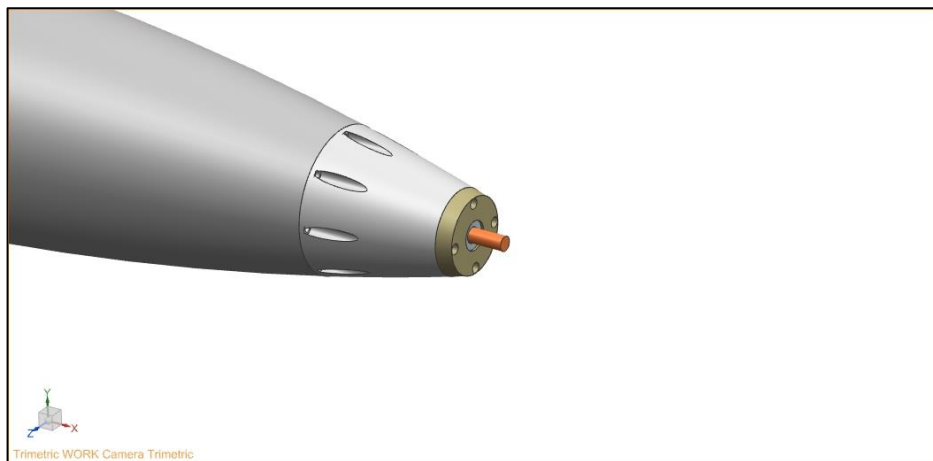


Figure 27. Designed 155 mm Munition with Bearings

Two bearing are used in front of motor to assure motor concentricity with the munition's axial moment of inertia axis. The bearings must provide mechanism angular velocity and torque request. Fins are fastened to motor by the bearings.

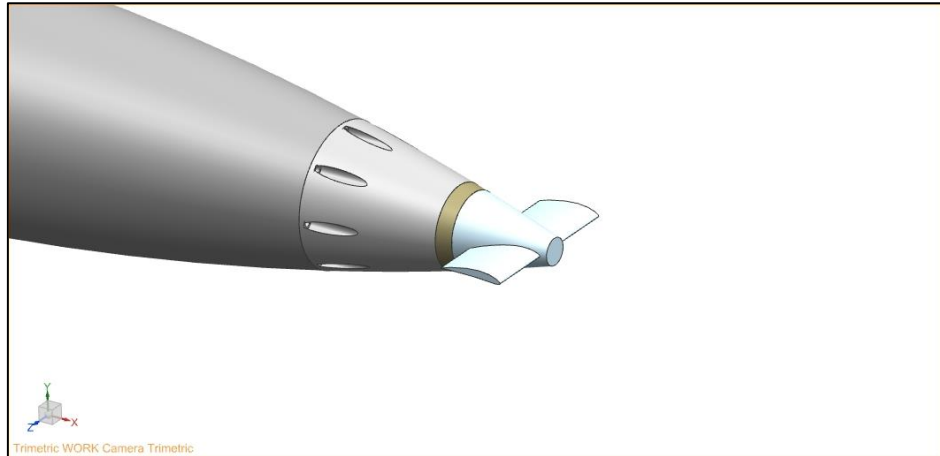


Figure 28. Designed 155 mm Munition with Bearings

The fins are assembled to the mechanism and draft format of the mechanism design is created basically. This section helps to understand how the mechanism works to control the munition. The fins have NACA 6412 airfoil section, whose drag and lift coefficients could be found from literature easily [27]. Airfoil data are given in Figure 29. Lift coefficient of mechanism wings is taken from NACA 6412 data [27]. The munition total angle of attack does not exceed about 10 degrees and it usually takes about 5 degrees so lift coefficient is taken about 1 according to Figure 29. Drag force effect is also considered on munition. Drag coefficient which is necessary to calculate drag force could be also taken from Figure 29 as well. If the lift coefficient is taken about 1, drag coefficient should be taken about 0.02 and drag force could be calculated for that drag coefficient.

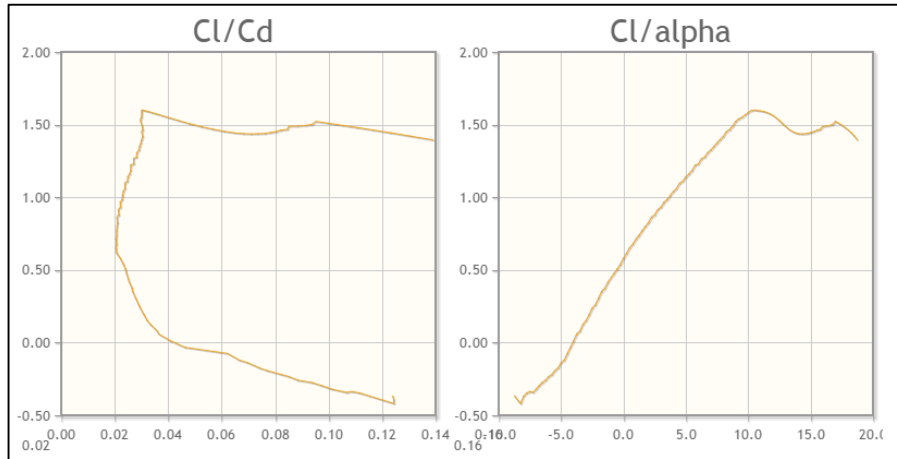


Figure 29. NACA 6412 Data [27]

4.1.2 Selection of Standard Elements

Motor of the mechanism is the most important component in the nose actuation kit because while the mechanism spins with same angular velocity in inverse direction according to body spin velocity, the fins could be hold at the fix angle in earth fixed coordinate. It should be better to choose motor and bearings according to angular velocity and torque request of the mechanism. Angular velocity of the munition is known and it is given in Figure 45. Therefore, selected motor and bearings reach maximum about 1670 rad/s angular speed at the beginning of the flight.

Moreover, maximum torque, which the mechanism encounters, must be calculated. Motor viscous friction is given in 4.2.3 and there is also some torques, which try to stop mechanism due to frictions. These are bearing torque due to bearing frictions and wings torque due to air resistance. Calculation of bearing torque due to bearing friction is given in (4.1).

$$F_s = N\mu \quad (4.1)$$

Constant of bearing friction is shown by μ and it could be found any bearing catalog for selected bearing. The bearings friction constant for the mechanism could be taken about 0.001 and N is radial force on bearing. Selected bearings have to

provide angular velocity and forces of the mechanism. Radial force could be calculated according to Figure 30, which implies that P and R_1 are radial forces on bearings respectively.

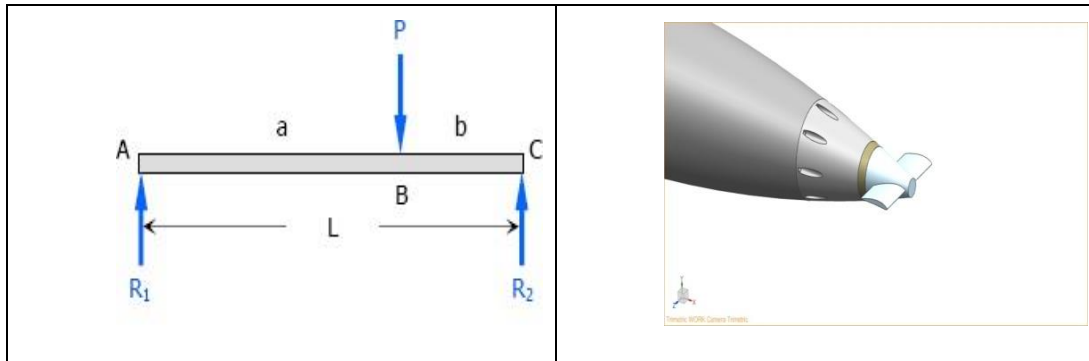


Figure 30. Forces on Bearings [28].

If P and R_1 are thought as radial forces on bearings, R_2 is force on wings. The metal bar is given with L length in Figure 30. This metal bar is also shaft of motor which rotate the mechanism fins. Some basic calculations are done to find P , R_1 and R_2 forces.

$$F_t = 0, \quad R_1 + R_2 = P \quad (4.2)$$

$$M_t = 0, \quad R_1 \times L - P \times b = 0 \quad (4.3)$$

R_2 is fin lift force and it is taken from the developed code, which is given in Figure 31. Fin lift force is calculated by mechanism force analysis in developed code for $3.e-4 \text{ m}^2$ fin surface area, which is found in 6.1. Fin surface area is decided according to stability criteria and ability of the munition control. It is seen from Figure 31 that mechanism force changes through the flight because although fin surface area is fixed, air density and especially velocity change through the flight. Thus, mechanism force, which is in Figure 31, is obtained.

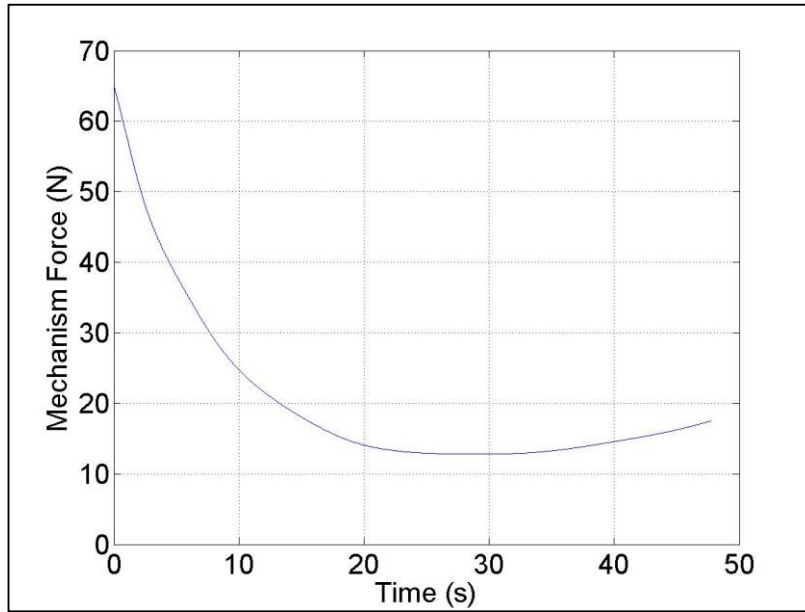


Figure 31. Mechanism Forces during the Flight

It is understood from Figure 31 that fins produces maximum about 65 N lift force. Lengths, which are L , a and b , are found from mechanical design parameters in solid model, which is given in Figure 28. Therefore, there are only two unknowns, which are P and R_1 radial forces on bearings and two equations. Equations (4.2) and (4.3) are recalled and rewritten with known. Moreover, r_l , which is given in (4.8), is distance between bearing outer surface and center line. The distance is also taken from solid model, which is given in Figure 28.

$$F_t = 0, \quad R_1 + 65 = P \quad (4.4)$$

$$M_t = 0, \quad R_1 \times 73.2 - P \times 59.2 = 0 \quad (4.5)$$

$$(R_1 + P)\mu = F_s \quad (4.6)$$

$$(275 + 340) \times 0.001 = 0.615 \text{ N} \quad (4.7)$$

$$T_b = F_s r_1 = 0.615 \text{ N} \times 4.5 \times 10^{-3} \text{ m} = 2.8 \times 10^{-3} \text{ N.m} \quad (4.8)$$

The torque, which is calculated in (4.8), should be provided by motor. Moreover, the other torque on motor is due to fins drag force. The body of the munition rolls with between 1600 rad/s and 800 rad/s during the flight so the mechanism rolls with same angular velocity. There is linear velocity on fins because of angular velocity of body. Mechanism fins are subjected to drag force due to this linear force on wings.

$$D = \frac{1}{2} \rho V^2 S C_D \quad (4.9)$$

$$S = 3 \times 10^{-4} \text{ m}^2 \quad (4.10)$$

The fins get out from the mechanism after about five seconds. W is Angular velocity of the mechanism, which is about maximum 1200 rad/s when fins get out the mechanism after five seconds. Other parameter, which is in equation (4.11), is r_2 . This distance is between midpoint of fins and munition center line.

$$V = w \times r_2 = 1200 \times 3 \times 10^{-2} \text{ m} = 36 \text{ m/s} \quad (4.11)$$

C_D is drag coefficient and it is taken for flat surface because the fins roll with an angular velocity. According to literature survey, drag coefficient could be taken about 1.05 [29].

$$D = \frac{1}{2} \times 1.225 \times 36^2 \times 3 \times 10^{-4} \times 1.05 = 0.2 \text{ N} \quad (4.12)$$

$$T_w = D r_2 = 0.2 \times 3 \times 10^{-2} \text{ m} = 6 \times 10^{-3} \text{ N.m} \quad (4.13)$$

Total torque, which applies to motor to stop, could be calculated in (4.14).

$$T_t = T_b + T_w = 2.8 \times 10^{-3} + 6 \times 10^{-3} \cong 8.8 \text{ mN.m} \quad (4.14)$$

There are a few alternatives to choose standard motor according to size, torque and velocity requirements of the mechanism. Some DC brushless motors could satisfy the requirements and EC 22, whose properties are given in Table 6, brushless motor is chosen.

Motor parameters are input to mathematical model of the nose actuation kit in 4.2.3. Especially, motor torque constant, inertia and viscous friction are needed to calculate transfer function of mechanism model. The motor is chosen according to package limits, velocity, torque limits and controller performance. If the requirements are changed because of some problems, the motor could be change and chosen from catalogs again.

Table 6. EC 22 Brushless Motor Properties

Motor type	Description	Brushless EC
Nominal voltage	The applied forces between max and min power	48 V
No load speed	The speed at which unloaded motor runs	12900 rpm
No load current	Typical current at which unloaded motor runs	384 mA
Nominal speed	The speed at nominal torque and voltage	8560 rpm
Nominal torque	The torque at nominal voltage and current	149 mN.m
Stall torque	The torque produced by motor when at standstill	460 mN.m
Torque constant	Specific torque	34.4 mN.m/A
Velocity constant	Specific velocity	278 rpm/V
Mechanical Time Constant	The time from standstill to %63 of its no load speed	2.31 ms
Motor inertia	Mass moment of inertia	7.63×10^{-7} kg.m ²
Max. permissible speed	Maximum recommended speed	20000 rpm
Viscous friction	Dynamic friction	2×10^{-7} N.m/rpm
Weight		160 g
Length		44.5 mm
Diameter		22 mm

4.2 Kit Control

In this thesis, control block must be designed to guard mechanism forces. A simple and effective controller could be enough to check to mechanism angular velocity and position. PI and PID controllers are investigated and these controllers are sufficient for tracking angular position and velocity.

Controllers produce a signal according to difference between reference value and output value in close loop systems. The PI and PID controllers include proportional and integral terms for tracking the reference signal with a minimum error. Proportional term could arrange by multiplying with current error. Proportional

term is responsible of sensibility of response. Integral term is multiplied with sum of errors for the time interval and this term could eliminate steady error of system response. However if integral term is increased too much, it cause to overshoot. The last term is derivative term, which is used in PID controller, is determined by multiplying rate of change error over time. This term develops settling time and stability of the system [30], [12].

Inertia of the mechanism and transmission ratio should also be determined because these parameters are input to control block of the mechanism. After calculation of inertia of the mechanism and transmission ratio, one of PI and PID controllers will be selected and coefficients of controller will also be calculated according to response of the transfer function.

4.2.1 Mechanism Moment of Inertia

Inertias of the mechanism components, which are motor, shaft and fins, are determined. All components spin about the munition center line, which is shown with dashed line in Figure 32. Motor moment of inertia could be found from motor properties, which are given in standard motor catalogs. Shaft moment of inertia could be calculated easily according to equation (4.17). Inertia of fins is taken from solid model. Thus, total inertia effect on motor could be calculated by summation of these three results.

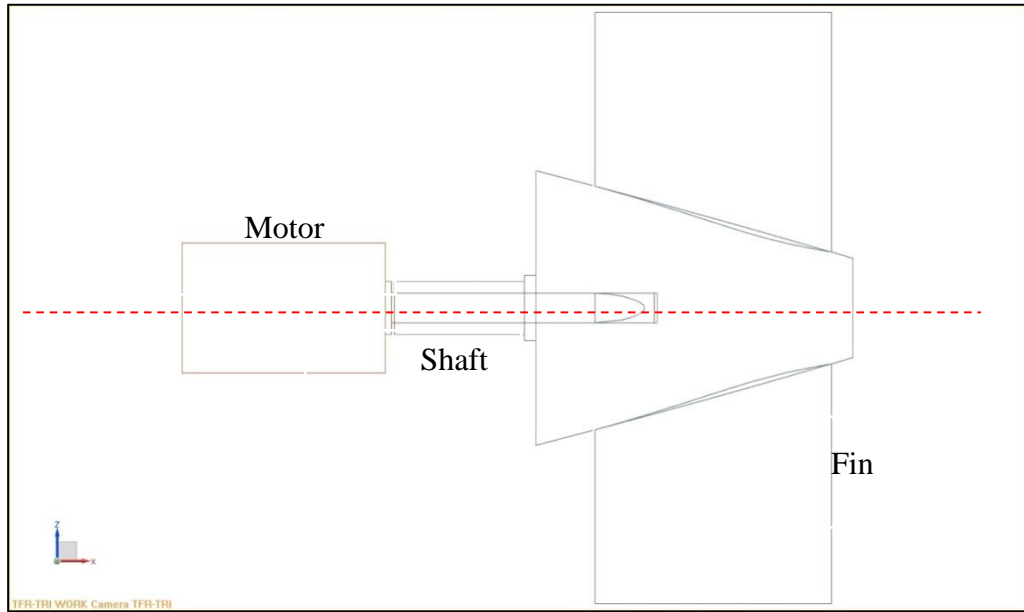


Figure 32. Motion of Dynamic Mechanism

Total inertia system could be found with equation (4.15)

$$J_{total} = J_{motor} + J_{shaft} + J_{fins} \quad (4.15)$$

After the mechanism is designed according to requirements and assign material properties, fins moments of inertia could be taken from solid model, which is given in Figure 28.

$$J_{fins} = 146.5 \times 10^{-6} \text{kgm}^2 \quad (4.16)$$

Another effect on motor is shaft moment of inertia. Shaft moment of inertia could be determined with simple calculations in (4.17).

$$J_{ballscrew} = \frac{1}{12} mL^2 = \frac{1}{12} 0.00744.5^2 = 1.2 \times 10^{-6} \text{kgm}^2 \quad (4.17)$$

The last inertia effect is motor moment of inertia, which could be taken from Table 6 and motor catalogs.

$$J_{motor} = 0.12 \times 10^{-6} \text{kgm}^2 \quad (4.18)$$

Therefore, total moments of inertia could be calculated now easily.

$$J_{total} = J_{motor} + J_{ballscrew} + J_{mechanism} \quad (4.19)$$

$$J_{total} = 0.12 + 1.2 + 146.5 = 148 \times 10^{-6} \text{ kgm}^2 \quad (4.20)$$

4.2.2 Transmission Ratio of the Mechanism

The mechanism is designed and used to provide forces and moments which change trajectory of the munition according to orders. The mechanism must satisfy about 12000 rad/s roll velocity and 8.6 mNm pause torque.

The mechanism includes brushless EC 22 motor, fins, shaft and power supply, which are shown in Figure 33.

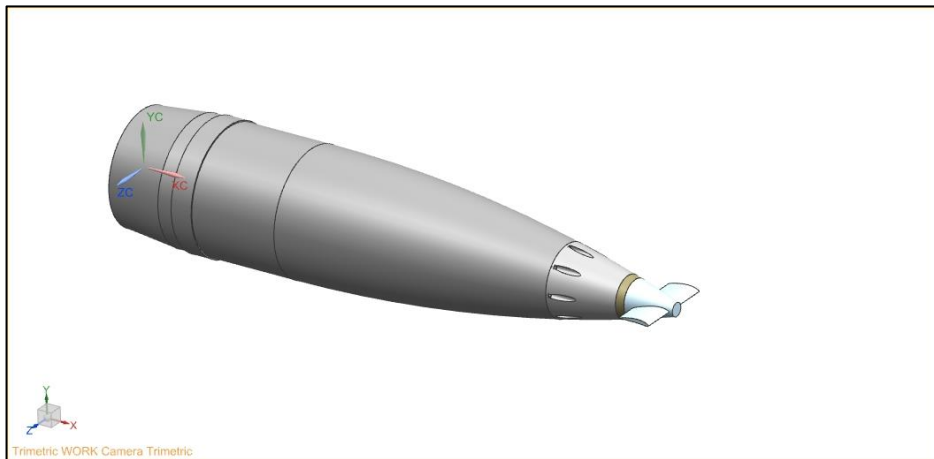


Figure 33. Mechanism with Munition

Motor is chosen according to mechanism roll velocity and pause torque requirement. The mechanism transmission ratio is also needed to create the transfer function of mechanism. Motor roll velocity is divided by mechanism roll velocity to determine transmission ratio [31]. The equation is given in (4.21).

$$N = \frac{\omega_{motor}}{\omega_{mechanism}} \quad (4.21)$$

As seen in Figure 32, fins are related to motor directly so it could be assumed that motor roll angle and velocity are equal to mechanism roll angle and velocity. Thus, the transmission ratio could be found.

$$N = 1 \quad (4.22)$$

The mechanism mathematical model could be obtained in 4.2.3 by using transmission ratio (N) and motor properties.

4.2.3 Mechanism Mathematical Model

Brushless motor, which is Maxon EC 22, is chosen and used for mechanism movement according to performance and packaging requirements. EC 22 brushless motor has high roll velocity with high torque, small size and small weight. Moreover, torque and velocity constants are critical parameters to choose motor. The motor has also high torque and velocity constant. Brushless EC motors have almost same properties with brushes motors except structural differences so brushless EC motor could be modeled like brushes motors.

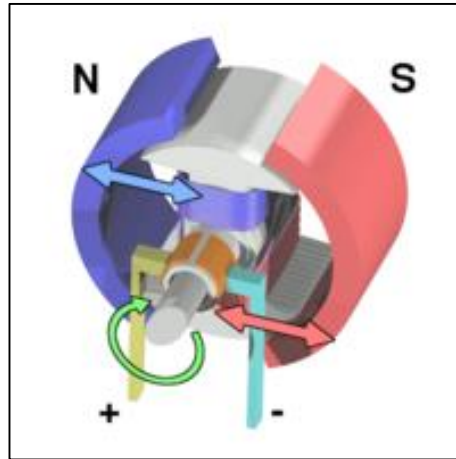


Figure 34. Motor Basic Work Principle [32]

The instant torque could be obtained for a pole of rotor in equation (4.23)

$$\tau_m(\theta) = r_r F_m(\theta) = r_r \left(l_m \frac{i}{c} B(\theta) \right) \quad (4.23)$$

Total torque could be calculated by taking integral of instant torque. Instant torque is assumed equal for all poles of rotor. Thus, the equation (4.24) is obtained.

$$\tau_m = r_r l_m \frac{i}{c} B_{avg} \quad (4.24)$$

Moreover, total torque could also be determined like equation (4.25).

$$\tau_m = k_t \Phi i \quad (4.25)$$

Total inverse electro motor force could be calculated in equation (4.26) like equation (4.24).

$$e = r_r w l_m B_{avg} \quad (4.26)$$

If the equation (4.26) is rewritten,

$$e = k_v \Phi w \quad (4.27)$$

Equation (4.27) could be obtained.

Motor torque constant and velocity constant, which include flux (Φ), could be found from motor product catalogs.

$$K_t = k_t \Phi = \frac{\tau_m}{i} \quad (4.28)$$

$$K_v = k_v \Phi = \frac{e}{w} \quad (4.29)$$

Mathematical model of motor circuit is shown in Figure 32. Motor circuit equation includes two different parts, which are rotational part circuit and mechanical part circuit.

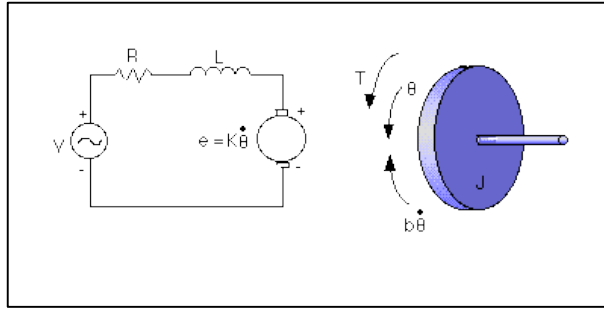


Figure 35. Brushless Motor Circuit

Equation (4.30) is written for rotational part circuit by using Kirchhoff law.

$$V = Ri + L \frac{di}{dt} + e \quad (4.30)$$

Equation (4.31) is also written for mechanical part circuit.

$$\tau_m = Bw + J \frac{dw}{dt} + \tau_L \quad (4.31)$$

If equation (4.29) and (4.30) are rewritten and combined, equation (4.32) is got to find voltage.

$$V = Ri + L \frac{di}{dt} + K_v w \quad (4.32)$$

Laplace transform is taken for equation (4.32). Thus, the below equation is found.

$$V(s) = (R + Ls)i(s) + K_v w(s) \quad (4.33)$$

If equation (4.28) and (4.31) are also rewritten and combined, equation (4.34) is obtained.

$$K_t i = J \frac{dw}{dt} + Bw \quad (4.34)$$

Laplace transform is also taken for equation (4.34) is taken. Therefore,

$$i(s) = \frac{(B + Js)w(s)}{K_t} \quad (4.35)$$

Equation (4.35) is written into the equation (4.33) for examination of current. Therefore;

$$V(s) = (R + Ls) \frac{(B + Js)w(s)}{K_t} + K_v w(s) \quad (4.36)$$

$$\frac{V(s)}{w(s)} = \frac{(R + Ls)(B + Js) + K_v K_t}{K_t} \quad (4.37)$$

with

$$\theta_m = \theta_w N \quad \text{and} \quad w = s\theta \quad (4.38)$$

$$\frac{\theta_w(s)}{V(s)} = \frac{\frac{K_t}{NLJ}}{s^3 + \left(\frac{R}{L} + \frac{B}{J}\right)s^2 + (RB + K_v K_t)s} \quad (4.39)$$

The relation between given voltage and output angle is extracted according to motor parameters, component's moments of inertia and transmission ratio [33], [34].

Driver of the brushless motor uses current to control the velocity and position of motor. In other words, current is controlled to change mechanism position. Because voltage control on brushless motor is harmful for life time of motors. Moreover application area of current control on brushless motor is more suitable compare to voltage control. Thus, current is input and roll angle of mechanism is output.

The Simulink model is given Figure 36 for current input and roll angle of mechanism output.

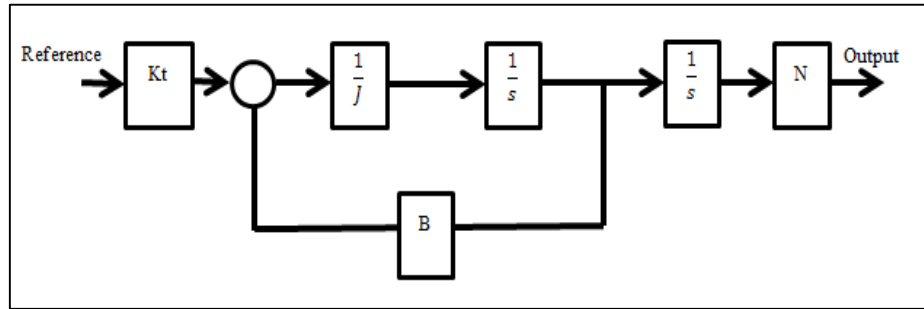


Figure 36. Simulink Model for Current Input and Roll Angle Output

The transfer function between current and roll angle of mechanism could be obtained according to Figure 36 easily. The transfer function for current input and roll angle of mechanism output is given in (4.40).

$$M(s) = \frac{\theta_w(s)}{i(s)} = \frac{\frac{K_t}{N}}{s(Js + B)} \quad (4.40)$$

When selected motor parameters are used in equation (4.40), the equation could be rewritten in (4.41).

$$M(s) = \frac{\theta_w(s)}{i(s)} = \frac{\frac{0.0344 \text{ Nm/Amp}}{1}}{s(s * 148 * 10^{-6} \text{ Nmsec}^2 + 2 * 10^{-6} \text{ Nmsec})} \quad (4.41)$$

$$M(s) = \frac{\theta_w(s)}{i(s)} = \frac{17200}{74s^2 + s} \quad (4.42)$$

Equation (4.42) is a transfer function for open loop system.

$$M(s) = \frac{N(s)}{D(s)} \quad (4.43)$$

Equation (4.43) is transfer function of system which is already found. Upper part of transfer function implies numerator of function and its roots are zeroes of system. Lower part of transfer function implies denominator and its roots are poles of system. Poles have to be left side of s plane to guarantee stability of system.

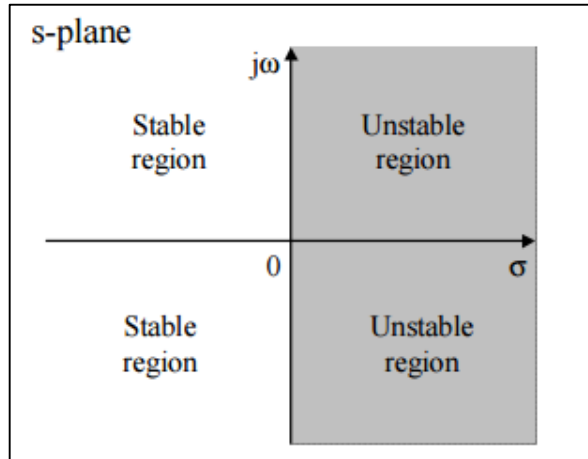


Figure 37. S-Plane

Therefore, there is no zeroes of equation (4.42). However, there are two poles, which are 0 and -0.0135. All poles of transfer function must be negative or zero to satisfy the stability condition of dynamic systems. Therefore, the poles, which are found from (4.42), are in stable region.

4.2.4 Controller Design

The controller is responsible to adjust angular velocity and position of the mechanism. Although PI controller, which is usually used for system need only position and velocity control, could be enough, this system has a high angular velocity, which cause to oscillation. Derivative term is used to avoid from oscillation so the controller should be better to have derivative term. Classic PID controller is determined by a weighted sum and it could be shown in equation (4.44).

$$C = K_p + \frac{K_i}{s} + K_d s \quad (4.44)$$

The PID controller has proportional, integral and derivative terms and they are denoted by K_p , K_i , K_d respectively.

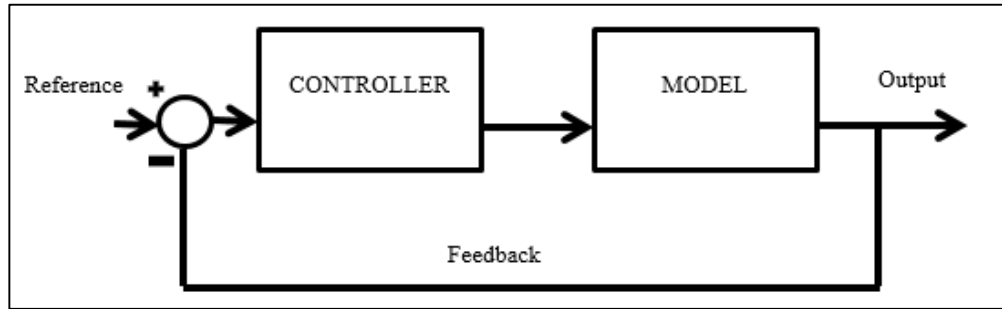


Figure 38. Close Loop Model from Reference to Output

Simple close loop model of the system is given at Figure 38. The controller is denoted by C and model is denoted by M . Transfer function of the close loop model, shown in Figure 38, could be determined like equation (4.45).

$$G(s) = \frac{CM}{CM + 1} \quad (4.45)$$

When $G(s)$ is rewritten by using controller, given in equation (4.44), and the model, given in equation (4.40), equation (4.46) is got.

$$G(s) = \frac{\frac{K_t}{B} K_d s^2 + \frac{K_t}{B} K_p s + \frac{K_t}{B} K_i}{\frac{J}{B} s^3 + \left(\frac{K_t}{B} K_d + 1\right) s^2 + \frac{K_t}{B} K_p s + \frac{K_t}{B} K_i} \quad (4.46)$$

The roots of the function could be calculated according to PID controller coefficients after determining of close loop transfer function.

There are a lot of ways to calculate controller coefficients in literature. The ways, which are tried to control the mechanism in this thesis, are using polynomials like Butterworth and Chebyshev, tuning method in Matlab. Therefore, Butterworth polynomial, which minimizes overshoots of system response, is used in this thesis. Damping ratio is taken 0.707 and third orders Butterworth polynomial could be written like equation (4.47) [31].

$$B_s(s) = \frac{s^3}{w_c^3} + \frac{2s^2}{w_c^2} + \frac{2s}{w_c} + 1 \quad (4.47)$$

W_c is, in equation (4.47), is bandwidth of control system. Bandwidth is the difference between the upper set of frequencies and lower set of frequencies. Bandwidth is typically measured in hertz [35]. W_c is chosen 50 Hz for the nose actuation kit mechanism. All parameters are known from previous parts according to motor and mechanism parameters. Thus, coefficients of controller are calculated by using equation (4.46) and (4.47).

$$K_p = \frac{2w_c^2 \frac{J}{B}}{\frac{K_t}{B}} = 22 \quad (4.48)$$

$$K_i = \frac{w_c^3 \frac{J}{B}}{\frac{K_t}{B}} = 538 \quad (4.49)$$

$$K_d = \frac{2w_c \frac{J}{B} - 1}{\frac{K_t}{B}} = 0.43 \quad (4.50)$$

The controller checks the roll angle and velocity of the mechanism for the spinning munition. Controller input is an error, which is difference between roll angle of the mechanism and desired roll angle, which is given. The output of controller, which is current, is input for transfer function of model as well. The input of transfer function could be found by this procedure.

Real life disturbances and errors should be thought when the mechanism model is designed. The real life effects, like measurement error, mechanism problems and other effects, should be added to the simulation model of the mechanism as a disturbance. These disturbances are defined as a current errors and measurement errors.

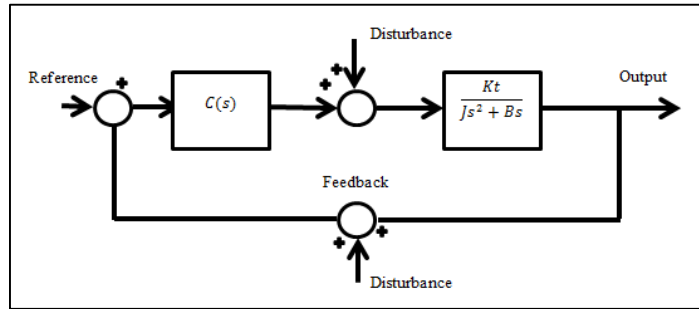


Figure 39. Simulink Model for Desired Roll Angle Input and Roll Angle Output

The basic Simulink model for this system is given in Figure 39. Moreover, coefficients of controller are calculated and given in equation (4.48), (4.49), (4.50).

Stability analysis should be done for the closed loop transfer function, given in (4.46), after finding of K_p , K_d , K_i controller coefficients according to Butterworth equation in (4.47). Pole zero calculation help to understand of stability of the system proportional to the transfer function.

Poles and zeroes of the closed loop system are calculated by using Matlab tool. Close loop transfer function have 2 zeroes and 3 poles which are $-25,6 \pm 24,4i$ zeroes, $-26,1 \pm 44i$ and $-47,7$ poles respectively. All poles are in left side of s-plane so the system could be said stable.

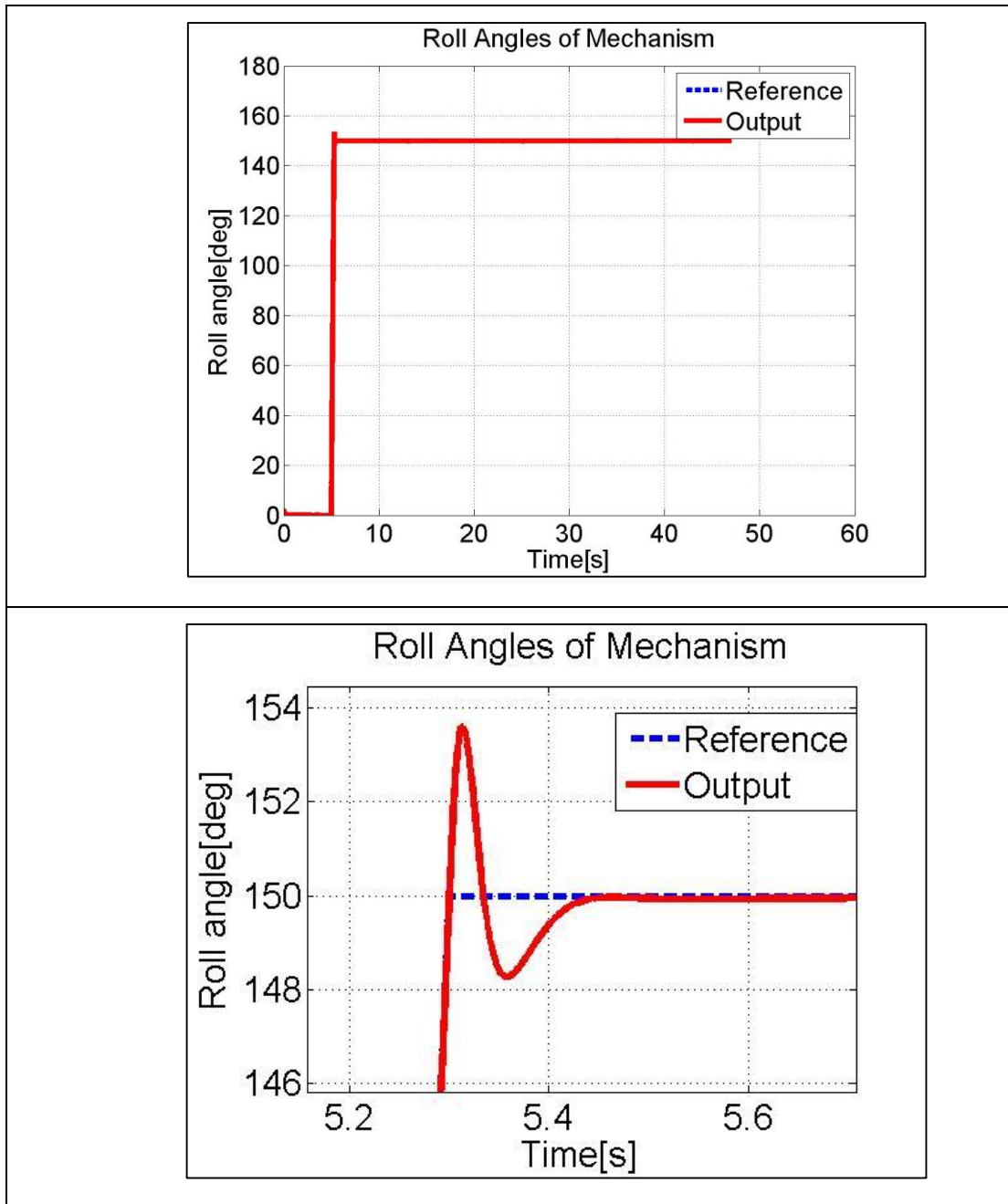


Figure 40. Roll Angles of Mechanism

The model has two inputs, which are reference angle of mechanism and roll angle of body, according to Simulink model. Reference angle of the mechanism is an angle, which is demanded by guidance, and it is given in Figure 40. It is wanted to hold the mechanism fins with fix angle in earth fixed frame. The mechanism fins with fix angle creates forces and moments to change the trajectory of standard 155

mm spin stabilized munition. Reference roll angle, which is given in Figure 40, could be changed according to guidance orders to track the trajectory.

On the other hand, the result of the mechanism's output roll angle is also given in Figure 40. It is expected that the mechanism follows the reference roll angle with minimum error. It is known that reference roll angle is given through the flight. However, there is no position control for mechanism in first five seconds because mechanism fins are inside of shield and there is no effect of fins on the munition trajectory. Another reason is roll acceleration of the munition is too high to follow in first five seconds because the munition roll velocity reaches about 1669.1 rad/s in 0.01 sec. Thus, motor of the mechanism needs too much power.

Fins rotate with same acceleration and reach same angular velocity with body velocity after five seconds. Fins are opened after five seconds and position control of the mechanism is done with body angular position. Roll angle difference of the mechanism is maximum about 180 degrees with body roll angle when fins of the mechanism are opened. Therefore, this difference is taken 150 degrees and motor tries to close this difference at five seconds after muzzle exists.

Oscillations could be problem for munition control but oscillation amplitude is not exceeding 1 degree so it does not affect trajectory of the munition. Moreover, it is understood from Figure 40 easily that the mechanism converges itself about reference roll angle. Second graph of the Figure 40 is the detail part of the Figure 40's first graph. It is at about 5.3 seconds, when the maximum difference is seen between reference and output orders.

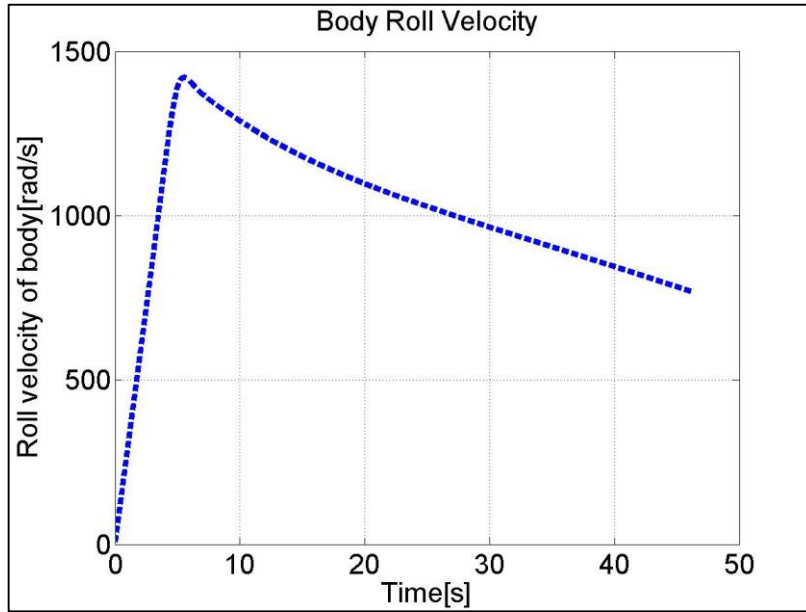


Figure 41. Roll Velocity of Body

It was already talked that position of the mechanism does not controlled in first five seconds so it is also assumed that mechanism does not follow the munition body and speeds up with a same acceleration in first five seconds. Roll velocity of the munition body, which is angular velocity from zero second to end of the flight, is given in Figure 41 with this assumption. Roll velocity increases from zero angular velocity to about 1400 rad/s linearly in Figure 41. However, after 5 seconds the mechanism angular velocity must match with body angular velocity. Then the munition spins with a velocity, which decreases to about 800 rad/s at the end of the flight.

Figure 41 is a roll angle, which the mechanism follows. It is thought that mechanism fins are hidden inside the mechanism for first five seconds. The fins of the mechanism exist from shell after the mechanism starts to follow the body roll angle. The mechanism fins should be opened after about 5 seconds when the munition is launched because of current limit of electric motor, used in the mechanism. In other words, if the mechanism is wanted to track the body spin velocity from the muzzle exists, motor reaches about 1669.1 rad/sec in 0.01 sec. thus, motor needs too high current to reach the spin velocity in short time.

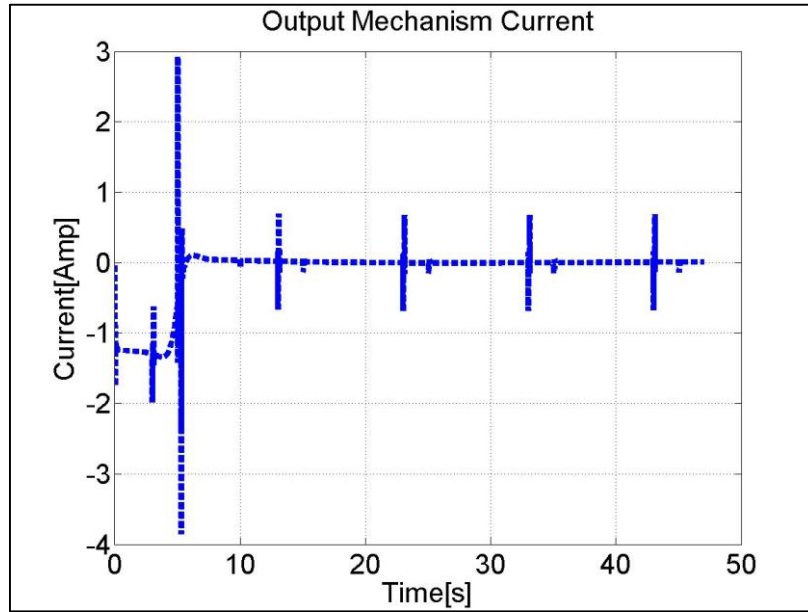


Figure 42. Necessary Current of Motor

The current, which is used by motor according to demand angle, is given in Figure 42 though the flight. Knowing the necessary current, which motor needs, is a critical subject for control of the mechanism because the power supply can supply a limited current. The current, which is used by motor and mechanism, does not exceed 3 amperes trough the flight. Therefore, this condition is suitable for our design.

CHAPTER 5

RESULTS AND DISCUSSION

5.1 Ballistic Flight Database

Aerodynamic coefficients are calculated by using the PRODAS software, equations of motion are determined and the developed code is prepared to obtain mechanism and wind effect on spin stabilized munitions. Results of the developed code, which is given in APPENDICES, are discussed in 5.2 and then the results of the developed code are compared with PRODAS results to check in 5.3. However, a step size frequency of the developed code should be decided, before comparing the results.

Before comparing the developed code and PRODAS results, step size frequency of the developed code should be chosen. The developed code is run for same model of the munition and initial conditions for varying step size frequency. Analyses are done with same code and same initial conditions time and again for finding optimal step size frequency, which give both minimum run time and the best results.

Table 7. Ballistic Flight Database for Longitudinal Dispersion

Elevation Angle (deg)	Step Size Frequency (Hz)							
	100	200	250	500	1000	2000	5000	10000
3	NaN	5408.88	5408.32	5408.32	5408.32	5408.05	5407.88	5407.88
6	NaN	8863.2	8861.97	8861.97	8861.56	8861.56	8861.4	8861.4
9	NaN	11257.49	11257.49	11256.83	11256.51	11256.51	11256.38	11256.38
12	NaN	13085.47	13085.18	13084.6	13084.31	13084.31	13084.31	13084.31
15	NaN	14599.35	14599.07	14599.07	14598.8	14598.8	14598.75	14598.72
18	NaN	15913.23	15912.97	15912.46	15912.2	15912.07	15912.1	15912.07
21	NaN	17074.82	17075.06	17074.57	17074.33	17074.33	17074.28	17074.28
24	NaN	18109.48	18109.25	18108.79	18108.79	18108.79	18108.74	18108.74
27	NaN	19027.06	19027.06	19026.62	19026.62	19026.62	19026.62	19026.59
30	NaN	19831.34	19831.76	19831.34	19831.34	19831.24	19831.18	19831.18
33	NaN	20515.59	20515.4	20515	20514.8	20514.8	20514.73	20514.73
36	NaN	21067.94	21067.57	21067.21	21067.21	21067.11	21067.06	21067.06
39	NaN	21476.4	21476.4	21476.4	21476.4	21476.4	21476.36	21476.34
42	NaN	21729.16	21729.35	21729.03	21729.03	21728.95	21728.9	21728.88
45	NaN	NaN	21805.37	21805.37	21805.22	21805.22	21805.19	21805.18
48	NaN	NaN	21687	21687	21686.87	21686.87	21686.81	21686.81
51	NaN	NaN	21365.2	21365.2	21365.07	21365.01	21364.97	21364.97
54	NaN	NaN	20822.63	20822.64	20822.53	20822.47	20822.44	20822.44
57	NaN	NaN	20006.17	20006.55	20006.45	20006.4	20006.37	20006.36
60	NaN	NaN	NaN	18910.12	18910.03	18910.03	18910.03	18910.03

Table 7 shows the longitudinal dispersion of the munition when the munition is launched with the initial conditions, which is given in Table 5. Left column of the Table 7 shows elevation angles. The top row is the step size frequency. Therefore, longitudinal dispersions of the munition can be found for different elevation angles and it can be seen effect of the step size frequency on results.

Table 8. Ballistic Flight Database for Lateral Dispersion

Elevation Angle (deg)	Step Size Frequency (Hz)							
	100	200	250	500	1000	2000	5000	10000
3	NaN	-11.33	-11.32	-11.32	-11.32	-11.32	-11.32	-11.32
6	NaN	-44.55	-44.54	-44.54	-44.53	-44.53	-44.53	-44.53
9	NaN	-89.22	-89.22	-89.2	-89.19	-89.19	-89.19	-89.19
12	NaN	-135.18	-135.17	-135.16	-135.15	-135.15	-135.15	-135.15
15	NaN	-176.87	-176.86	-176.86	-176.86	-176.86	-176.86	-176.85
18	NaN	-215	-214.99	-214.98	-214.97	-214.96	-214.96	-214.96
21	NaN	-249.76	-249.77	-249.75	-249.74	-249.74	-249.74	-249.74
24	NaN	-281.47	-281.47	-281.45	-281.45	-281.45	-281.45	-281.45
27	NaN	-310.1	-310.1	-310.09	-310.09	-310.09	-310.09	-310.09
30	NaN	-335.28	-335.29	-335.28	-335.28	-335.27	-335.27	-335.27
33	NaN	-357.24	-357.23	-357.22	-357.21	-357.21	-357.21	-357.21
36	NaN	-375.95	-375.94	-375.92	-375.92	-375.92	-375.92	-375.92
39	NaN	-391.1	-391.1	-391.1	-391.1	-391.1	-391.1	-391.1
42	NaN	-402.47	-402.48	-402.47	-402.47	-402.47	-402.46	-402.46
45	NaN	NaN	-409.43	-409.43	-409.42	-409.42	-409.42	-409.42
48	NaN	NaN	-411.63	-411.63	-411.62	-411.62	-411.62	-411.62
51	NaN	NaN	-405.25	-405.25	-405.24	-405.24	-405.23	-405.23
54	NaN	NaN	-387.07	-387.08	-387.07	-387.07	-387.06	-387.06
57	NaN	NaN	-360.51	-360.61	-360.61	-360.6	-360.6	-360.6
60	NaN	NaN	NaN	-314.41	-314.41	-314.41	-314.41	-314.41

Table 8 shows the lateral dispersion of the munition when the munition is launched with the initial conditions given in Table 5. Left column of the table shows elevation angles. The row is the step size frequency as well. Thus, lateral dispersions of the munition can be found for different elevation angles and it can be seen the effect of the step size frequency on results.

Different muzzle elevation angles, which are from 3 degrees to 60 degrees, are used and the results are shown at the tables. Spin stabilized munitions reach the maximum range with 45 degrees muzzle angle as seen in Table 7 and Table 8, so the analyses are done for maximum 60 degrees. First analyses are done for 100 Hz step size frequency but no solution is obtained. Because step size frequency is not enough for these analyses due to high spin rate. Spin and linear velocity of the munition are out of boundary limits at any muzzle elevation angle when step size frequency is chosen 100 Hz. If the step size frequency is 200 Hz or more, the solutions can be taken with same initial conditions, which are given in Table 5. Thus, the code is run with same initial conditions for 500 Hz step size frequency and more than it. The solutions converge in each other. However, run time of the developed code is very

long for 1000, 2000, 5000 and 10000 Hz 500 Hz step size frequency. Thus, 500 Hz sampling time is chosen for the developed code and comparisons are done for the step size frequency.

Moreover, this work help to not only choose step size frequency of the developed code but also give an opinion about range and lateral deflection of 155 mm spin stabilized munitions for different elevation angles of muzzle. Circular error probable is given at Figure 43 is about 267 m for standard 155 mm spin stabilized munitions [14]. In the military science, circular error probable (CEP) is a measure of a weapon system's precision. It is defined as the radius of a circle, centered about the mean, whose boundary is expected to include the landing points of 50% of the rounds [36].

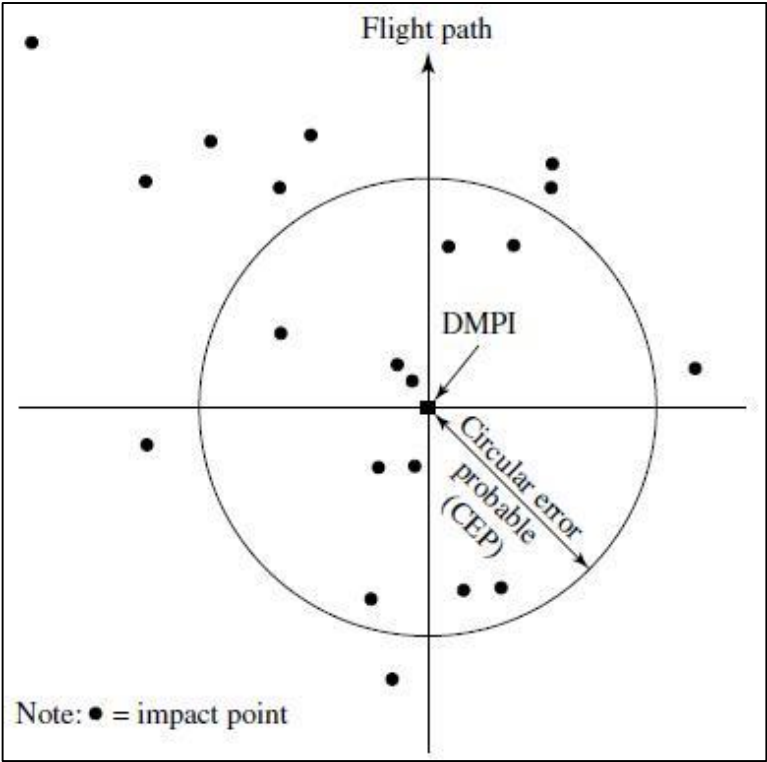


Figure 43. Circular Error Probable [36]

5.2 Results and Discussion of the Developed Code

Equations of motion of ballistic flight are set and all forces and moments on the munition are obtained.

The developed code uses modified Euler method as an iteration method. As it could be seen from Table 7 and Table 8, step size frequency is increased step by step and it is understood that range and lateral deflection do not change anymore for more than 500 Hz step size frequency so it could be said that 500 Hz step size frequency is optimum value for the modified Euler method. The developed code is run with 500 Hz sampling frequency according to 5.1. Therefore, the results of the developed code, which are obtained with 500 Hz step size frequency with the initial conditions, are given and discussed in this section.

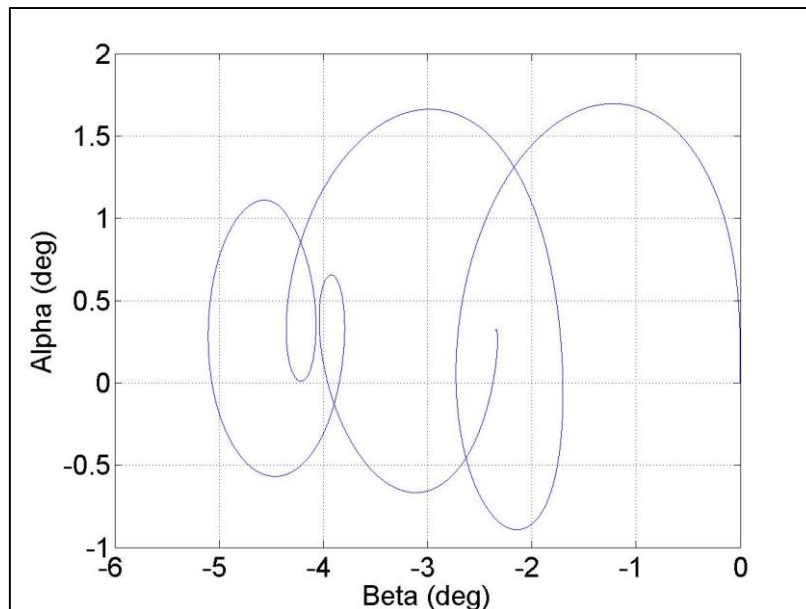


Figure 44. Alpha vs Beta for the Developed Code

Figure 44 shows angle of attack and side slip angle of the munition. The vertical axis of the figure, which is called alpha, is angle of attack of the munition in degree and the horizontal axis, which is called beta, is side slip angle in degree. A point (0, 0) could be thought as a velocity direction of the munition. Alpha and beta give an opinion about angle, which is between munition nose vector and velocity vector. Alpha angle of the munition does not exceed 1.7 degree along the flight. Beta

angle of the munition is bigger than alpha due to Magnus moment effect but it does not exceed 5 degree. Thus, the munition nose vector follows the ellipse in the flight.

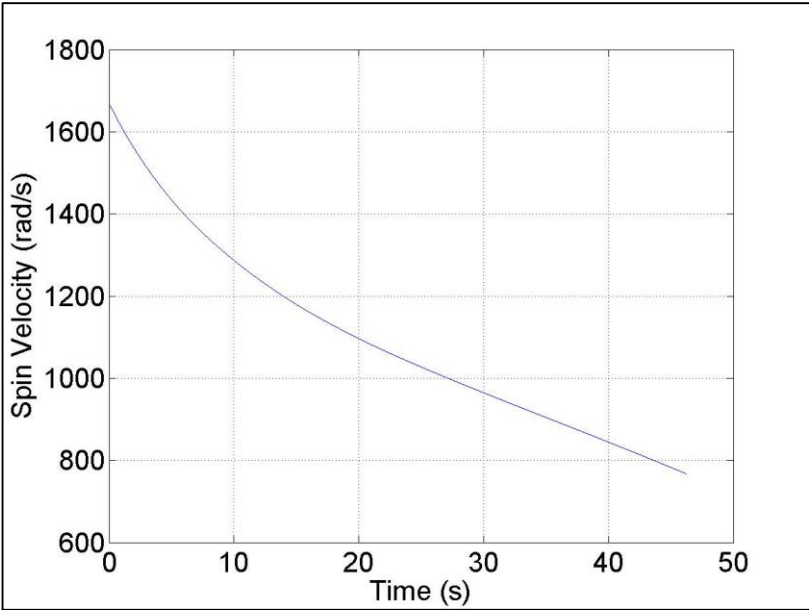


Figure 45. Spin Velocity vs Time for the Developed Code

Figure 45 shows spin velocity of the munition in radian per second through the flight. The vertical axis of the figure is spin velocity and the horizontal axis is time in second.

A spin velocity is a variable like elevation angle. The initial spin velocity can be determined according to muzzle design so analyses of the developed code are also run for different spin velocities in APPENDICES to observe the effect of the spin velocity on the munition. It can be understood from the analyses that higher spin velocity is preferred for stability of the munition. However, the spin velocity decreases to about half of it along the flight due to spin damping moment on the munition.

The stability of these munitions is provided by high spin velocity so if the munition flies without spin, the munition becomes unstable and it does not reach the target position. The initial spin velocity of standard spin stabilized munitions is related to the design of the muzzle. Thus, the initial spin velocity of the munition can be determined according to muzzle design and some analyses, which can show spin

effect on the munition directly, are repeated with zero, lower and high spin velocity than 1669.1 rad/s at this section.

The developed code is run with zero spin velocity. It is expected that the munition is unstable through the flight due to zero spin velocity. There are two criteria to stable flight. One of them is dynamic stability must be between zero and two. The other one is gyroscopic stability must be bigger than one. Instability of the munition causes to high total angle of attack. The munition faces with high drag force due to high total angle of attack. The velocity of munition is also expected to decrease dramatically because of high drag force. Results of the munition flight with zero spin velocity are given in APPENDICES. The solutions are given for about five seconds because the velocity of the munition is out of boundary after five seconds. In other words, aerodynamic coefficients are defined between 0.6 and 3 Mach number. It could be understood from Figure 62 that velocity of munition for zero spin velocity decrease dramatically so aerodynamic coefficients cannot be calculated for the velocity at about five seconds. That solutions are given trough the flight is not necessary anyway because it could be understood from Figure 64 that the munition is totally unstable.

After it was seen that the munition is unstable for zero spin velocity, the developed code is run with smaller spin velocity to analyze spin velocity effect on the munition. It is expected that if the spin velocity of munition is increased, the munition is more stable and hit the target position with smaller error [2]. The calculations and results of the developed code, is run for 1669.1 rad/sec spin velocity, are talked about in 3.3, 3.4 and 5.2. In other words, if the spin velocity is chosen smaller than 1669.1 rad/sec, the munition is less stable. Therefore, 1000 rad/sec spin velocity is chosen and the munition is launched with this spin velocity. All results are given in APPENDICES. It is understood from figures in APPENDICES that the munition is less stable because total angle of attack increases around 7 degrees in Figure 63 and the stability factor is smaller according to higher spin velocity in Figure 64.

Similarly, it is expected that the munition is more stable when it is launched with higher spin velocity than 1669.1 rad/sec. Spin velocity affects stability of the

munition directly according to ballistic research [2]. The calculations, whose results are given in APPENDICES, are done with higher spin velocity 2500 rad/sec and same linear velocity 826 m/sec. Therefore, more stable flight, less deflection and smaller total angle of attack are got at the end of flight. If the results given in APPENDICES are examined carefully, it is understood that the munition is more stable. First of all, the total angle of attack does not exceed 4 degrees in Figure 63 and this value reaches about 5 degrees for 1669.1 rad/sec spin velocity. Then, stability factors, which are given in Figure 64, are higher according to lower spin velocities because gyroscopic moment for higher spin velocities is bigger than the other for smaller spin velocities and this means the munition is more stable trough the flight. In other words, deflections are also smaller because of stability.

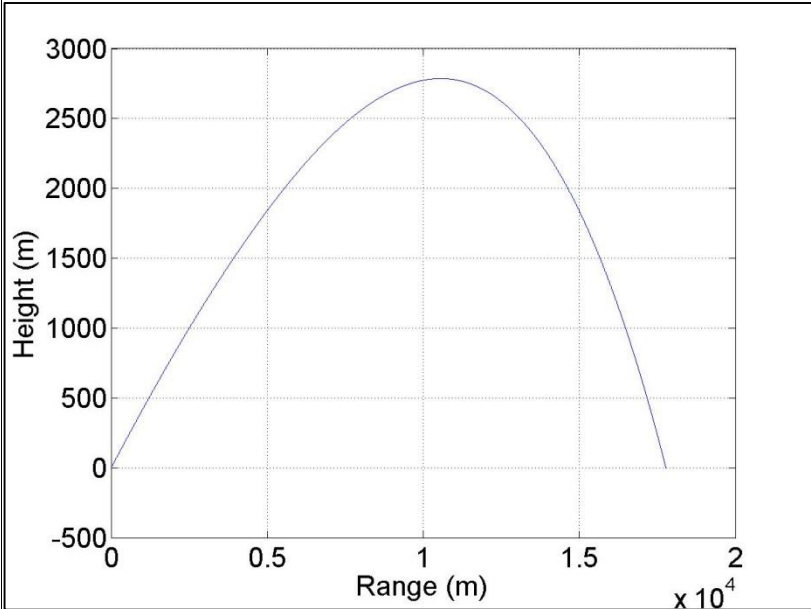


Figure 46. Height vs Range for the Developed Code

Figure 46 shows the height vs the range of the munition in meter along the flight. The vertical axis of the figure is the height of the munition, and the horizontal axis is the range of the munition. The figure shows side view of the munition during the flight without any control mechanism.

It could be understood from Figure 46 that munition rises with the elevation angle about 2786 m and then fell the ground due to the gravity effect when the munition reaches maximum 17778 m range with 23 degrees elevation angle. If the

elevation angle is increased up to 45 degrees, the height and range of the munition increase as well.

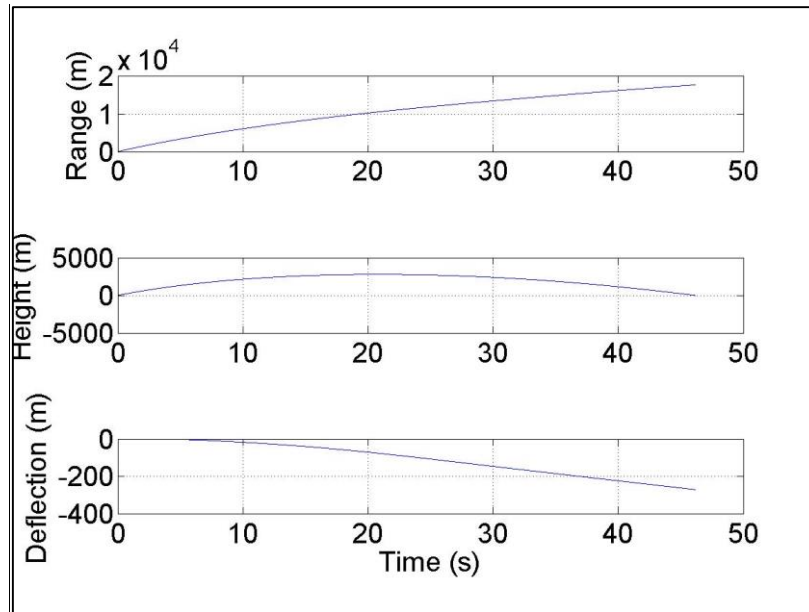


Figure 47. Positions vs Time for the Developed Code

Figure 47 shows all positions of the munition in meter according to time in second. Figure 47 includes three figures, which show position of the munition according to directions of the coordinate system. The vertical axes of the figure are the range, height and deflection of the munition respectively. The horizontal axis is time about 46.2 seconds.

The munition flight takes about 46, 2 second and it reaches maximum 2786 m about middle of the flight like Figure 46. The first figure, which implies the range of the munition, is about 17778 m and its deflection from target is about 271 m like standard 155 mm spin stabilized munitions, whose circular error probable is about 267 m.

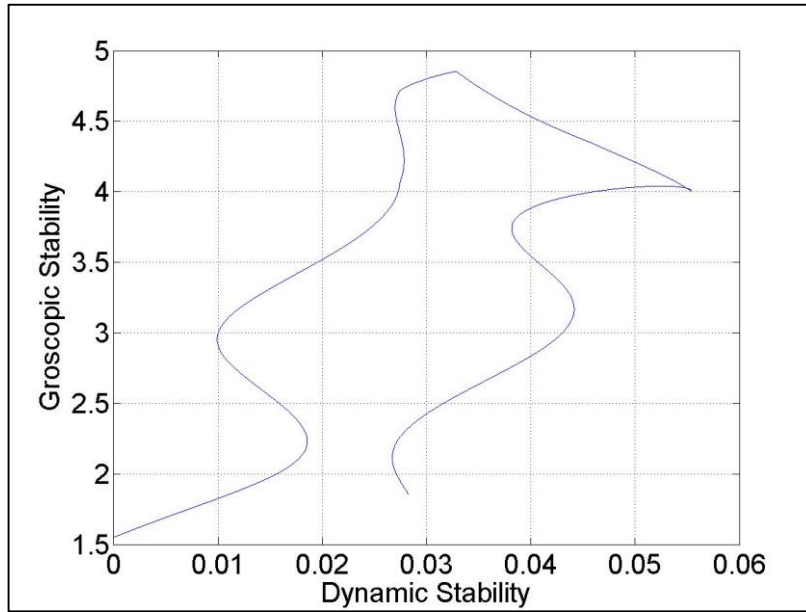


Figure 48. Gyroscopic Stability vs Dynamic Stability for the Developed Code

Figure 48 shows the gyroscopic (S_g) and dynamic stability (S_d) of the munition through the flight. The stability factors are unitless and they are shown in the same figure. The vertical axis of the figure is the gyroscopic stability, and the horizontal axis is the dynamic stability.

The most essential part of this section is the gyroscopic stability, which must be bigger than 1 to stable flight [2]. The gyroscopic stability relates to spin velocity, magnitude of linear velocity, pitch moment coefficient of munition directly. Gyroscopic stability differs between about 1.5 and 5 in Figure 48 and it means that the gyroscopic stability is satisfied. If the gyroscopic stability factor increases, the munition is more stable.

On the other hand, S_d is dynamic stability and it must be between 0 and 2. It should be better to be close to zero [2]. Dynamic stability relates to the aerodynamic coefficients of the munition, which are given Table 2, so it depends to design of the munition. Dynamic stability differs between 0 and 0.05 in the Figure 48 as the condition is satisfied for dynamic stability. Therefore the munition is stable through the flight because both stability conditions must be satisfied.

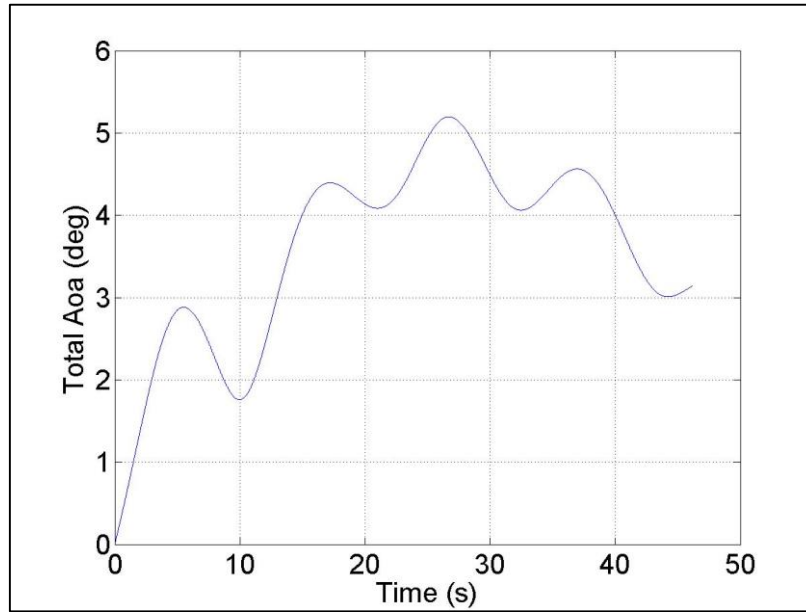


Figure 49. Total Angle of Attack vs Time for the Developed Code

Figure 49 shows the total angle of attack of the munition in degree vs time. The vertical axis of the figure is the total angle of attack of the munition, which is combination of the angle of attack and side slip angle of the munition. The total angle of attack is talked in depth in 3.2. The horizontal axis is the time in second.

The total angle of attack depends to alpha and beta angles. It is critical for stability of the munition because nearly all forces and moments depend on total angle of attack. The munition follows the trajectory better as long as total angle of attack is smaller. Analyses imply that when total angle of attack exceeds about 10 degrees, the munition becomes unstable and leaves from the trajectory. However, the total angle of attack reaches maximum 5 degrees along the flight as seen in Figure 49.

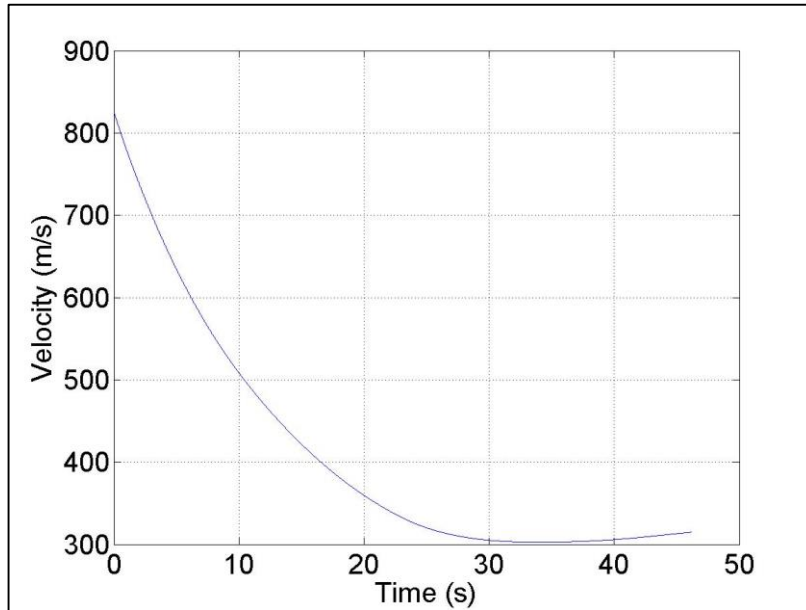


Figure 50. Velocity vs Time for the Developed Code

Figure 50 shows the velocity of the munition in meter per second and time in second. The vertical axis of the figure is the velocity of the munition, which is from muzzle exist to end of the flight. The horizontal axis is the time.

The velocity, which is given in Figure 50, is mainly affected from gravity force. The munition velocity decreases dramatically up to half of the flight about 24 second due to negative gravity force. And then it is seen from Figure 50 that the velocity decreases until about 320 m/s. The munition muzzle velocity is 826 m/s and it decreases because of axial force and gravity force.

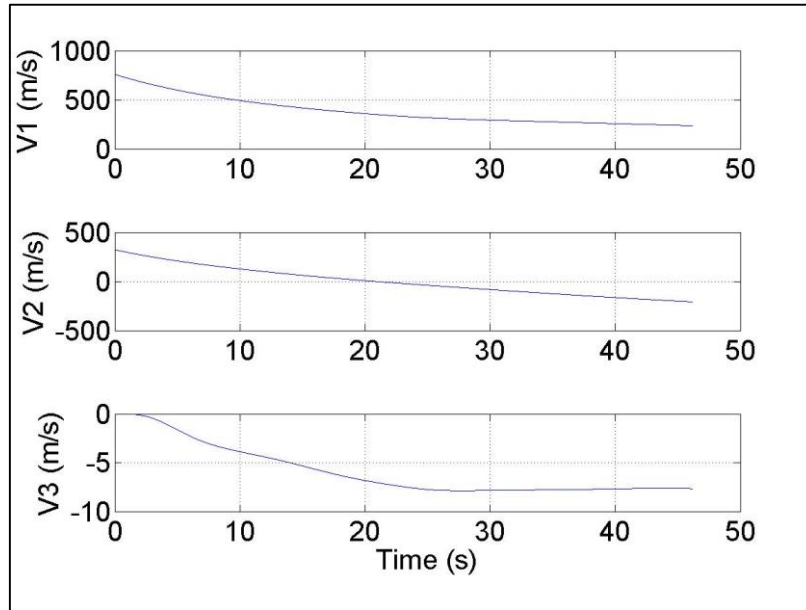


Figure 51. Velocities vs Time for the Developed Code

Figure 51 shows all velocities of the munition in meter per second according to time in second. Figure 51 includes three figures, which show velocity of the munition according to directions of the coordinate system. The vertical axes of the figure are the velocity 1, velocity 2 and velocity 3 respectively. The horizontal axis is the time.

It is expected that velocity 1 should decrease along the flight because of axial force on the munition. The other one is velocity 2 is upward velocity and it is affected from negative gravity force up to half of flight and then positive gravity force affects the munition up to end of the flight. Thus, velocity 2 decreases and reaches to 0 and then increases. The last one is the velocity 3, which is side velocity. The velocity 3 causes to the munition's deflection. It is better to be close to 0 because side velocity causes to deflection.

5.3 Comparison between PRODAS and the Developed Code

Equations of motion of the munition are determined to describe flight behavior of the spin stabilized munitions under the aerodynamic forces and moments in 3.3 and 3.4.

The results of the munition’s flight behavior are shown and discussed about their feasibility in 5.2. However, software should be used to check the results and be sure of results accuracy. Thus, PRODAS software is used to check the results of the developed code. It is known that the software does not give exact results but it gives an opinion for the validity of the developed code.

Differences between the developed code and PRODAS are obtained for all results. However, the differences are not so critical to evaluate reliability and feasibility of the results because trend of the results are more important to evaluate reliability and feasibility of the results. The figures in this section are not same completely with the figures in 5.2 because of limited PRODAS results.

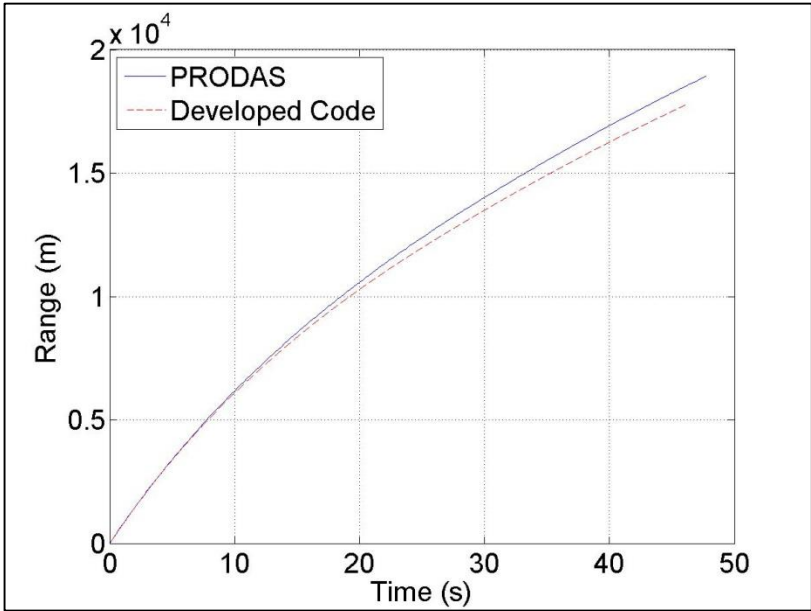


Figure 52. Range vs Time for Comparison

Figure 52 shows the range of the munition in meter vs time in second though the flight. The vertical axis of the figure is the range of the munition, and the horizontal axis is the flight time. The figure is given to obtain the difference between the ranges for PRODAS and developed code. The solid line of the figure is result of the developed code and dashed line shows PRODAS result.

Figure 52 shows the difference of the range between PRODAS solutions, which is talked about at 2.5, and the developed code without any control, which is also discussed at 5.2. The range is about 17788 meters according to the developed

code and 18920 meters according to PRODAS results. It is known that PRODAS is not exact solution for spin stabilized munitions. However, similarity of solutions gives an opinion about reliability and accuracy of the results.

$$Difference \% = \frac{|PRODAS - Calculation|}{PRODAS} \quad (5.1)$$

$$\frac{|18920 - 17788|}{18920} = 6\% \quad (5.2)$$

The difference of the ranges between the developed code and PRODAS is 6%, which is found in (5.2).

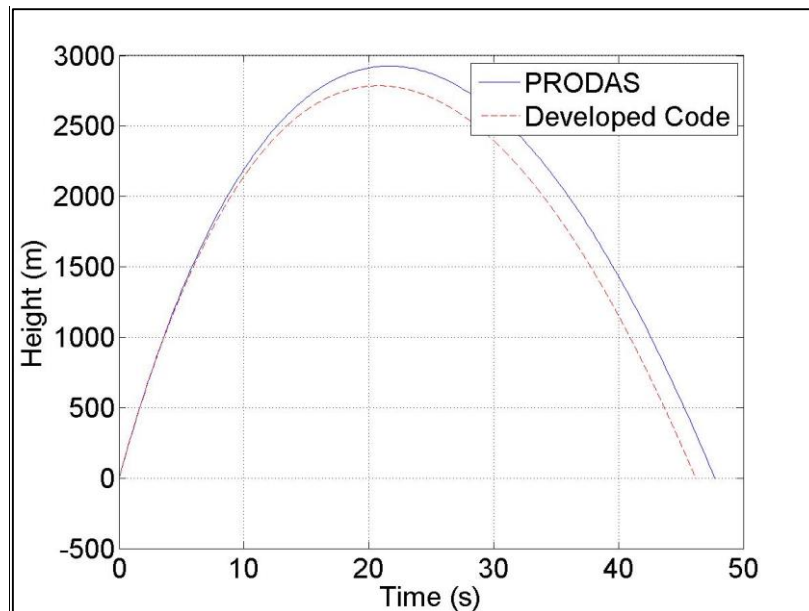


Figure 53. Height vs Time for Comparison

Figure 53 shows the height of the munition in meter vs time in second during the flight. The vertical axis of the figure is the height of the munition, and the horizontal axis is the flight time. Figure 53 is side view of the munition during the flight without control mechanism. The dashed line of the figure is result of the developed code and solid line shows PRODAS result.

Figure 53 is side view of the munition trajectory. The munition rises up to about 2920 m above the ground according to PRODAS solution. The calculation of

ballistic flight is done with same initial conditions, which are used also in PRODAS, by using developed code. The figure shows height of the trajectory and its maximum value is about 2787 m in the developed code. It could be understood from Figure 53 that results are very close each other and their trends are very similar. The height of the munition is 5% is found in (5.3) at the end of flight.

$$\frac{|2920 - 2787|}{2787} = 5\% \tag{5.3}$$

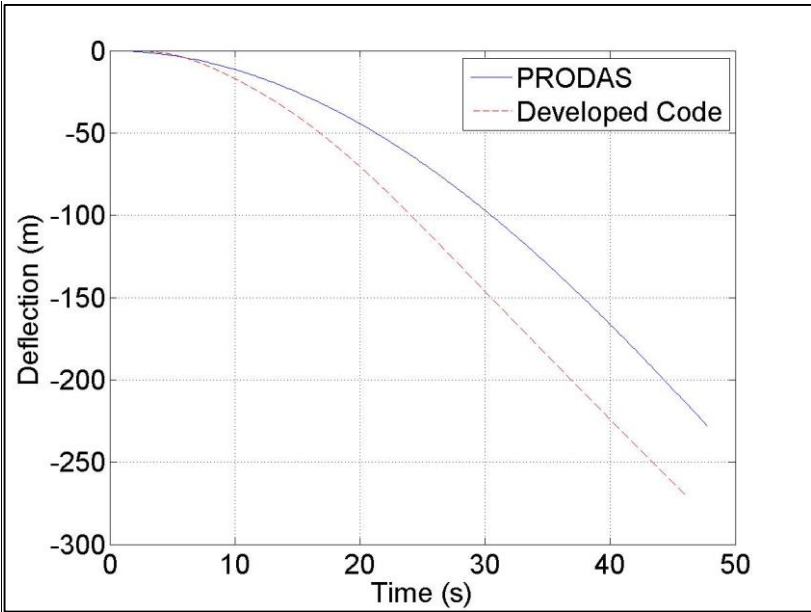


Figure 54. Deflection vs Time for Comparison

Figure 54 shows the deflection of the munition in meter vs time in second though the flight. The vertical axis of the figure is the lateral deflection of the munition, and the horizontal axis is the flight time. Figure 54 is top view of the munition during the flight without control mechanism. The dashed line of the figure is result of the developed code and solid line shows PRODAS result.

Comparison of lateral deflection for PRODAS and the developed code is given in Figure 54. Standard 155 mm spin stabilized munitions always deflect from the target to left side naturally due to Magnus effect of the spin velocity vector.

Lateral deflection of PRODAS is 227 meters to left side. On the other hand, the munition deflects from the target about -271 meters for developed code.

Deflection directions of munitions are the same. Although the difference is about 15%, the trends of results are very similar to each other.

$$\frac{|(-227) - (-271)|}{271} = 15\% \quad (5.4)$$

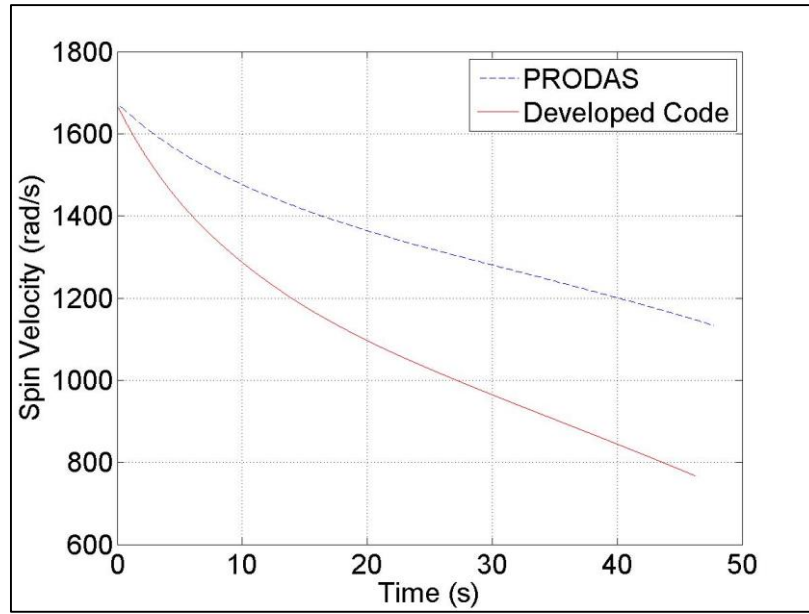


Figure 55. Spin Velocity vs Time for Comparison

Figure 55 shows spin velocity in radian per second of the munition through the flight. The vertical axis of the figure is spin velocity and the horizontal axis is time in second. The solid line of the figure is result of the developed code and dashed line shows PRODAS result.

The other parameter is spin velocity or roll velocity of the munition. Figure 55 differs from other figures because error of Figure 55 is the highest one. Both analyses are done with same initial condition and start from 1669.1 rad/s the spin velocity, which decreases to 1133 rad/s for PRODAS analysis. However, the spin velocity decreases to 768 rad/s for the developed code due to spin damping moment.

$$\frac{|1133 - 768|}{1133} = 30\% \quad (5.5)$$

Although the difference is the highest one, they have a similar trends and it is also known that PRODAS does not give an exact solutions. Therefore, the results support in each other.

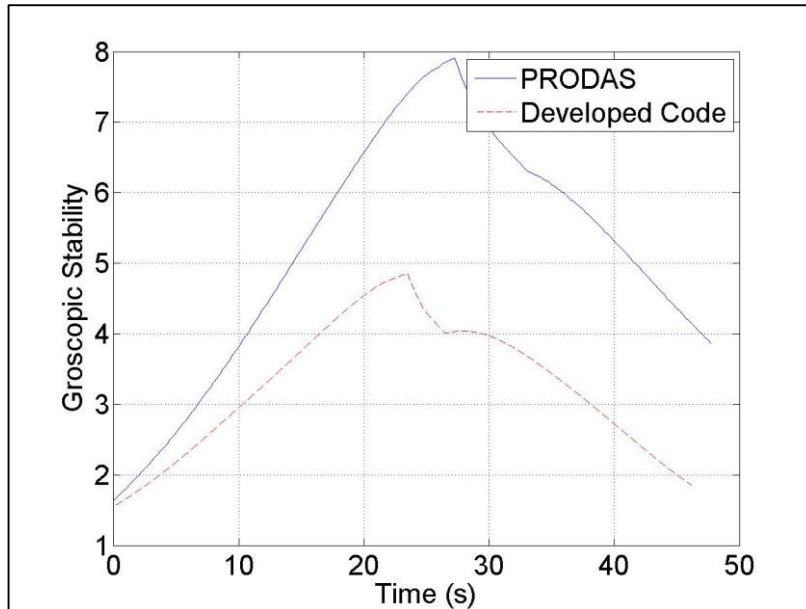


Figure 56. Gyroscopic Stability vs Time for Comparison

Figure 56 shows the gyroscopic stability of the munition through the flight. The vertical axis of the figure is the gyroscopic stability and the horizontal axis is time in second. The solid line of the figure is result of the developed code and dashed line shows PRODAS result.

Comparison of the gyroscopic stability is done and given in Figure 56. The gyroscopic stability varies with time and trends of analysis are very similar along the flight. The stability increases from beginning of the flight to about half of the flight for both analyses because the velocity of the munition decreases up to half of the flight significantly. Both of them also decrease from half of the flight to end of the flight.

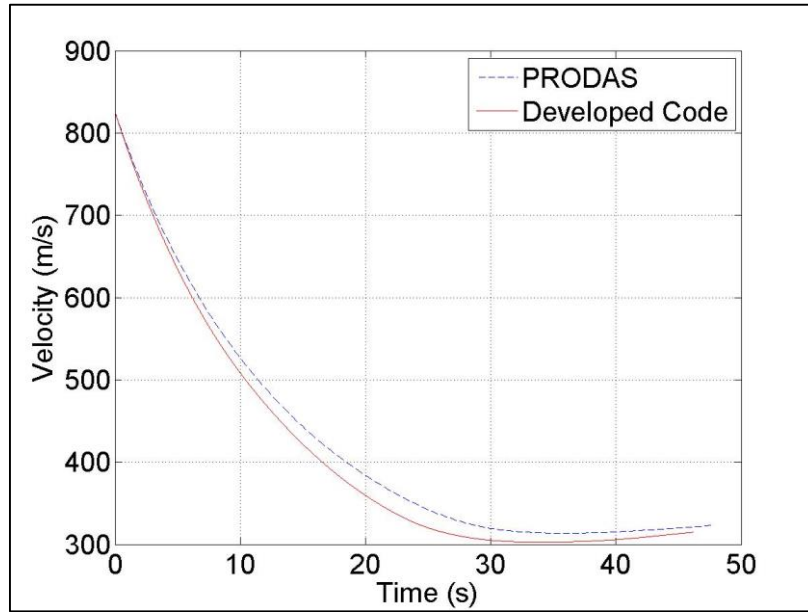


Figure 57. Velocity vs Time for Comparison

Figure 57 shows the velocity of the munition in meter per second and time in second. The vertical axis of the figure is the velocity of the munition, which is from muzzle exist to end of the flight. The horizontal axis is the time. The solid line of the figure is result of the developed code and dashed line shows PRODAS result.

The velocities of the analyses coincide in each other along the flight. Velocities start from about 826 m/s and then decrease about 300 m/s at half of the flight. However, the velocities increase up to about 325 m/s at the end of flight.

$$\frac{|323 - 315|}{323} = 3\% \quad (5.6)$$

The error is 3%, which is the smallest difference. As well as, the trends are so similar along the flight.

5.4 Control Authority Results and Discussion

Classic spin stabilized munitions, which are unguided munitions, are used with a high circular error probable in a war zone. The circular error probable of these munitions, which is discussed in 5.2, is about 267 meters. It means that the munition cannot usually hit the target at the first attempt. In other words, chance of hitting the

target passes through an enemy because there is generally only one chance to hit the target in a war zone due to detection of own position in first launch. Thus, it is very important to hit the target position at the first attempt under any disturbance. There are some studies about the modification of unguided spin stabilized munitions to convert guided spin stabilized munitions to hit the targets precisely under the disturbance and especially wind. Therefore, a control authority, which can change the trajectory of the munition and hit the target position under high wind effect, is needed. An actuation system is needed to guide the munition and obtain the control authority. The Nose Actuation Kit is designed and added to the nose part of the standard 155 mm spin stabilized munition for creating the control authority and position correction of spin stabilized munitions under wind effect.

The munition, whose stability is supported by high spin velocity, could fly very long time in its trajectory, which is planned before. The range of the munition and a natural deflection due to Magnus effect are known before the launch without any disturbance according to initial elevation and azimuth angle of the muzzle. However, if there is some disturbance especially the wind effect on the munition, the trajectory of the munition can change significantly. The wind effect changes the final position of the munition considerably. The wind effect is added to the developed code, whose accuracy is checked by PRODAS and results are given 5.2 and 5.3 respectively, to obtain deflection of the munition under wind effect. Before the wind effect is added to the developed code, wind velocities in the World and especially Turkey were researched because maximum wind velocity, which is encountered in a war zone, is not known. The maximum wind velocity can be taken 15 m/s according to weather reports in Turkey [37]. However, maximum wind velocity is taken about 30 m/s in defense industry [38] so the control authority with the nose actuation kit must be able to cover 30 m/s wind velocity deflection zone. The analyses are also done for 10 m/s, 20 m/s and 30 m/s wind velocities to understand maximum capability of mechanism control authority. Analyses are run for several times to determine wind deflection zones. The analyses are repeated with different wind directions, which are from 0 degree to 360 degrees with 30 degrees increments, and wind magnitudes for 10 m/s, 20 m/s and 30 m/s. Therefore, three deflection zones for

10 m/s, 20 m/s and 30 m/s wind velocities are determined and given with base point, which is the final position of the munition without wind and mechanism forces, in Figure 58.

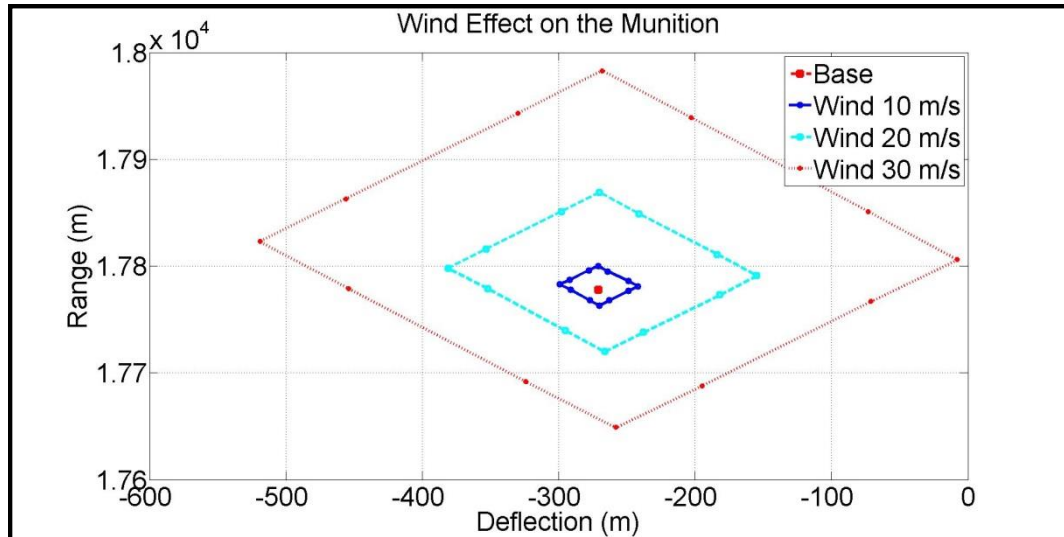


Figure 58. Wind Effects on the Munition

The horizontal axis of Figure 58 is deflection in meter. It is the lateral dispersion of the munition. The vertical axis of Figure 58 is range in meter. The range is also called the longitudinal dispersion of the munition. The base point at (-271, 17778) is shown with a square point. When the munition is launched with the initial conditions, which are given in Table 5, the final position is the square point, which is given in 5.2. The lateral dispersion of the munition occurs due to Magnus effect so it is called a natural deflection. The deflection zones in Figure 58 are diamond shape because constant wind velocities are taken though the flight. In other words, when the wind velocity on the munition is taken 10 m/s and it is applied to 90 degrees direction in short the positive lateral direction, the munition reaches to right point of the 10 m/s wind deflection zone. However, when the wind velocity is applied to 270 degrees direction in short the negative lateral direction, the munition reaches to left point of the 10 m/s wind deflection zone. The analyses are done for different wind velocity directions with 30 degrees increments and diamond shape comprises. Therefore, the boundaries of the 10 m/s wind deflection zone is created and shown with solid line in Figure 58. If the wind velocity is lower than 10 m/s, the final position of the munition is in 10 m/s wind deflection zone in Figure 58. The

other wind deflection zones are for 20 m/s and 30 m/s, which are shown with dashed and dotted line respectively. They are created with same procedure of 10 m/s wind deflection zone. The deflection zones for 20 m/s and 30 m/s wind velocities are much bigger than the deflection zones for 10 m/s wind velocity because wind velocity affect the trajectory and final position of the munition exponentially. Therefore, wind effects on the munition are surveyed without mechanism force and wind deflection zones are obtained for different wind velocities.

The effect of the mechanism is added to the developed code to investigate a control capacity of the mechanism without wind effect. The variables of the mechanism, which are inputs to the developed code, are mechanism force and its direction. One of the variables is mechanism force, which is calculated according to equation (5.7).

$$\vec{F}_{Mec} = \frac{1}{2} \rho V^2 S C_{L_mec} \quad (5.7)$$

Air density (ρ) in equation (5.7) is determined according to altitude of the munition. The velocity (V), which is also given in Figure 18, is also calculated in the developed code though the flight and lift coefficient of the mechanism fins (C_{L_mec}) is calculated for NACA 6412 airfoil [27]. The last one in equation (5.7) is surface area of fins (S), which must be chosen to design the nose actuation kit. $1 \times 10^{-4} \text{ m}^2$, $2 \times 10^{-4} \text{ m}^2$, $3 \times 10^{-4} \text{ m}^2$, $4 \times 10^{-4} \text{ m}^2$ and $5 \times 10^{-4} \text{ m}^2$ fin surface areas are entered into equation (5.7) respectively. However, fin surface areas, which are bigger than $5 \times 10^{-4} \text{ m}^2$, are not entered into the developed code because high mechanism effects cause to instability on the munition. After the fin surface areas in the developed code were stated, the other variable, which is a force direction, is also entered into the developed code.

The developed code with $1 \times 10^{-4} \text{ m}^2$ fin surface area is run for different force directions, which are from 0 degree to 360 degrees with 30 degrees increment similar to determining wind effect zone. The direction of the mechanism is given according to x axis of the munition's body fixed frame. In other words, the mechanism force, which direction is 0 degree, implies upward direction. The mechanism force, which

direction is 90 degree, implies positive side direction. About 12 analyses are run to generate the mechanism effect zone for $1 \times 10^{-4} \text{m}^2$ fin surface area. The points, which the munition reaches at the end of the flight, are determined according to analyses results. These points constitute the border of mechanism effect zone for $1 \times 10^{-4} \text{m}^2$ fin surface area. Then, the other analyses are run for $2 \times 10^{-4} \text{m}^2$, $3 \times 10^{-4} \text{m}^2$, $4 \times 10^{-4} \text{m}^2$, $5 \times 10^{-4} \text{m}^2$ fin surface areas with variable force directions. Thus, mechanism effect zones are obtained for different fin surface areas similar to wind effect zones and Figure 59 is obtained.

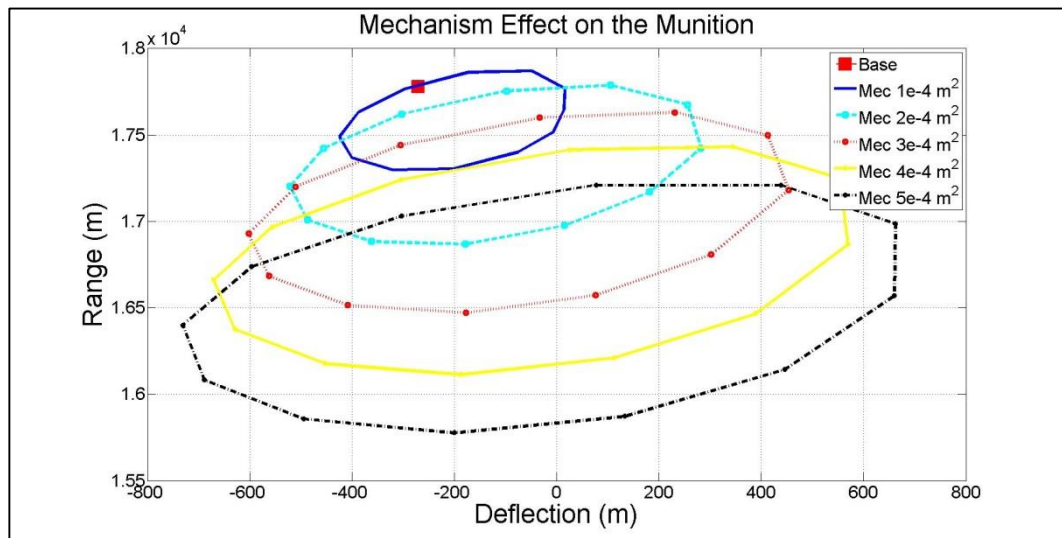


Figure 59. Mechanism Effect on the Munition

Figure 59 shows the mechanism control zones for different fin surface areas without wind effect. The horizontal axis of Figure 59 is deflection in meter. It is also called the lateral dispersion of the munition. The vertical axis of Figure 59 is the range in meter. It is also called the longitudinal dispersion of the munition. The base point is also shown with square point. When the munition is launched with the initial conditions, that are given in Table 5, the final position is square point $(-271, 17778)$, that is given in 5.2. The smallest zone is for $1 \text{e-}4 \text{ m}^2$ fin surface area, that is the smallest fin surface area, and it is given in Figure 59 by solid line. The final positions of the munition for $1 \times 10^{-4} \text{m}^2$ fin surface area and different force directions comprise the border of the solid line. It also means that the munition can reach any point in this zone with the mechanism force, whose fin surface area is $1 \times 10^{-4} \text{m}^2$, when guidance control workout is done and added. The shape of the mechanism

effect zones is different from the shape of the wind effect zones because of some reasons. One of the reasons is that moments on the munition, which is due to wind force, is too small to affect the munition final position but moments of the mechanism force on the munition bigger. The moments affect the total angle of attack and the final position of the munition significantly. The other reason is that wind force is taken constant and it affects the munition final position linearly but mechanism force varies according to altitude and velocity of the munition. When the fin surface area is bigger, the mechanism effect zone is bigger. However, maximum range, that the munition can reach, decrease because the mechanism moment affects the total angle of attack of the munition and so the munition loses its energy due to drag force.

It is seen that when the mechanism force increases, mechanism effect zone is much bigger. However, this does not mean that the fin surface area could be chosen as big as possible because all analyses are done with stability calculations, which are gyroscopic and dynamic stability. The munition becomes unstable for fin surface area, which is bigger than $3 \times 10^{-4} \text{m}^2$, because fin forces and moments change the munition trajectory significantly. The forces and moments of the mechanism affect the linear, spin velocities and nose direction of the munition so stability of the munition is affected by the mechanism directly. An optimum fin surface area, which is the biggest surface area and does not cause to instability, should be found and fins are designed according to the optimum fin surface area. The fin surface area value should be also enough to cover at least 30 m/s wind deflection zone.

Gyroscopic and dynamic stability factors are calculated for all analyses when the borders of the mechanism effect zones are obtained. It is seen that the munition becomes unstable for $4 \times 10^{-4} \text{m}^2$ and $5 \times 10^{-4} \text{m}^2$ fin surface areas. Therefore, the biggest value of the fin surface area, which is also smaller than $4 \times 10^{-4} \text{m}^2$ surface area and cover maximum wind effect area, is $3 \times 10^{-4} \text{m}^2$ so it is chosen to design the mechanism fins.

Final positions of the munition were described under wind effects with different direction in Figure 58. In addition, mechanism effect on the munition was also described without wind effect for maximum fin surface area in Figure 59.

In other words, maximum control zone with $3 \times 10^{-4} \text{m}^2$ fin surface area was determined and maximum wind effect zone, which is covered by the mechanism, was obtained. The critic wind velocity is 30 m/s because this velocity is used as a maximum wind velocity in defense industry projects. Therefore, the mechanism effect zone for $3 \times 10^{-4} \text{m}^2$ fin surface area is added to Figure 58 and finally Figure 60 is obtained.

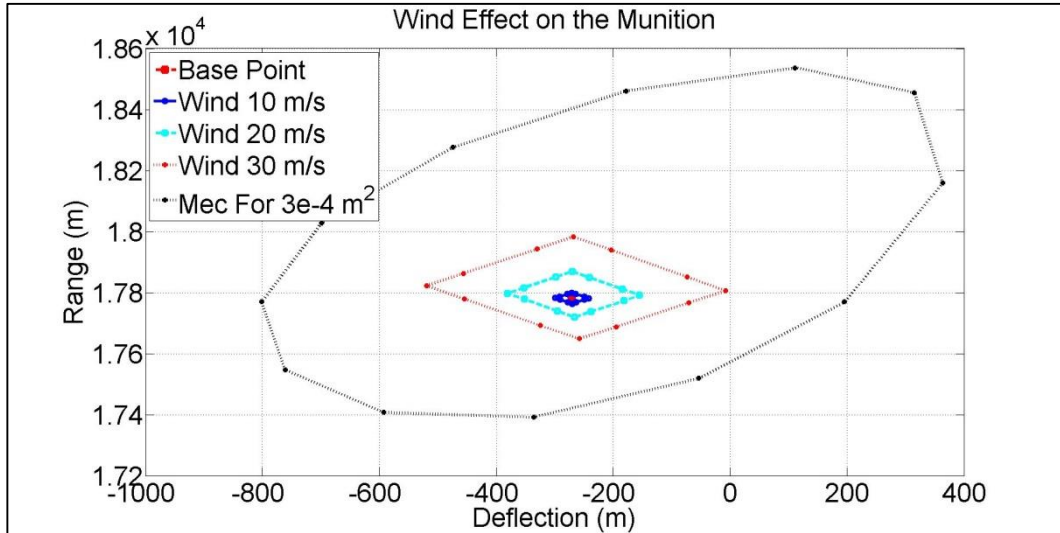


Figure 60. Mechanism and Wind Effects on the Munition

The figure properties are same with Figure 58 and Figure 59. The base point, which is given in Figure 60, is also final position of the munition without any disturbance and mechanism force. Wind velocity zones were also described and known from Figure 58. It is important in Figure 60 that 30 m/s wind zone, which is the biggest velocity zone, is covered by the mechanism or not. The mechanism control zone with $3 \times 10^{-4} \text{m}^2$ fin surface area can cover the all velocities zone easily so it can be said that the control authority with $3 \times 10^{-4} \text{m}^2$ fin surface area is enough in battle conditions. Therefore, the munition could be launched and reach the desired final position with effective guidance under maximum 30 m/s wind velocity. It is not ensured that the munition follows the its trajectory effectively under more than 30 m/s wind velocity, which is not expected in the standard air conditions. Defense industry projects take maximum 30 m/s wind velocity in operations. The mechanism can cover all wind velocity zones with the fin surface area.

CHAPTER 6

CONCLUSION AND FUTURE WORK

6.1 Conclusion

In this thesis the possibility of controlling standard 155 mm spin stabilized munitions to reduce miss distances under the wind effect is investigated. There are limited mechanism options to control spin stabilized munitions because they are launched from muzzle with high spin velocity [15]. After a thorough literature survey about mechanism design options, an original mechanism is designed to control the munition. The mechanism is added to nose part of the munition and mechanism fins create the control surfaces to change the trajectory of the munition. Although the trajectory of spin stabilized munitions can be obtained by only the software like PRODAS, a code is developed to obtain equations of motion with aerodynamic forces and moments for spin stabilized munitions so exact wind and mechanism effects on the munition can be observed as well. PRODAS software extracts the trajectory of the munition statistically and it is known that the software is not correct a hundred percent. However, the comparison is done between results of the developed code and the software to check the results of the developed code. Moreover, analyses are repeated for different spin velocity, which are zero, lower and higher than the spin velocity given in Table 5. The analyses for different spin velocities are compared in each other to observe the flight behavior changes. Mechanism effect, which is added to the developed code, must provide necessary forces and moments so that the munition reaches the desired final position. Mechanism design options of the mechanism are interviewed and searched in literature surveys and original mechanism design is decided to control the munition. The original mechanical design contains a selection of standard components like motor and bearings, fin profiles of the mechanism and designing of the other components. Mathematical model of the mechanism, which contains motor parameters, transmission ratio of the mechanism and moments of inertia of

components, is obtained to design control block by using PID controller. Wind velocities are searched for defense industry applications. The maximum wind velocity, which can be encountered in war zone, is found. Calculations with the developed code are repeated for the munition under different wind velocities. Hundreds of calculations are done for different wind velocities and wind directions to obtain wind effect zones. Similar calculations with the developed code are repeated for different fin surface areas and force directions to obtain mechanism effect zones, which also cover the wind effect areas.

Aerodynamic coefficients of the munition have to be obtained to determine equations of motion. There are some software options to get aerodynamic coefficients like ANSYS and PRODAS. PRODAS is chosen for these coefficients due to fast running and shareware license opportunity. Moreover, there is a standard 155 mm spin stabilized munition model in PRODAS database for users. Initial conditions, like linear and spin velocities, are also chosen according to vehicles like tanks and howitzers. Aerodynamic coefficients, which does not contain mechanism fin lift coefficient, are obtained between 0.6 Mach and 3 Mach. After getting the coefficients, trajectory of the munition can be determined easily with the initial conditions.

Moreover, transformation matrix is obtained to extract relationship between body fixed and earth fixed coordinate system. All aerodynamic coefficients, which are given with physical meanings of linear and nonlinear parts, are discussed and vector quantities of forces and moments are defined according to nose and velocity vector of the munition. Linear and rotational accelerations are determined by using aerodynamic forces and moments. Linear, rotational velocities and positions are found according to these accelerations in body and earth fixed coordinate systems. Munition body parameters like weight, moments of inertia and dimensions of the munition are also given. Body parameters of the munition are taken for standard 155 mm spin stabilized munitions, whose parameters could be found easily in literature, because it is a common munition all over the World. After equations of motion are calculated, the developed code is created and run.

On the other hand, solid model and controller design of the mechanism are discussed. Similar systems are interviewed and unique design is done for the mechanism. Mechanism fins could be plate with initial angle of attack but drag force of plate surfaces is larger than NACA fin profiles so NACA 6412 is chosen for mechanism fins. NACA 6412 lift and drag coefficients are given proportional to angle of attack of the munition. The mechanism design contains shell, fins, power supply and standard elements, which are motor and bearings. The standard elements are selected according to spin velocity and maximum torque, which comes from the mechanism. The spin velocity for though the flight is calculated by using the developed code. Mechanism forces and moments are also determined according to drag and lift forces of the mechanism fins. A lot of bearings can be selected from catalogs, which satisfy maximum angular velocity of system and radial and axial force on bearings. However, limited options are found for motor, which satisfy maximum angular velocity with needed torque. Selected motor must satisfy the requirements, which are spin velocity and maximum torque of the mechanism. Another challenge is controller design of the mechanism to fix the fins at desired roll angle. Moments of inertia of the mechanism components are determined but motor moment of inertia could be taken from catalog, which gives motor properties. Transmission ratio is also needed and determined between roll velocity of motor and the mechanism. Mechanism mathematical model is created by using moments of inertia, transmission ratio of mechanism. PI Controller was tried to use in control block. However, it is seen that PID controller performance with suitable coefficients is better due to derivative effect of the controller. The PID controller coefficients can be calculated by two ways, which are tune method of Matlab and Butterworth method. The mechanism needs less current to track the reference angle for PID controller, whose coefficients are calculated with Butterworth method, so the PID controller coefficients are calculated by using Butterworth method.

To conclude, an optimum step size frequency of the developed code is searched according to speed and accuracy of calculations so 500 Hz step size frequency is decided because there are negligible changes at the final positions of the munition but run time of calculations increase dramatically for higher step size

frequency more than 500 Hz. The analyses of the developed code are done and the results are given. Moreover, the analyses are repeated for different spin velocity of the munition to obtain effect of the spin velocity on the munition. The results of developed code are compared with PRODAS results and an average 10% difference is seen. However, trends of results are more important than differences because it is not sure that the results of PRODAS are a hundred percent accurate. Thus, all trends between developed code and PRODAS results are too similar to continue works. The munition is launched with the initial conditions in Table 5 without wind and mechanism effect. Final position is determined under these circumstances. The munition is also launched under different wind velocities and directions again and again so wind effect zones are obtained and given. On the other hand, the munition is launched under mechanism effect with different force direction and fin surface areas, which cause different mechanism forces, several times so mechanism effect zones are obtained and given as well. Maximum fin surface area is also determined because of stability problem. Therefore, a control authority is obtained and showed that wind effect zones are covered by the maximum fin surface area.

6.2 Future Work

This thesis is created with some assumptions and the calculations are done by using these assumptions. However, these assumptions create uncertainty about behavior of the munition in real conditions. Future works include proving of the assumptions, which are control performance in reality, accuracy of aerodynamic coefficients and sensor data, so the performance of the munition is ensured in real conditions. The PID controller with calculated coefficients generally shows a good performance in theory. However, when the controller with calculated coefficients is used in real systems, its performance can decrease due to disparity between controller coefficients, which are designed theoretically, and real system. It is planned to produce the mechanism with a dummy standard 155 mm spin stabilized munition body and design controller coefficients according to real system. Moreover, while controller coefficients are designed again with real mechanism and test

apparatus, sensor data will be verified because the accuracy of the sensor is assumed perfect. The other assumption is accuracy of aerodynamic coefficients. All forces and moments on the munition are calculated by using these aerodynamic coefficients so their accuracy is so important to get accurate results. The coefficients are taken from PRODAS software, which runs statistically, but any other method is not used to check accuracy of the coefficients of this software so it is planned to do wind tunnel test of mechanism solid model with 155 mm munition body and get aerodynamic coefficients experimentally.

It is discussed that there is a control authority under wind effect for 155 mm spin stabilized munitions in the thesis. The mechanism, which can change the trajectory according to guidance orders, is designed. Wind effect areas are created with different wind magnitudes and directions for the munition. The maximum fin surface area is found to satisfy stability condition of the munition and cover the wind effect zones. The control authority shows that the munition could reach any point under the wind effect. Thus, guidance and control section will be designed for this control authority to reach the target position with guidance orders under the wind effect precisely.

REFERENCES

- [1] M. D. Ilg, Guidance, Navigation and Control for Munitions, PhD Thesis, Drexel University, 2008.
- [2] R. McCoy, Modern Exterior Ballistic, Schiffer Publ. Co., 1999.
- [3] "CP Library," Rocket Reviews, [Online]. Available: <http://www.rocketreviews.com/what-is-cp.html>. [Accessed 1 January 2016].
- [4] "Actuation Systems," UTC Aerospace System, [Online]. Available: <http://utcaerospacesystems.com/cap/systems/Pages/actuation-systems-business.aspx>. [Accessed 3 September 2015].
- [5] T. U. Ölçer, "H₂/H_∞ Mixed Robust Controller Synthesis for a Fin Actuation System, MSc Thesis," Middle East Technical University, Ankara, 2013.
- [6] İ. Yavrucuk, "Flight Dynamics Course Notes," Middle East Technical University, Ankara, 2011.
- [7] "Gyroscope," Oxford Dictionary, [Online]. Available: <http://www.oxforddictionaries.com/definition/english/gyroscope>. [Accessed 4 March 2015].
- [8] T. A. Guide, "Long Range Shooting," The Arms Guide, [Online]. Available: <http://thearmsguide.com/6211/long-range-shooting-external-ballistics-static-stability/>. [Accessed 1 January 2016].
- [9] E. R. Courtney and M. W. Courtney, "Aerodynamic Drag and Gyroscopic Stability," *arXiv preprint arXiv*, vol. 1309, no. 5039, 2013.
- [10] J. S. Francisco and E. Kristopher, "An Evaluation of Yuma Proving Grounds Ballistic Arsenal Scoring Methods," Naval

Postgraduate School, 2005.

- [11] "PRODAS Software Products Catalog," Arrow Tech, Burlington Vermont, 2013.
- [12] "PID Controller," Wikipedia, [Online]. Available: http://en.wikipedia.org/wiki/PID_controller. [Accessed 24 September 2015].
- [13] "Joint Direct Attack Munition," Navy Military, [Online]. Available: http://www.navy.mil/navydata/fact_display.asp?cid=2100&tid=400&ct=2. [Accessed 28 February 2015].
- [14] P. J. B., "XM1156 Precision Guidance Kit," in *Fuze Conference*, 2010.
- [15] M. Eroğlu, A. Kutay, G. Tombul and B. Özkan, "Kanatçıklı Dönü Kararlı Mühimmatların Dinamik Modellenmesi ve Denetim Yaklaşımlarının İncelenmesi," UMTS, İzmir, 2015.
- [16] "Smart 155," Wikipedia, [Online]. Available: https://en.wikipedia.org/wiki/SMArt_155. [Accessed 30 January 2015].
- [17] "External Ballistic," Wikipedia, [Online]. Available: https://en.wikipedia.org/wiki/Ballistics#External_ballistics. [Accessed 5 January 2015].
- [18] M. Khali, H. Abdalla and O. Kamal, "Dispersion Analysis for Spinning Artillery Projectile," in *In: Proc., 13th Int. conf. on Aerospace Science and Aviation Technology, ASAT-13-FM-03, Military Technical College,, Cairo, Egypt*, 2009.
- [19] "Long Range Shooting: External Ballistics – Spin Drift," The Arms Guide, [Online]. Available: <http://thearmsguide.com/5346/long-range-shooting-external-ballistics-spin-drift-13-theory-section/>. [Accessed 13 March 2015].
- [20] C. Theodore, "Helicopter Flight Dynamics Simulation With

Refined Aerodynamic Modeling, PhD Thesis," University of Maryland, College Park., 2000.

- [21] "Aerodynamic Force," Wikipedia, [Online]. Available: http://en.wikipedia.org/wiki/Aerodynamic_force. [Accessed 14 March 2015].
- [22] "PRODAS Aerodynamic Forces & Moments," Arrow Tech, Burlington Vermont, 2015.
- [23] "Dynamic Pressure," NASA, [Online]. Available: <https://www.grc.nasa.gov/www/k-12/airplane/dynpress.html>. [Accessed 29 March 2015].
- [24] F. Fresconi and G. Cooper, "Flight Mechanics of a Novel Guided Spin-Stabilized Projectile Concept," *Proceedings of the Institution of Mechanical Engineers, Part G: Journal of Aerospace Engineering*, no. 0954410011408385, 2011.
- [25] "Equations of Motion," Wikipedia, [Online]. Available: https://en.wikipedia.org/wiki/Equations_of_motion. [Accessed 3 January 2016].
- [26] "Engineering Design Service," Design Tech, [Online]. Available: <http://www.designtechsys.com/articles/engineering-design-services.php>. [Accessed 23 April 2015].
- [27] "NACA 6412," Airfoil Tools, [Online]. Available: <http://airfoiltools.com/airfoil/details?airfoil=naca6412-il>. [Accessed 12 June 2015].
- [28] "Deflections in Simply Supported Beams," Mathalino, [Online]. Available: <http://www.mathalino.com/reviewer/mechanics-and-strength-materials/solution-problem-659-deflections-simply-supported-beams>. [Accessed 8 September 2015].
- [29] "Drag Coefficient," Wikipedia, [Online]. Available: https://en.wikipedia.org/wiki/Drag_coefficient. [Accessed 2 November

- 2015].
- [30] K. Ogata, *Modern Control Engineering*, New Jersey: Prentice Hall Inc., 2002.
- [31] E. Daş, *Güdümlü Bir Mühimmat Kanatçık Tahrik Sistemi İçin İki Döngülü Kontrol Sistemi Tasarımı*, MSc Thesis, İstanbul Technical University, 2014.
- [32] "DC Motor," Wikipedia, [Online]. Available: https://en.wikipedia.org/wiki/DC_motor. [Accessed 3 August 2015].
- [33] İ. İ. Delice, G. S. Tombul and B. Özkan, "Kesir Dereceli Denetim Yaklaşımının Kanatçık Eyletim Sistemine Gerçek," TOK, Niğde, 2012.
- [34] E. Daş, İ. İ. Delice and L. Gören, "Güdümlü Bir Mühimmat Kanatçık Tahrik Sistemi İçin İki Döngülü Kontrol," TOK, Kocaeli, 2014.
- [35] "Bandwidth," Wikipedia, [Online]. Available: [https://en.wikipedia.org/wiki/Bandwidth_\(signal_processing\)](https://en.wikipedia.org/wiki/Bandwidth_(signal_processing)). [Accessed 9 January 2016].
- [36] "Circular Error Probable," Word Press, [Online]. Available: <https://metinmediamath.wordpress.com/2013/10/10/missile-accuracy-cep/>. [Accessed 10 January 2016].
- [37] H. Edremitoğlu, K. Toydemir and O. Başkan, *Economical, Environmental Outcomes of Wind Energy Production in Turkey*, Worcester Polytechnic Institute (degree of Bachelor of Science), 2007.
- [38] J. C. Baker, A. Bouferrouk, J. Perez and S. D. Iwnicki, "The Integration of Cross Wind Forces into Train Dynamic Calculations," *In: World Congress on Railway Research*, pp. 18-22, 2008.
- [39] "NACA 6412," Airfoil Tools, [Online]. Available: <http://airfoiltools.com/airfoil/details?airfoil=naca6412-il>. [Accessed 8 June 2015].

- [40] M. Green and D. J. Limebeer, *Linear Robust Control*, Courier Corporation, 2012.
- [41] M. J. Grimble, *Robust Industrial Control Systems-Optimal Design Approach for Polynomial Systems*, John Wiley & Sons, 2006.

APPENDICES

Appendix A: PRODAT Results

Table 9. Munition Trajectory Analysis by PRODAT Software

Time	X	Y	Z	Slant	Velocity	Spin	A_Bar	Gyro
sec	m	m	m	m	m/sec	rad/sec	deg	
0	0	0	0	0	826	1674.81	0	1.64
0.5	375.53	-0.03	158.16	407.48	804.08	1660.36	0.02	1.73
1	742.06	-0.12	310.11	804.25	783.2	1646.61	0.04	1.81
1.5	1100.02	-0.27	456.1	1190.82	763.29	1633.52	0.04	1.9
2	1449.81	-0.47	596.34	1567.66	744.3	1621.02	0.04	2
2.5	1791.82	-0.74	731.04	1935.21	726.16	1609.09	0.05	2.09
3	2126.4	-1.06	860.4	2293.87	708.84	1597.68	0.05	2.19
3.5	2453.88	-1.44	984.61	2644.04	692.27	1586.75	0.05	2.29
4	2774.58	-1.88	1103.82	2986.09	676.42	1576.27	0.06	2.39
4.5	3088.79	-2.37	1218.2	3320.34	661.22	1566.21	0.06	2.5
5	3396.76	-2.92	1327.9	3647.1	646.59	1556.55	0.07	2.61
5.5	3698.74	-3.53	1433.04	3966.65	632.51	1547.25	0.07	2.72
6	3994.92	-4.19	1533.76	4279.23	618.95	1538.3	0.08	2.83
6.5	4285.54	-4.91	1630.16	4585.11	605.89	1529.68	0.09	2.95
7	4570.78	-5.68	1722.36	4884.52	593.3	1521.36	0.09	3.07
7.5	4850.84	-6.5	1810.47	5177.69	581.16	1513.33	0.1	3.19
8	5125.91	-7.38	1894.59	5464.84	569.47	1505.54	0.1	3.31
8.5	5396.15	-8.32	1974.82	5746.17	558.21	1497.96	0.11	3.44
9	5661.75	-9.3	2051.25	6021.88	547.36	1490.59	0.12	3.56
9.5	5922.86	-10.35	2123.97	6292.18	536.9	1483.41	0.13	3.69
10	6179.63	-11.44	2193.07	6557.24	526.8	1476.41	0.13	3.82

Time	X	Y	Z	Slant	Velocity	Spin	A_Bar	Gyro
sec	m	m	m	m	m/sec	rad/sec	deg	
10.5	6432.21	-12.59	2258.62	6817.24	517.07	1469.59	0.14	3.96
11	6680.74	-13.79	2320.7	7072.35	507.67	1462.94	0.15	4.09
11.5	6925.34	-15.05	2379.39	7322.71	498.6	1456.44	0.16	4.23
12	7166.16	-16.36	2434.75	7568.49	489.84	1450.1	0.17	4.37
12.5	7403.29	-17.72	2486.85	7809.83	481.39	1443.88	0.18	4.5
13	7636.86	-19.14	2535.75	8046.86	473.22	1437.79	0.19	4.64
13.5	7866.98	-20.6	2581.5	8279.73	465.34	1431.81	0.2	4.78
14	8093.74	-22.12	2624.18	8508.55	457.72	1425.95	0.21	4.92
14.5	8317.25	-23.7	2663.82	8733.45	450.35	1420.2	0.22	5.06
15	8537.6	-25.32	2700.49	8954.55	443.23	1414.55	0.23	5.2
15.5	8754.88	-27	2734.23	9171.95	436.35	1409.02	0.24	5.34
16	8969.16	-28.73	2765.09	9385.75	429.7	1403.62	0.25	5.48
16.5	9180.54	-30.51	2793.12	9596.08	423.27	1398.33	0.27	5.62
17	9389.08	-32.35	2818.35	9803.01	417.06	1393.16	0.28	5.76
17.5	9594.87	-34.23	2840.84	10006.6	411.05	1388.09	0.29	5.9
18	9797.96	-36.16	2860.61	10207.1	405.25	1383.13	0.3	6.04
18.5	9998.43	-38.15	2877.71	10404.4	399.63	1378.26	0.31	6.17
19	10196.3	-40.18	2892.18	10598.7	394.21	1373.48	0.33	6.31
19.5	10391.8	-42.27	2904.05	10790	388.97	1368.77	0.34	6.44
20	10584.7	-44.4	2913.36	10978.4	383.9	1364.12	0.35	6.57
20.5	10775.3	-46.59	2920.14	11164.1	379.01	1359.51	0.37	6.7
21	10963.6	-48.82	2924.42	11347	374.29	1354.96	0.38	6.83
21.5	11149.5	-51.1	2926.24	11527.3	369.72	1350.45	0.39	6.96
22	11333.3	-53.43	2925.62	11704.9	365.32	1346	0.4	7.08
22.5	11514.8	-55.81	2922.59	11880.1	361.07	1341.58	0.42	7.2

Time	X	Y	Z	Slant	Velocity	Spin	A_Bar	Gyro
sec	m	m	m	m	m/sec	rad/sec	deg	
23	11694.2	-58.24	2917.19	12052.7	356.98	1337.22	0.43	7.3
23.5	11871.5	-60.71	2909.44	12223	353.06	1332.92	0.44	7.41
24	12046.8	-63.23	2899.36	12391	349.31	1328.68	0.45	7.51
24.5	12220.1	-65.79	2886.99	12556.7	345.72	1324.49	0.47	7.6
25	12391.5	-68.41	2872.34	12720.2	342.3	1320.35	0.48	7.67
25.5	12560.9	-71.06	2855.44	12881.6	339.1	1316.25	0.49	7.74
26	12728.6	-73.77	2836.31	13041	336.08	1312.2	0.49	7.79
26.5	12894.6	-76.52	2814.96	13198.5	333.27	1308.18	0.5	7.85
27	13058.8	-79.32	2791.41	13354.1	330.65	1304.2	0.51	7.89
27.5	13221.5	-82.16	2765.68	13507.9	328.22	1300.25	0.52	7.78
28	13382.6	-85.05	2737.78	13660.1	326.04	1296.32	0.5	7.55
28.5	13542.3	-87.99	2707.71	13810.6	324.11	1292.38	0.48	7.34
29	13700.7	-90.97	2675.47	13959.7	322.4	1288.45	0.48	7.16
29.5	13857.7	-93.99	2641.08	14107.5	320.89	1284.52	0.48	7.02
30	14013.6	-97.05	2604.53	14253.9	319.56	1280.59	0.46	6.91
30.5	14168.3	-100.16	2565.83	14399.1	318.41	1276.67	0.46	6.8
31	14321.8	-103.31	2524.99	14543.1	317.41	1272.74	0.46	6.7
31.5	14474.3	-106.5	2482.01	14686	316.55	1268.81	0.45	6.6
32	14625.8	-109.72	2436.9	14827.8	315.82	1264.87	0.44	6.51
32.5	14776.3	-112.99	2389.66	14968.7	315.22	1260.93	0.44	6.41
33	14925.8	-116.3	2340.3	15108.6	314.73	1256.99	0.43	6.32
33.5	15074.4	-119.65	2288.83	15247.6	314.34	1253.03	0.42	6.27
34	15222	-123.03	2235.26	15385.7	314.03	1249.07	0.42	6.23
34.5	15368.7	-126.45	2179.6	15523	313.8	1245.11	0.42	6.17
35	15514.5	-129.91	2121.86	15659.5	313.64	1241.14	0.41	6.12

Time	X	Y	Z	Slant	Velocity	Spin	A_Bar	Gyro
sec	m	m	m	m	m/sec	rad/sec	deg	
35.5	15659.4	-133.41	2062.06	15795.1	313.55	1237.16	0.41	6.05
36	15803.4	-136.94	2000.19	15930.1	313.53	1233.17	0.4	5.99
36.5	15946.5	-140.51	1936.29	16064.3	313.57	1229.17	0.39	5.91
37	16088.7	-144.11	1870.36	16197.7	313.67	1225.15	0.39	5.84
37.5	16230.1	-147.74	1802.41	16330.5	313.81	1221.12	0.38	5.76
38	16370.5	-151.41	1732.46	16462.6	314.01	1217.07	0.37	5.68
38.5	16510.1	-155.11	1660.52	16594.1	314.25	1213	0.37	5.59
39	16648.8	-158.84	1586.62	16725	314.54	1208.92	0.36	5.5
39.5	16786.6	-162.6	1510.76	16855.2	314.86	1204.81	0.35	5.41
40	16923.5	-166.39	1432.96	16984.9	315.22	1200.68	0.35	5.32
40.5	17059.5	-170.21	1353.25	17114	315.61	1196.53	0.34	5.22
41	17194.6	-174.06	1271.63	17242.5	316.03	1192.35	0.33	5.13
41.5	17328.9	-177.93	1188.13	17370.5	316.47	1188.15	0.32	5.03
42	17462.2	-181.82	1102.77	17497.9	316.94	1183.92	0.31	4.94
42.5	17594.6	-185.74	1015.56	17624.8	317.43	1179.67	0.31	4.84
43	17726.1	-189.68	926.53	17751.3	317.94	1175.39	0.3	4.74
43.5	17856.6	-193.64	835.7	17877.2	318.46	1171.08	0.29	4.65
44	17986.3	-197.62	743.1	18002.7	319	1166.73	0.28	4.55
44.5	18115	-201.62	648.73	18127.7	319.54	1162.36	0.27	4.46
45	18242.7	-205.63	552.63	18252.2	320.1	1157.96	0.27	4.36
45.5	18369.5	-209.67	454.82	18376.3	320.66	1153.52	0.26	4.27
46	18495.3	-213.71	355.32	18500	321.22	1149.05	0.25	4.18
46.5	18620.2	-217.77	254.17	18623.2	321.79	1144.54	0.24	4.09
47	18744.1	-221.84	151.37	18746	322.36	1140.01	0.24	4
47.5	18867	-225.92	46.96	18868.4	322.93	1135.43	0.23	3.91

Time	X	Y	Z	Slant	Velocity	Spin	A_Bar	Gyro
sec	m	m	m	m	m/sec	rad/sec	deg	
47.7224	18921.4	-227.74	0	18922.7	323.18	1133.39	0.23	3.87

Appendix B: The Developed Code

```
clc, clear all,
close all

%% Sabit deęerlerin ve bařlangıç kolullarının atanması
%%%%%%%%%%%%%%%%%%%%%%%%%%%%%%%%%%%%%%%%%%%%%%%%%%%%%%%%%%%%%%%%%%%%%%%%
%% Sabit deęerlerin ve bařlangıç kolullarının atanması %%
%%%%%%%%%%%%%%%%%%%%%%%%%%%%%%%%%%%%%%%%%%%%%%%%%%%%%%%%%%%%%%%%%%%%%%%%

%% Mühimmat Deęerleri
T = 0.002; % Örnekleme Zamanı
g = 9.80665; % Yerçekimi deęerini m/s^2 cinsinden ifade
ettim.
d = 154.74*10^-3; % metre
S = (pi*d*d)/4; % m^2
m = 40.78; % kg

Ixx = 0.142; % kg.m2
Iyy = 1.82; % kg.m2
Izz = Iyy; % kg.m2

%% Bařlangıç Kořulları
konum = [0 0 0]';
% [m] sırasıyla 123 koordinat sistemi mesafe, yükseklik, yanal

p = 1669.1; % rad/s
roll_rate= p; % rad/s
q = 0; % rad/s
r = 0; % rad/s

omega = [p q r]'; % rad/s

% Kuzey doęrultusunda, 23 derecelik açıyla atıldığını varsayalım.
% (Euler Angles, NED->Body)
phi = 0; % radyan
theta = 23*pi/180; % radyan
psi = 0; % radyan

alpha = 0; % radyan
beta = 0; % radyan

zaman = 0; % s

% İlk hızın sadece burnu yönünde (kuzey yönünde) olduğunu düşünelim.
u = 826; % m/s
v = 0; % m/s
w = 0; % m/s

%%
```

```

% Gövde ekseninde tanımladığımız hızı, 123 dünya ekseninde
dönüştürüyoruz.
Vi = u*[cos(theta)*cos(psi) sin(theta)*cos(psi) sin(psi) ]';

V1 = Vi(1);           % Dünya ekseninde 1 eksenindeki hızı.
V2 = Vi(2);           % Dünya ekseninde 2 eksenindeki hızı.
V3 = Vi(3);           % Dünya ekseninde 3 eksenindeki hızı.

V = norm(Vi);         % Toplam doğrusal hız.

x = [cos(theta)*cos(psi) sin(theta)*cos(psi) sin(psi) ]';
% Dünya ekseninde unit burun vektörü
h = [Ixx/Iyy*p*x(1,1) Ixx/Iyy*p*x(2,1) Ixx/Iyy*p*x(3,1) ]';
% Dünya ekseninde açısal hız vektörü
i = (Vi(:,end)/V(end));
% Dünya ekseninde hız doğrultusundaki unit vektör

delta = 0;            % delta = sin(total_aoa)
total_aoa = 0;        % [rad] total_aoa= sqrt(alpha^2+beta^2)

sure = 50;            % sn cinsinden maksimum simulasyon süresi

% de = 0; dr = 0; da = 0; % Kontrolsüz olduğu için 0 aldım.

Tr=0;                 % Thrust olmadığından 0 alınır

%% Dış Etkiler
% Rüzgar hızı

V_wind_mag = 0 ;     % m/s
V_wind_ang = 10;     % deg
V_wind = [V_wind_mag*cosd(V_wind_ang) 0
V_wind_mag*sind(V_wind_ang) ]'; % m/s

% Mekanizma Kuvveti

Fmec(1) = 0;
Smec = 3e-4;         % m^2
mec_angle = 30;      % deg
bas_zaman = 500;     % s

%%
%% Tablolanmış Aerodinamik Veriler 57 numaralı Dispersion Analysis
Machpoints = [ 0.6000  0.7000  0.7500  0.8000
0.8500...
0.8750  0.9000  0.9250  0.9500  0.9750  1.0000
1.0250...
1.0500  1.1000  1.2000  1.3500  1.5000  1.7500
2.0000...
2.2500  3.0000];
Cx0_data = [ 0.1170  0.1190  0.1190  0.1200
0.1270...
0.1320  0.1360  0.1600  0.1920  0.2430  0.2940
0.3130...

```

```

    0.3280    0.3320    0.3240    0.3120    0.3000    0.2790
0.2550...
    0.2390    0.2230];
Cxa2_data   = [ 5.0000    5.0000    5.0000    5.5000
5.7000...
    5.8500    6.0000    6.2000    6.7000    7.0000    7.2000
6.9000...
    6.0000    5.5000    5.3000    5.1000    5.0000    4.8000
4.6000...
    4.4000    4.2000];
Cxa4_data   = [      0      0      0      0
0 ...
    0      0      0      0      0      0      0
...
    0      0      0      0      0      0      0
...
    0      0];
Cna_data    = [ 1.5000    1.5000    1.5000    1.5000
1.5500...
    1.6000    1.6500    1.7000    1.7500    1.8000    1.8500
1.9000...
    1.9500    2.0000    2.1000    2.2300    2.3500    2.4800
2.6000...
    2.6800    2.7500];
Cna3_data   = [ 10.0000   10.0000   10.0000   10.0000
10.0000...
    10.0000   10.0000   10.0000   10.0000   10.0000   10.0000
10.0000...
    10.0000   10.0000   10.0000   10.0000   10.0000   10.0000
10.0000...
    10.0000   10.0000];
Cpn_data    = [ 0.7200    0.7100    0.6600    0.6000
0.6200...
    0.6400    0.6400    0.6000    0.5600    0.8600    1.2300
1.3000...
    1.3800    1.4300    1.5300    1.6500    1.7500    1.8600
1.9400...
    2.0000    2.0400];
Cypa_data   = [-0.9600   -0.9600   -0.9600   -0.9600   -
1.0200...
    -1.0400   -1.0700   -1.2100   -1.3500   -1.3000   -1.2400   -
1.1900...
    -1.1300   -1.0700   -0.9600   -0.9600   -0.9600   -0.9600   -
0.9600...
    -0.9600   -0.9600];
Cxf_data    = [ 0.0820    0.0830    0.0830    0.0840
0.0890...
    0.0910    0.0940    0.1140    0.1340    0.1700    0.2060
0.2180...
    0.2300    0.2320    0.2270    0.2180    0.2100    0.1950
0.1780...
    0.1670    0.1560];
Cxb_data    = [ 0.0350    0.0360    0.0360    0.0360
0.0380...
    0.0410    0.0420    0.0460    0.0580    0.0730    0.0880
0.0950...

```

```

0.0980    0.1000    0.0970    0.0940    0.0900    0.0840
0.0760...
0.0720    0.0670];
Cnq_data   =   [      0      0      0      0
0 ...
0      0      0      0      0      0      0
...
0      0      0      0      0      0      0
...
0      0];
Cma_data   =   [ 4.2100  4.2300  4.3000  4.4000
4.5100...
4.6200  4.7700  4.9850  5.2000  4.8000  4.2500
4.2300...
4.2000  4.1900  4.1900  4.1800  4.1700  4.1500
4.1300...
4.1100  4.0900];
Cma3_data  =   [-1.2500 -1.2500 -1.2500 -1.2500 -
2.0000...
-2.5000 -3.0000 -3.0000 -3.0000 -3.0000 -3.0000 -
2.0000...
-2.0000 -1.0000 -1.0000      0      0      0
0 ...
0      0];
Cma5_data  =   [      0      0      0      0
0 ...
0      0      0      0      0      0      0
...
0      0      0      0      0      0      0
...
0      0];
Cmq_data   =   [-10.6000 -10.6000 -13.5000 -14.6900 -
14.9400...
-15.0600 -15.1900 -15.5900 -15.9900 -17.9400 -22.2000 -
23.0000...
-23.7900 -24.4900 -25.9900 -26.8000 -27.3800 -27.7000 -
27.7000...
-27.7000 -27.7000];
Cmq2_data  =   [      0      0      0      0
0 ...
0      0      0      0      0      0      0
...
0      0      0      0      0      0      0
...
0      0];
Cnpa1_data =   [ 0.4500  0.4500  0.4500  0.4500
0.5300 ...
0.5600  0.6000  0.6000  0.6000  0.7700  0.9300
1.1000 ...
1.2700  1.2700  1.2200  1.1600  1.1100  1.0200
1.0200 ...
1.0200  1.0200];
Cnpa3_data =   [ 0.5300  0.5500  0.5600  0.5700
0.6300 ...
0.6600  0.6800  0.7200  0.7500  0.8300  0.9100
0.9800...

```

```

1.0600    1.0600    1.0400    1.0100    0.9900    0.9500
0.9500 ...
0.9500    0.9500];
Cnpa5_data = [ 0.5600    0.6100    0.6300    0.6500
0.6900...
0.7100    0.7200    0.7900    0.8600    0.8800    0.9000
0.9000...
0.9000    0.9000    0.9000    0.9000    0.9000    0.9000
0.9000...
0.9000    0.9000];
Clp_data = [-0.0270   -0.0270   -0.0270   -0.0270   -
0.0270 ...
-0.0270   -0.0270   -0.0270   -0.0270   -0.0265   -0.0260   -
0.0260 ...
-0.0260   -0.0260   -0.0250   -0.0250   -0.0240   -0.0230   -
0.0230 ...
-0.0230   -0.0230];
Cld_data = [
0 ...
0    0    0    0    0    0    0
...
0    0    0    0    0    0    0
...
0    0];

```

```

%%%%%%%%%%%%%%%%%%%%%%%%%%%%%%%%%%%%%%%%%%%%%%%%%%%%%%%%%%%%%%%%%%%%%%%%
%%%%%%%%%%%%%%%%%%%%%%%%%%%%%%%%%%%%%%%%%%%%%%%%%%%%%%%%%%%%%%%%%%%%%%%%

```

```

ix = cross(i(:,end),x(:,end)); % hız ve burun vektörü cross
çarpımı
xix = cross(x(:,end),ix); % xix = xix/norm(xix);

```

```

maxit = sure/T;
inc=0; % iteration number

```

```

while inc<maxit & konum(2,end) >= 0
% maksimum simulasyon süresi bittiğinde veya yükseklik 0
olduğunda bitir

```

```

zaman(end+1) = (inc+1)*T;

```

```

Aero_Katsayi_Hesapla_ME_151206_R7 %

```

```

Kuvvet_Moment_Hesapla_ME_151206_R7 %

```

```

% Kararlılık Analizi
Sg(inc+1) =
(2*Ixx^2*roll_rate(end)^2)/(pi*rho*Iyy*d^3*V(end)^2*Cma) ;
% Maccoy chapter 10 gyroskopik kararlılık>1
Sd(inc+1) = 2*(Cn-Cx0*(m*d^2/Ixx/2)*Cyp)/((Cn-Cx0-
(m*d^2/Iyy)*Cmq+...
(m*d^2/Ixx/2)*Clp));
% Maccoy chapter 10 dinamik kararlılık [0 2]

```

```

EOM_1_151206_R7

%%%%%%%%%%%%%%%%%%%%%%%%%%%%%%%%%%%%%%%%%%%%%%%%%%%%%%%%%%%%%%%%%%%%%%%%
%%%%%%%%%%%%%%%%%%%%%%%%%%%%%%%%%%%%%%%%%%%%%%%%%%%%%%%%%%%%%%%%%%%%%%%%

Aero_Katsayi_Hesapla_ME_151104_R6 %
Kuvvet_Moment_Hesapla_ME_151104_R6 %

EOM_2_151206_R7

    inc = inc + 1; % increment iteration
end %% end of for

%%%%%%%%%%%%%%%%%%%%%%%%%%%%%%%%%%%%%%%%%%%%%%%%%%%%%%%%%%%%%%%%%%%%%%%%
%%% PLOTTINGS %%%
%%%%%%%%%%%%%%%%%%%%%%%%%%%%%%%%%%%%%%%%%%%%%%%%%%%%%%%%%%%%%%%%%%%%%%%%

if konum(2,end)<=0

    button = questdlg('Füze yere düştü.','Bildirim',...
        'Figürleri göster','Kapat','Figürleri göster');

elseif inc>=maxit

    button = questdlg('Maksimum simulasyon süresine ulaşıldı',...
        'Bildirim','Figürleri göster','Kapat','Figürleri göster');

else
    msgbox('konum2 NaN oldu sanırım');
    button = 'x';
end
%%
if strcmp(button,'Figürleri göster')
    f1= figure('units','normalized','outerposition',...
        [0.02 0.75 0.3 0.24]); plot(Sd,Sg); grid on;...
        title('Stability'); xlabel('Sd'); ylabel('Sg');
    f2= figure('units','normalized','outerposition',...
        [0.35 0.75 0.3 0.24]); plot(zaman,total_aoa*(180/pi));...
        grid on; title('Time vs. Total Aoa'); xlabel('Time (s)');...
        ylabel('Total Aoa (deg)');
    f3= figure('units','normalized','outerposition',...
        [0.68 0.75 0.3 0.24]); plot(konum(1,:),konum(2,:)); grid
on;...
        title('Position1 vs. Position2'); xlabel('Position1
(m)');...
        ylabel('Position2 (m)');
    f4= figure('units','normalized','outerposition',...
        [0.02 0.51 0.3 0.24]); plot(zaman,V1); grid on; ...
        title('Time vs. V1'); xlabel('Time (s)'); ...
        ylabel('Vx (m/s)');
    f5= figure('units','normalized','outerposition',...
        [0.35 0.51 0.3 0.24]); plot(zaman,V2); grid on; ...
        title('Time vs. V2'); xlabel('Time (s)'); ...

```

```

        ylabel('Vy (m/s)');
f6= figure('units','normalized','outerposition',...
    [0.68 0.51 0.3 0.24]); plot(zaman,V3); grid on; ...
    title('Time vs. V3'); xlabel('Time (s)'); ...
    ylabel('Vz (m/s)');
f7= figure('units','normalized','outerposition',....
    [0.02 0.27 0.3 0.24]); plot(zaman,konum(1,:));...
    grid on; title('Time vs. Position1'); ...
    xlabel('Time (s)'); ylabel('Position1 (m)');
f8= figure('units','normalized','outerposition',...
    [0.35 0.27 0.3 0.24]); plot(zaman,konum(2,:)); ...
    grid on; title('Time vs. Position2'); ...
    xlabel('Time (s)'); ylabel('Position2 (m)');
f9= figure('units','normalized','outerposition',...
    [0.68 0.27 0.3 0.24]); plot(zaman,konum(3,:)); ...
    grid on; title('Time vs. Position3'); ...
    xlabel('Time (s)'); ylabel('Position3 (m)');
f10= figure('units','normalized','outerposition',...
    [0.02 0.03 0.3 0.24]); plot(zaman,V); grid on; ...
    title('Time vs. V'); xlabel('Time (s)'); ...
    ylabel('V (m/s)');
f11= figure('units','normalized','outerposition',...
    [0.35 0.03 0.3 0.24]); plot(zaman,roll_rate); ...
    grid on; title('Time vs. p'); xlabel('Time (s)'); ...
    ylabel('p(rad/s)');
f12= figure('units','normalized','outerposition',...
    [0.68 0.03 0.3 0.24]); plot(beta*(180/pi),
alpha*(180/pi));...
    grid on; title('Alpha vs. Beta'); xlabel('Beta (deg)');...
    ylabel('Alpha (deg)');

end

```

Appendix C: The Developed Code Analyses for Spin Velocities

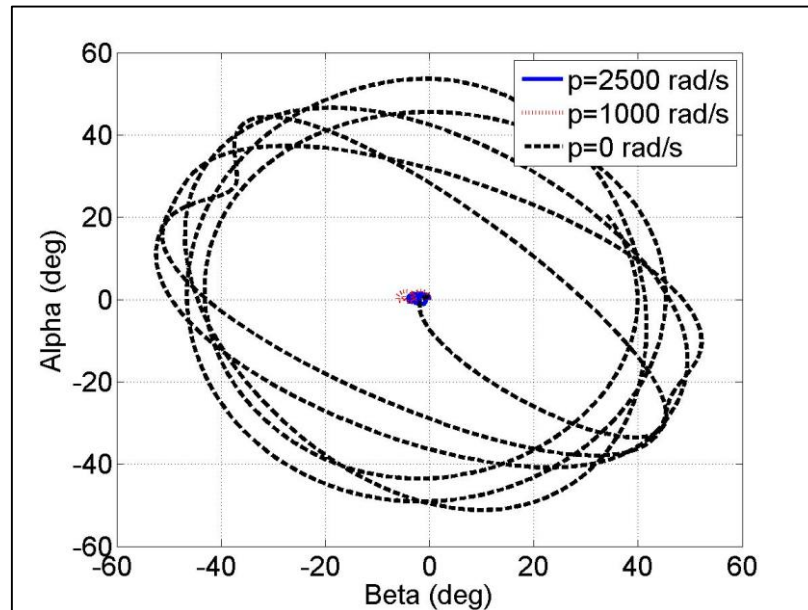


Figure 61 Alpha vs Beta for Different Spin Velocities

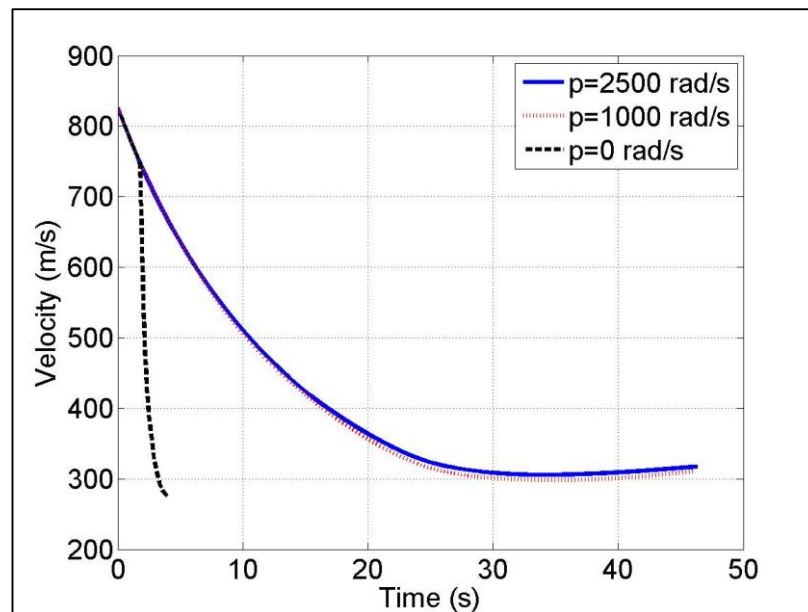


Figure 62 Velocity vs Time for Different Spin Velocities

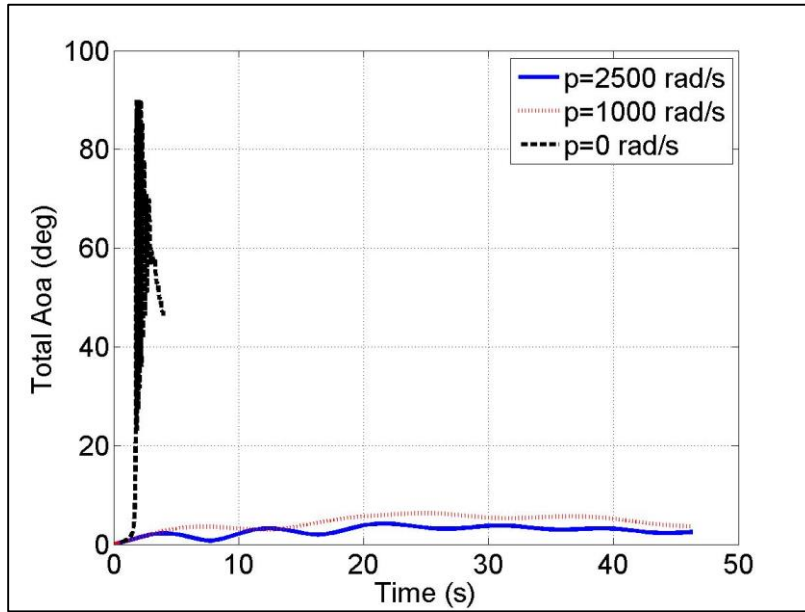


Figure 63 Total Aoa vs Time for Different Spin Velocities

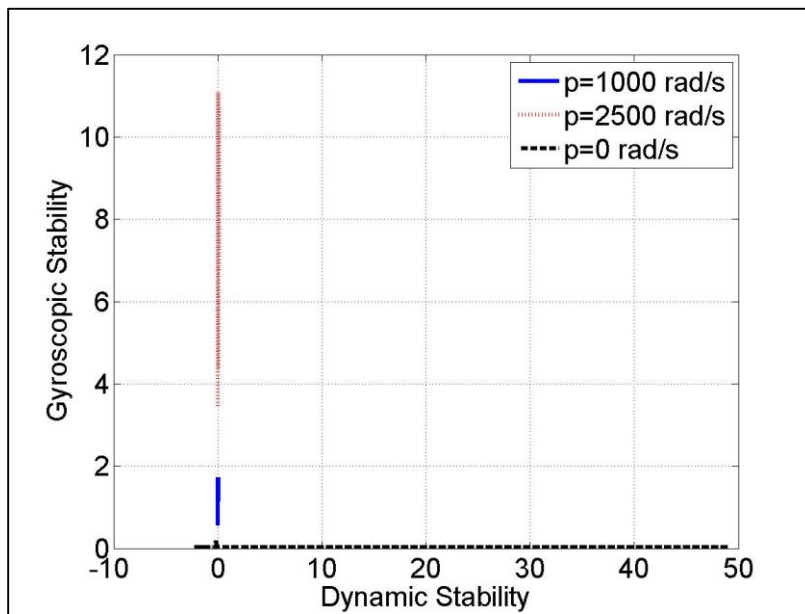


Figure 64 Gyroscopic vs Dynamic Stability for Different Spin Velocities

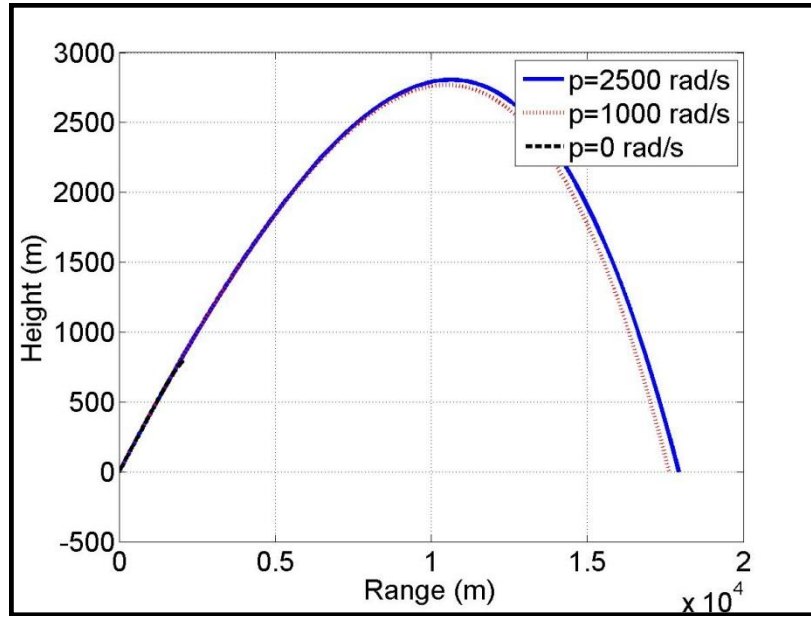


Figure 65 Height vs Range for Different Spin Velocities